

A SEARCH FOR ANTIMATTER IN THE PRIMARY COSMIC RAYS

A THESIS

submitted by

ASHLEY REGINALD CLARKE

for the degree of

DOCTOR OF PHILOSOPHY

in the

UNIVERSITY OF LONDON

February 1971

...

The fault, dear Brutus, is not in our stars,  
But in ourselves, that we are underlings.

...

Julius Caesar Act I scene 1.

ABSTRACT

Two heavy nuclei detectors were flown on high altitude balloons from Kampala ( $15^{\circ}N, 32^{\circ}E$ ), Uganda in May 1970. The balloon borne detectors consisted of two scintillator elements which determined the effective opening angle of the detector, and a gas Cerenkov element. The geometrical factor of each detector was  $200 \text{ cm}^2$  steradians.

The large geometrical factor together with a charge resolution of  $\Delta Z < 0.5$  units of charge up to silicon,  $Z=14$  enabled us to obtain information on the charge composition of the primary cosmic radiation for rigidities,  $R$  greater than 10 GV. The detector was supported at an angle of  $50^{\circ}$  to the vertical, and it was free to rotate in azimuth. By using the variation of geomagnetic cut-off rigidity with azimuth, and the pulse height information from the gas Cerenkov, it was possible to determine the integral rigidity spectra of the dominant nuclear species, and the charge groups from boron to iron nuclei. There is some evidence to suggest that, if one assumes the integral rigidity spectra to be a power law in rigidity, the exponent  $\gamma_Z$  is a function of the charge  $Z$ . The implication of this result to currently accepted views on the propagation and acceleration of cosmic rays is discussed.

Flux estimates of the splash and re-entrant proton albedo are presented and compared with previous results.

Due to the different geomagnetic cut-off rigidities for charged particles of opposite sign, the detector can be used to look for antinuclei

(ii)

in the primary cosmic radiation while pointing due East ( $\pm 45^\circ$ ). As no antinuclei events were recorded during either flight, it was possible to place an upper limit to the ratio of antinuclei to nuclei ( $Z \geq 6$ ) in the rigidity range  $10 < R < 18$  GV of

$$\frac{n_{\bar{A}}}{n_A} < 7.5 \% \quad (95\% \text{ confidence limit})$$

The significance of this result is discussed in relation to current cosmological models.

Physical processes which are capable of producing spurious antinuclei events are discussed together with the ultimate sensitivity of the detector to the antinuclei to nuclei ratio. It is suggested that, with longer exposure times at altitude, the upper limit could be reduced to  $10^{-2}\%$  with the present detector.

CONTENTS

	Page number
ACKNOWLEDGEMENTS .....	1
<u>CHAPTER 1</u> <u>INTRODUCTION TO HEAVY NUCLEI IN THE COSMIC</u>	
<u>RADIATION</u> .....	2
1.1.            General Introduction .....	2
1.2.            Origin of Cosmic Radiation .....	3
1.3.            Sources and Accelerating Mechanisms .....	7
1.4.            Propagation and Age of Cosmic Rays .....	10
1.5.            Introduction to Antinuclei .....	19
1.6.            Cosmological Implications of Antimatter .....	23
<u>CHAPTER 2</u> <u>THE DETECTOR</u> .....	28
2.1.            Description of Apparatus .....	28
2.1.1. Electronics .....	30
2.1.2. Ground Equipment .....	34
2.2.            Scintillator Elements .....	36
2.2.1. Design Criteria and Calibration .....	36
2.2.2. Uniformity of Light Collection .....	44
2.2.3. Efficiency of Scintillator Elements .....	46
2.2.4. Preflight Gain Setting .....	47
2.3.            Gas Cerenkov .....	50
2.3.1. Design Criteria .....	50
2.3.2. Preflight Calibration .....	56

2.3.3.	Efficiency of Cerenkov .....	57
2.3.4.	Scintillation Light in Gas Tank .....	60
2.4.	Hall-Probe Magnetometer .....	60
2.4.1.	Description .....	60
2.4.2.	Calibration .....	66
2.4.3.	Limitations .....	69
2.4.4.	Determination of Azimuth .....	72
2.5.	Pulse Height Analysers .....	73
<u>CHAPTER 3</u>	<u>BALLOON FLIGHTS AND DATA ANALYSIS</u> .....	76
3.1.	Balloon Flights .....	76
3.2.	Data Analysis .....	79
3.2.1.	Raw Data .....	79
3.2.2.	In-Flight Calibration .....	79
3.2.3.	Correlation of Events with Azimuth .....	80
3.2.4.	Scintillator and Cerenkov Response to Heavy, Nuclei .....	81
3.2.5.	Dead-Time Correction .....	91
3.2.6.	Ionization and Recombination Light in Gas Cerenkov .....	93
<u>CHAPTER 4</u>	<u>BACKGROUND EFFECTS IN THE DETECTOR</u> .....	94
4.1.	Discussion of Background .....	94
4.2.	Jets .....	96
4.3.	Albedo .....	101
4.3.1.	Splash and Re-entrant Proton Flux .....	104

4.4.	Spallation in the Detector .....	111
	4.4.1. Splash Alpha Albedo - Differential Flux	
	Values .....	117
<u>CHAPTER 5</u>	<u>RIGIDITY SPECTRA OF HEAVY NUCLEI</u> .....	118
5.1.	Derivation of Spectral Exponents .....	118
5.2.	Review of Rigidity Spectra ( $10 < R < 40$ GV) ...	133
5.3.	Significance of Spectra in Range $10 < R < 40$ GV	136
	5.3.1. Leakage from the Galaxy .....	136
	5.3.2. Ionisation .....	137
	5.3.3. Solar Modulation .....	137
	5.3.4. Fragmentation .....	138
	5.3.5. Interstellar Acceleration Mechanisms .....	138
5.4.	Discussion of the Results .....	141
	5.4.1. Conclusion .....	145
<u>CHAPTER 6</u>	<u>NUCLEAR COMPOSITION OF COSMIC RAYS - CHARGE</u>	
	<u>SPECTRUM</u> .....	147
6.1.	Extrapolation to the Top of the Atmosphere .....	147
	6.1.1. Light to Medium Nuclei Ratio .....	150
	6.1.2. Carbon to Oxygen Ratio .....	155
	6.1.3. Nitrogen to Medium Nuclei Ratio .....	155
	6.1.4. Fluorine to Oxygen Ratio .....	157
	6.1.5. Heavier ( $Z \geq 10$ ) to Medium Nuclei Ratio .	157
6.2.	Source Composition .....	158
	6.2.1. Extrapolation to Source Region .....	158
	6.2.2. Source Composition .....	160

6.3.	Discussion .....	161
6.4.	Conclusion on Source Composition .....	164
<u>CHAPTER 7</u>	<u>UPPER LIMIT TO ANTINUCLEI IN THE PRIMARY COSMIC</u>	
	<u>RAYS</u> .....	167
7.1.	Experimental Method .....	167
	7.1.1. Derivation of Upper Limit .....	172
	7.1.2. Spurious Antinuclei Events and Detector	
	Sensitivity .....	173
	(a) Chance Coincidences .....	174
	(b) Albedo .....	175
	(c) Isotopic Composition .....	176
	(d) Pion Production in Jets .....	179
	(e) Stars .....	180
	(f) Fragmentation of High-Z Primary .....	180
7.2.	Antimatter in the Galaxy - Significance of Gamma	
	Ray Astronomy .....	187
7.3.	Antimatter in the Galaxy - Conclusions .....	190
<u>APPENDIX A</u>	<u>HALL PROBE MAGNETOMETER</u> .....	197
<u>APPENDIX B</u>	<u>SOLAR MODULATION</u> .....	201
<u>APPENDIX C</u>	<u>PREFERENTIAL LOSS BY DIFFUSION</u> .....	204
REFERENCES	.....	205



ACKNOWLEDGEMENTS

Firstly, I would like to thank Professor H. Elliot for his excellent advice and unfailing good humour at all times.

I would like to thank all the members of the Cosmic Ray and Space Physics Group who helped with the construction of the detectors, in particular Mr. K.E. Moss and Mr. Manu Joshi.

This work would not have been possible without the cooperation of Professor D.M. Thomson of Makerere University College, Kampala, who provided accommodation and base facilities in Uganda. I thank him and his staff in the Physics Department for their hospitality and help, and especially, my colleague Dr. R.K. Sood for constant encouragement during times of stress, whose help was instrumental to the success of the project.

I wish to thank Dr. J.G. Greenhill for the opportunity to work with him and the Science Research Council for their financial support.

I am very grateful to Miss Corri van de Stege for typing this thesis and, finally, I would like to thank, and dedicate this thesis to, my parents for their continuing support and encouragement.

CHAPTER I. - INTRODUCTION TO HEAVY NUCLEI IN THE COSMIC  
RADIATION.

1.1. General Introduction

The term 'primary cosmic radiation' refers to all those particles and electromagnetic radiations entering the Earth's atmosphere and originating in galactic and extragalactic sources. The study of this cosmic radiation is important because its constituents are natural space-probes, whose properties reflect the properties of the sources of the radiation and also the interstellar medium through which the radiation travels en route to the Earth.

Most of the cosmic radiation consists of protons and helium nuclei. The heavy nuclei, with charge  $Z > 3$  account for only 1.4% of the total radiation and so, in the past, experimental results pertaining to the charge composition and energy spectra of these nuclei have been associated with poor statistics, especially at very high energies.

These heavy nuclei fragment into lighter nuclei when traversing appreciable amounts of matter, and hence the incoming flux of heavy nuclei must be investigated near the top of the Earth's atmosphere in order to avoid the extrapolation of the flux values to the top of the atmosphere by using imprecise fragmentation probabilities. The experiment to be described employed a heavy nuclei detector with a large

collecting area which was flown on a high altitude balloon, and achieved an atmospheric depth of  $5.0 \text{ gm.cm}^{-2}$  residual atmosphere.

The composition of the heavy nuclei is expected to yield information on the composition of the source regions, after account has been taken of interstellar accelerative processes and the fragmentation of heavier nuclei into lighter nuclei. By comparing the ratios of one charge group to another, and, as techniques improve, investigating the isotopic composition of certain charge groups, it is possible to estimate the average amount of matter traversed and the age of the cosmic radiation. A study of the energy and rigidity spectra of the different charge groups gives information on the accelerating mechanism in interstellar space and also the mechanism responsible for the injection of cosmic rays into interstellar space.

In the following sections, the currently accepted models of the origin of the cosmic radiation (Section 1.2.) of the source regions and accelerating mechanisms (Section 1.3.) of propagation, confinement and age of cosmic radiation (Section 1.4.) are reviewed and discussed. The relevance of the results presented here to the models reviewed is discussed in chapters 5 and 6.

### 1.2. Origin of Cosmic Radiation

There are two schools of thought as far as the origin of the cosmic radiation is concerned. On the one hand, Burbidge et.al. (1, 2, 3) consider that the radiation is universal in extent and that the cosmic ray flux exists throughout the Universe with an intensity

almost comparable to the intensity observed at the earth. A variant of this proposal is due to Sciama (4) who supposes the radiation to be confined to the local group or cluster of galaxies. However, these suggestions are regarded as improbable because the original idea requires vast amounts of energy in the form of cosmic radiation and the latter proposal cannot account physically for a mechanism which would permit storage and confinement of the cosmic rays within a limited extragalactic volume. On the other hand, Ginzburg and Syrovatskii (5) suggest that the observable cosmic rayflux is essentially a galactic phenomenon, and predict that the flux of cosmic radiation in intergalactic space is very small. Their theory represents a steady state situation where cosmic rays are continuously produced in the galaxy and the observed distribution is determined by the net effect of creation mechanisms and loss via interstellar absorption and leakage from the galaxy. Yet another proposal has been put forward; Webber (6) and Durgaprasad (7) which maintains that cosmic rays may have been produced at a single well-defined past epoch. However, this is not regarded as a serious alternative because the presence of the recently detected superheavy nuclei with charge,  $Z > 80$ , as pointed out by Cowsik et.al. (8) cannot be understood in this theory. The interaction mean free path of such a nucleus is of the order of  $1 \rightarrow 2 \text{ gm.cm}^{-2}$  and with currently accepted values of the density of interstellar space, these particles cannot have survived for times,  $T > 10^8$  yrs. Another

experimental result which disagrees with this big bang picture of cosmic rays is the observed electron spectrum which extends up to 300 GeV. If the electrons had been produced at the same time as the rest of the cosmic radiation the present spectrum should show a sharp high energy cut-off due to energy losses. The lack of such a cut-off up to 300 GeV implies that the creation time  $< 10^6$  yrs in the past. However, Walker (9) has shown that the cosmic ray intensity has been constant to within 10% for the last  $10^7$  years and other experimenters e.g. Anders (10) have shown that it has been constant to within a factor of 2 over the past  $10^9$  years.

Hence, the situation at the present time is that the bulk of the observed cosmic radiation is thought to be confined to the galaxy by the resident magnetic fields. Cosmic rays with energies of the order of  $10^{17}$  eV are, however, of undoubtedly extragalactic origin because, in order to suppose that they were confined to the galaxy, one would have to exceed the strength of the galactic magnetic fields deduced from other observations. If the observation of the total energy spectra of EAS in the energy range  $10^{14} - 10^{18}$  eV can be verified, then there exists excellent corroborative evidence that the leakage phenomenon of these high energy particles from the galaxy is valid. As pointed out by Syrovatskii et.al.(11) the change in the total energy spectral exponent from

$$|\underline{\gamma}_F| \approx 2.5 \quad \text{for} \quad E < 3 \times 10^{15} \text{ eV}$$

to

$$|\gamma_{\underline{F}}| \approx 3.0 \quad \text{for} \quad 3 \times 10^{15} < E < 10^{16} \text{ eV}$$

can be understood in terms of the definite variation of the diffusion coefficient with the energy and charge of the diffusing particle. If the diffusion of cosmic rays in the galaxy depends upon size and strength of magnetic homogeneities then the spectral width of this leakage phenomenon is due to 'chemical blurring'. As the diffusion coefficient should start to change at the same rigidity for the different charge groups, the iron group nuclei will leak out at a total energy,  $E_{L,Fe}$  which is related to the energy at which protons leak out  $E_{L,p}$  by

$$E_{L,Fe} = Z_{Fe} F_{L,p}$$

Another interesting result on the spectral shapes, which has to be verified, is the apparent reversal of the total energy spectral exponent to

$$|\gamma_E| \approx 2.5 \quad \text{for} \quad E > 10^{16} \text{ eV.}$$

One could interpret this residual flux as the flux of the intergalactic cosmic radiation, and if this flux is extrapolated to lower energies, the ratio of the supposed intergalactic component to the galactic component is

$$n_{i.g./ng} \approx 10^{-2} \quad (1)$$

From the experimental point of view, the arguments are divided

between galactic and extragalactic origin for the cosmic radiation and a compromise of sorts has been achieved. The results of the present experiment cannot question either point of view and so the galactic model has been implicitly assumed as far as any conclusions are concerned.

### 1.3. Sources and Acceleration Mechanisms

Having accepted the equilibrium galactic model of Ginzburg and Syrovatskii, the main problem is to find sources capable of supplying the required cosmic ray energy. The total energy of the cosmic radiation can be determined experimentally by finding the detailed energy spectrum and integrating over all energies observed. In this way, the energy density of the cosmic radiation within the galaxy is found to be approximately  $1 \text{ eV/cm}^3$ , which is also the accepted figure for the magnetic field energy density and the energy density of the 'starlight' or radiation field within the galaxy. (As one is considering an equilibrium model, one would expect the total available energy to be shared equally between the different energy forms.)

Assuming that the volume of the galactic disk is  $3 \times 10^{66} \text{ cm}^3$  and that the average storage time within the galaxy is  $10^6$  yrs (see later) it follows that the energy input required from the integrated cosmic ray sources is

$$\frac{10^{-12} \times 3 \times 10^{66}}{10^6 \times 3 \times 10^7} \text{ ergs/sec.}$$

$$\sim 10^{41} \text{ ergs/sec} \quad \text{using } 1 \text{ eV/cm}^3 = 10^{-12} \text{ ergs/cm}^3$$

The most likely candidates for sources of cosmic radiation are supernovae and pulsars. The energy release from the explosion of a supernova is thought to be  $\sim 10^{51}$  ergs and, as the frequency of occurrence of these supernovae in the galaxy is  $\sim 1$  every century, the effective energy release is

$$\frac{10^{51}}{100 \times 3 \times 10^7} \text{ ergs/sec} \approx 3 \times 10^{41} \text{ ergs/sec.}$$

and so this source is energetically possible.

Tammann (Astron. Astrophysics, 8, p.458, 1970) has conducted a count of the supernovae occurring in galaxies and when he extrapolates the information to our own galaxy, deduces a possible frequency of occurrence of supernovae of 1 per 26 yrs (+ 10 yrs) - hence the supernovae could definitely be able to provide the energy for cosmic rays.

In a supernova, the nucleosynthesis of heavy elements is already far-advanced, and the pre-supernova core is composed of iron. When exothermic nuclear reactions are nearly exhausted, the star undergoes gravitational collapse into a neutron star, while the outer layers of the star explode and form a cloud like the Crab Nebula. Colgate et.al. (12) have developed a theory of hydrodynamical acceleration during the initial explosion stage. In their theory, the energy from a shock wave blows off a large fraction of the star and because the shock intensifies as it passes into lower density material, it imparts relativistic energies to the outermost layers.



There have been numerous theories of acceleration of the particles in supernovae remnants after the initial explosion. Layzer (13) supposes that acceleration occurs via stochastic processes in relatively dense, magnetized clouds of plasma (it is worthwhile noting that this is essentially the Fermi mechanism of acceleration). Kaplon and Skadron (14) develop a quantitative theory, specifically for the Crab Nebula, which supposes the post-explosion acceleration is due to either Fermi-type acceleration or the Hayakawa, hydromagnetic shock theory. Another suggestion from Michel (15) proposes acceleration of particles in neutral sheets within the magnetic fields of supernovae remnants. Finally, Melrose (16) and Tsytovich (17) discuss the possible preferential acceleration of heavy nuclei from thermal energies in the presence of special hydromagnetic conditions in ionized plasmas.

The added attraction of supernovae is the presence of large amounts of heavy elements. If the relative abundance of each nuclear species occurring in the flux of cosmic radiation is compared to the universal relative abundances, as given by Aller (18) or Cameron (19) obtained from mainly spectroscopic data on stellar atmospheres, it is found that cosmic radiation is overabundant in heavy nuclei (see Table VII). Any plausible source of the cosmic radiation must therefore be either overabundant in heavy nuclei as compared to the majority of main-sequence stars or the acceleration mechanisms must preferentially

accelerate the heavier in order to increase their abundances relative to the lighter nuclei. Most of the acceleration mechanisms have been mentioned already, and each will be discussed later in the light of the present experimental evidence on the spectra of the individual nuclear species in Chapter 5.

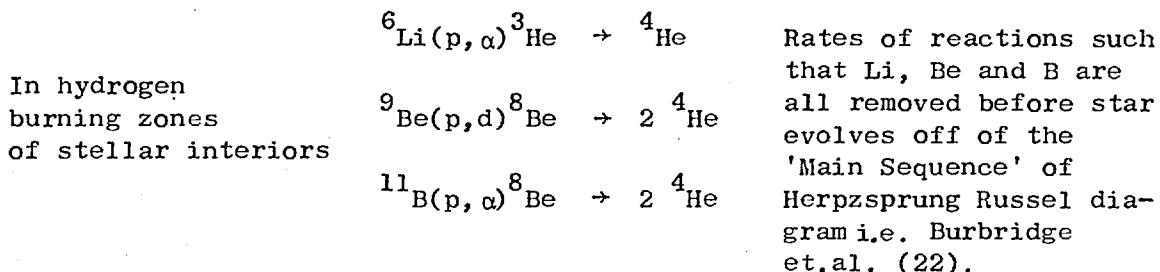
Gold (20) has proposed that pulsars are rapidly rotating neutron stars and there is evidence, from the pulsar in the Crab Nebula, that the rotational energy of the pulsar is slowly transformed into radiative energy. Ostriker and Gunn (21) predict that particles may be accelerated up to energies of the order of  $10^{21}$  eV in the radiation field of the pulsar, and so this could possibly explain the very highest part of the spectrum of cosmic radiation without the necessity of an extragalactic source.

#### 1.4. Propagation and Age of Cosmic Rays

It is generally believed that, after leaving the sources, cosmic rays diffuse through interstellar space with their motion being controlled and made random on a large scale by the galactic magnetic fields. In their passage through the interstellar material at least two mechanisms affect the cosmic ray composition and energy spectra, namely fragmentation of heavy ions into lighter ions in nuclear interactions with the interstellar hydrogen and Coulomb interactions including ionization energy loss. Additional processes which could affect the energy depen-

dence of the relative composition include Fermi acceleration, in collisions of the nuclei with magnetic irregularities in plasma clouds and a rigidity dependent escape from the galaxy. It is also possible that cosmic rays have traversed appreciable material before leaving the source region, in which case the above processes may also occur before the injection into interstellar space.

The simplest propagation model which can be used is the 'slab model' which assumes that all nuclear species present in the source regions traverse a fixed amount of interstellar material,  $x \text{ grm.cm}^{-2}$  which is independent of the particle energy. If one accepts this model, it is possible to extrapolate the observed flux of the  $i^{\text{th}}$  nuclear species  $j_i(x)$  back to the source,  $j_i(0)$ , if one knew the composition of the source. It was noticed that the flux of the L-nuclei (lithium, beryllium and boron) in the cosmic radiation was anomalously large. These nuclei have short lifetimes in stellar envelopes due to the favoured thermonuclear reaction which convert these nuclei to stable helium form by proton bombardment:



and hence, the natural explanation for the L-nuclei was that they were secondary nuclei from the fragmentation of the heavier nuclei in interstellar space. A similar argument applies for  ${}^3\text{He}$  and deuterium, D.

At relativistic energies, measurements of the ratio  ${}^3\text{He}/({}^3\text{He}+{}^4\text{He})$  as well as the  $L/M$  ratio, i.e. the ratio  $(\frac{\text{Li}+\text{Be}+\text{B}}{\text{C}+\text{N}+\text{O}})$  lead to similar values of the amount of interstellar material traversed.

$$\bar{x} \approx 3 \rightarrow 5 \text{ gm.cm}^{-2}$$

The theory of the 'slab model' was developed by Biswas et.al. (23), O'Dell et.al. (24). Once it has been established that the cosmic radiation has traversed,  $\bar{x}$  gm.cm<sup>-2</sup> of interstellar material, it is possible to find the age of the cosmic radiation,  $\tau_{\text{CR}}$  if one makes an assumption about the average density,  $n_{\text{H}}$  of protons in the interstellar medium

$$\begin{aligned} \bar{x} &= n_{\text{H}} m_{\text{p}} l \text{ gm.cm}^{-2} & l &= \text{path traversed (cm)} \\ &= n_{\text{H}} m_{\text{p}} c \cdot \tau_{\text{CR}} & m_{\text{p}} &= \text{proton mass (gm)} \\ & & c &= \text{vel. of light (cm/sec)} \end{aligned}$$

Rearranging

$$\tau_{\text{CR}} = \frac{\bar{x}}{n_{\text{H}} m_{\text{p}} c} = \frac{5}{1.1 \cdot 1 \times 10^{-24} \cdot 3 \times 10^{10} \cdot 3 \times 10^7} \text{ yrs.}$$

$$\tau_{\text{CR}} \approx 3 \times 10^6 \text{ yrs} \quad \text{assuming } n_{\text{H}} = 1 \text{ proton/cc}$$

In the equilibrium model of Ginzburg, this age of the cosmic radiation may be interpreted as the storage time within the galactic disk. If this model is correct, then it should be possible to detect a streaming of the cosmic radiation out of the galaxy. The streaming effect manifests itself in the form of a sidereal anisotropy,  $\delta$  whose value is given by

$$\delta = (2 + \gamma) v/c \quad \text{where } v = \text{bulk velocity}$$

$c = \text{velocity of light}$   
 $\gamma = \text{exponent of differential energy spectrum.}$

Taking the observed upper limit to the anisotropy of  $10^{12}$  eV particles as  $< 3 \times 10^{-4}$  Elliot (25) and a representative exponent  $\gamma = 2.5$  one finds that the bulk velocity of the cosmic radiation is less than 20 km/sec or 20 pc per  $10^6$  yrs. This implies an extremely short mean free path,  $\lambda$  for diffusion of cosmic rays in the galactic magnetic fields,

$$\lambda \approx 0.1 \text{ pc} \approx 1 \text{ light year}$$

and is a severe restriction on the possible modes of propagation in the galaxy.

It has been suggested by Ginzburg (26) that the non-thermal radio emission from high galactic latitudes is magnetic bremsstrahlung by cosmic ray electrons propagating in a galactic halo - a spheroidal system of tenuous gas extending around the galactic disk. If this halo region exists, the density of the hydrogen gas  $n_H \sim 10^{-2} \text{ p/cm}^3$  and this modifies the confinement of the cosmic rays to  $\tau_{CR} \approx 10^8$  yrs. Hence the expected anisotropy for confinement in the halo will be less than for confinement to the disk.

However, the existence of the halo has not been definitely proved and recent theoretical work by Wentzel (27) and Lerche (28) have shown that a high degree of isotropy can arise rapidly from interactions of cosmic rays with hydromagnetic waves in the interstellar medium.

Parker (29) has concluded that the deduced slow streaming of the cosmic ray gas (velocity  $< 20$  km/sec) and the length of the galactic arms (15 kpc) indicates that cosmic rays escape normally to the disk. It could also mean that the cosmic radiation which we observe originates in nearby portions of the galaxy.

As the cyclotron radius of particles of  $10^{12}$  eV is  $\sim 3$  A.U. in the solar system, it is remotely possible that the observed isotropy of the cosmic rays is due to solar modulation (Parker (30)), but the current body of opinion regards the isotropy as a real effect. Ramaty et.al. (31) on the basis of the anisotropy result suggest that the discrepancy between the relatively short confinement time and the slow streaming is resolved when one realises that the confinement time deduced refers to the heavy nuclei (because it is derived from fragmentation) whereas the slow streaming phenomenon refers to protons predominantly. As protons have a much longer lifetime than nuclei, if nuclear interactions predominate over leakage during propagation, then the slow streaming is possible.

The problem of propagation in the disk and/or halo may be resolved by accurate determination of the cosmic ray age. Hayakawa (32) and Peters (33) pointed out that the age of the cosmic radiation could be measured with an appropriate radioactive tracer. A suitable radioactive isotope is  $^{10}\text{Be}$  whose mean life at rest,  $\tau(0)$ , is  $3.9 \times 10^6$  yrs. When the isotope is moving relativistically, its lifetime  $\tau(\gamma)$  is dilated to larger values

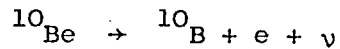
$$\tau(\gamma) = \gamma \tau(0) \quad \text{where } \gamma = (1 - \beta^2)^{-\frac{1}{2}}$$
$$\beta = \text{velocity} = v/c$$

and so, if the flux of  $^{10}\text{Be}$  in the cosmic radiation could be measured as a function of energy, the average lifetime of the cosmic radiation could be deduced.

In the past, the amount of  $^{10}\text{Be}$  has been crudely deduced by measuring the ratios of the individual L-nuclei, e.g.  $\text{Be}/\text{B}$  and  $\text{Be}/\text{Li}$  as a function of energy, and comparing these ratios with the expected ratios on the basis of  $^{10}\text{Be}$  survival and  $^{10}\text{Be}$  decay. Shapiro and Silberberg (34) have studied the problem extensively with up to date experimental cross sections for fragmentation of heavier into L-nuclei and they conclude that a definite statement of the age is elusive. However, using the recent results of von Rosenvinge and Webber (35) they find that the lifetime is consistent with substantial survival of  $^{10}\text{Be}$ , i.e.

$$\tau < 2 \times 10^7 \text{ yrs.}$$

and this result implies confinement to the galactic disk. The latest reported measurements on the isotopic composition of nuclei from  $\text{Li} \rightarrow \text{Mg}$  by Lund et.al. (36) indicate that  $^9\text{Be}$  and/or  $^{10}\text{Be}$  are the dominant isotopes for beryllium and  $^{11}\text{B}$  is the dominant boron isotope. This strengthens the argument above that the age of the cosmic radiation is such that the reaction



has not had chance to proceed.

An alternative radioactive tracer would be  $^{53}\text{Mn}$  whose half-life is  $\tau \sim 2 \times 10^6$  yrs. Reames (37) suggested this isotope and pointed out that it can decay only by K-capture. Above 0.5 GeV/n, the probability of electron capture is low and  $^{53}\text{Mn}$  should survive whereas at  $E_{\text{mn}} < 0.4$  GeV/n it could decay if the captured electron was not stripped off again. He deduces from present experimental evidence that  $\tau < 10^8$  yrs.

Other possibilities are  $^{26}\text{Al}$  and  $^{35}\text{Cl}$  for radioactive tracers, but the dual problems of

(a) adequate charge resolution and

(b) adequate statistics

make such isotopes impossible to use at the present time.

A number of other suggestions for the estimation of cosmic ray age have been proposed and are reviewed by Shapiro (38). All such methods do not contradict the result

$$\tau_{\text{CR}} \approx 10^6 \text{ yrs.}$$

It has been pointed out already that the simple slab model of propagation of cosmic rays gives consistent results (between unrelated data) for the mean quantity of matter traversed at relativistic energies.



When data became available for the energy region,  $E < 100$  MeV/n from satellite measurements, it became immediately obvious that the slab model was totally inadequate. A number of theorists, notably Fan et.al. (39); Cowsik et.al. (40); Balasubrahmanyam et.al. (41) and Fichtel and Reames (42) have discussed more realistic models in which the path length,  $x$ , was described by gaussian or exponential distributions and as a function of the energy of the particle. In other words they tried to deduce the equation of continuity for an equilibrium model in which the cosmic rays diffused through the galactic disk undergoing fragmentation and nuclear interactions and in which they were removed by diffusion in the galaxy or by ionization losses. Better fits to the data were achieved in this way, but some of the lowest energy results could still not be explained.

The basic discrepancy between the observations of Comstock (43) and Waddington and Freier (44) and the theory of the one-component model is that one would expect to see a large variation in the ratio of light to heavy nuclei with energy due to ionization losses at very low energies, but this behaviour is not seen. This has led some people, notably Comstock et.al. (45) and Burbidge et.al. (46) to speculate on the possibility of a 2-component model of propagation but many more have deferred judgement until the few satellite experimental results have been verified. Whereas the data of the Chicago group suggests a

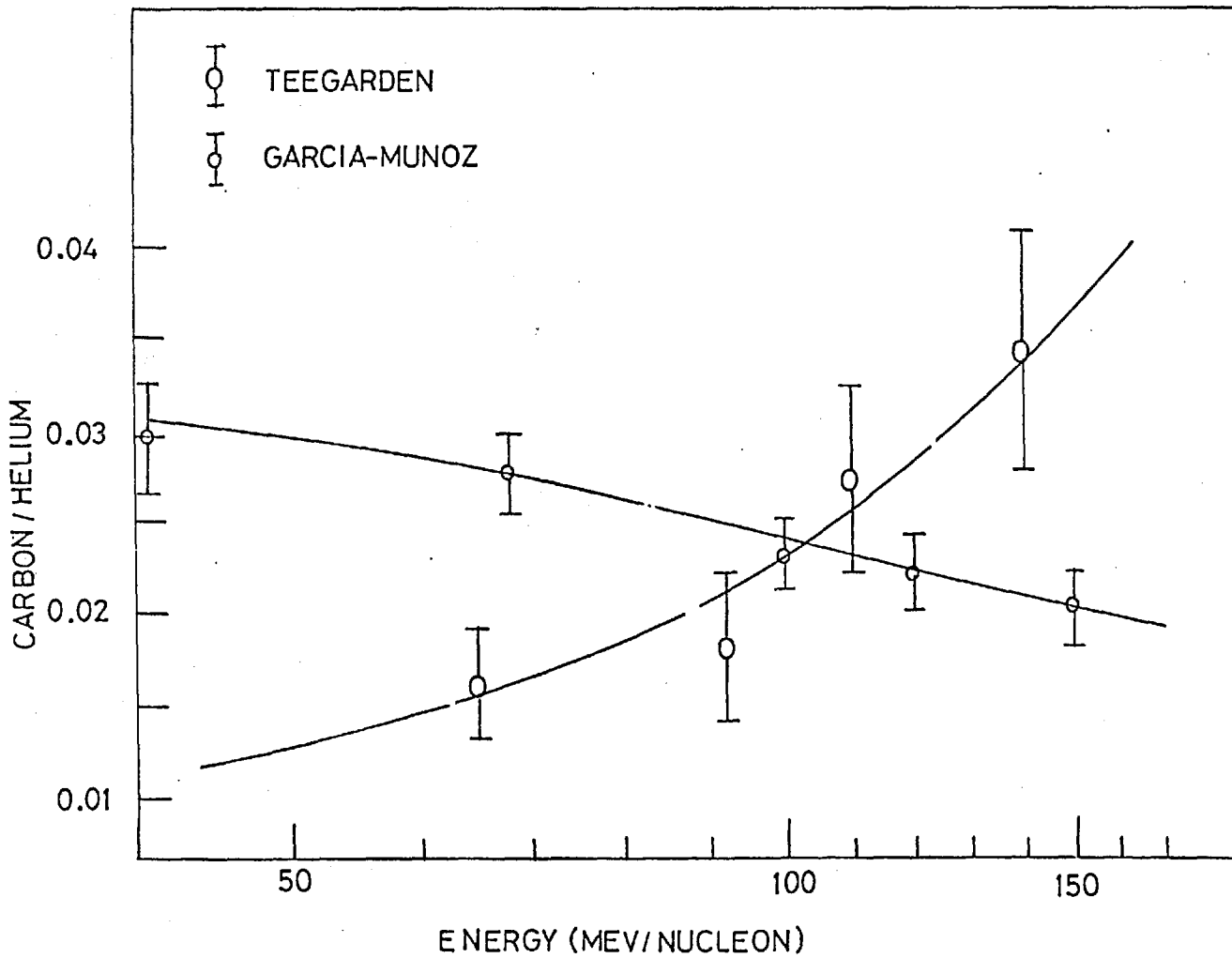


FIG. 1 SATELLITE MEASUREMENTS.

2-component model the data of the NASA Goddard group - Teegarden et. al (47) - is consistent with a one component model. As a typical example of the discrepancies, the ratio  $C/He$  is plotted at the lowest energies in Figure 1. It is worth noting that, even if the Chicago group results are accepted, Ramadurai (48) has shown that the energy dependence of the relative abundance could be reproduced by a one component model if the particles traverse a significant amount of matter while undergoing statistical Fermi acceleration at the source.

To summarise, there is much dispute over the propagation of the cosmic radiation, and as the measurements of the flux at the earth are the integrated effects of source injection and acceleration mechanisms as well as all the possible propagational effects, the exact behaviour of the radiation in the source regions must be in doubt also. The present experiment was conducted with a view to increasing the knowledge of heavy nuclei in the relativistic region of energies, and the relevance of the results to the currently accepted theories of origin and propagation are discussed in Chapters 5 and 6.

### 1.5. Introduction to Antinuclei

All matter, as we know it, is composed of elementary particles. Each particle is described in terms of a set of physical parameters, e.g. mass, charge, spin, etc. which assume discrete values - these ~~the~~ values are called quantum numbers. Theoretical physics seeks mathematical relationships or symmetries between these quantum numbers

in order to explain the finite number of allowed combinations of the quantum numbers which represent physically observed particles. The great test of any symmetry theory is not only to check that known particles fit the theory but also to predict the possible existence of hitherto unknown particles.

In 1928 Dirac (Proc. Roy. Soc. A118, p.351) had to postulate the existence of a set of particles which had identical quantum numbers to existing particles, i.e. they were identical to ordinary particles except that the sign of the electric charge was reversed. These particles were called 'antiparticles' and shortly afterwards the antielectron, or positron was discovered by Anderson (Phys. Rev. 43, p.491 (1933)) in an interaction induced by a high-energy cosmic ray particle. Dirac predicted that a catastrophic interaction could occur between a particle and antiparticle - all the initial mass energy would be completely converted on interaction to radiation energy, of wavelength  $\lambda$ , where

$$m_A c^2 + m_{\bar{A}} c^2 = \frac{hc}{\lambda}$$

$c$  = velocity of light  
 $h$  = Planck constant  
 $m_A = m_{\bar{A}}$  = mass of particle

Dirac's prediction explained in a natural way why these antiparticles are rare in the world as we know it. It is impossible to have a homogeneous mixture of particles and antiparticles due to the probability

of annihilation reactions.

Dirac also predicted that, if a  $\gamma$ -ray photon has sufficient energy, it is possible to reverse the annihilation reaction. This process is called pair-creation

$$\frac{hc}{\lambda} \rightarrow m_A c^2 + m_{\bar{A}} c^2$$

where a particle, and its equivalent antiparticle, materialise simultaneously.

High energy physicists, studying nuclear interactions induced by accelerators found that the fundamental particles could only be transformed into each other by nuclear collisions if a quantity called the Baryon number, B was conserved in the transformation. This observation was summed up by the Conservation of Baryon Number

$$\Delta B = 0$$

which physicists believe to be universally upheld.

If this law is and was universal, it implies that any acceptable theory for the 'origin' of the Universe must explain an initial materialisation of particles in which the Baryon Number was conserved. This led Alfven and Klein (see next section) to develop a theory in which half the Universe is composed of particles and half is composed of antiparticles.

The basic building block of the elements, which constitute the total matter in the world, is the atom. The atom consists of a central core,

or nucleus of positively charged protons and neutrons (which have zero charge) surrounded by a cloud of negatively charged electrons. The stability of this configuration is due to the electrical bond between positive and negative charges. Hence, once the positron and, later the antiproton had been shown to exist, there was no reason to believe that antiatoms, consisting of an antinucleus (of antiprotons and <sup>anti</sup>neutrons) and a cloud of positrons, could not exist and be as stable as ordinary atoms. Hence, if a satisfactory separation mechanism can exist which keeps predominantly matter regions of space away from predominantly antimatter regions, it is possible that half of the observable Universe is composed of antimatter.

Cosmic radiation is a sample of matter from the galaxy, and possibly also from other galaxies, and the discovery of antinuclei in the cosmic radiation would imply regions of antimatter. The presence of large amounts of antimatter in the Universe is attractive to astrophysicists because the annihilation mechanism is the most efficient energy transfer process known, and recently, certain celestial objects, e.g. quasars, have been discovered which radiate vast amounts of energy - possibly controlled annihilation energy.

A review of current cosmological models is presented in the following section.

### 1.6. Cosmological Implications of Antimatter

It has been seen in Section 1.5. that complete symmetry seems to exist between particles and antiparticles at the 'elementary-particle level'. Klein (49) and later Klein and Alfvén (50) were the first to develop a cosmological theory of matter and antimatter which postulated an initial state of low density gas containing equal numbers of protons and antiprotons (in order to conserve Baryon number) and electrons and positrons (for complete charge symmetry). This gas, or ambiplasma contracted under its mutual gravitational attraction, and as the density increased, annihilation increased. The annihilation products,  $\gamma$ -rays diffusing through the contracting ambiplasma, exerted a radiation pressure which eventually halted the collapse and turned the contraction into the present expansion. In order to avoid an annihilation catastrophe when the galaxies were forming, they had to assume the presence of a primeval magnetic field in the ambiplasma which separated the matter and antimatter by electrolysis. As this separation mechanism operates on a small cosmological scale, a necessary conclusion of the original cosmology is that half of the galaxy is matter and half is antimatter.

This cosmology is beset by theoretical difficulties outlined by Steigman (51). Firstly, there is no mechanism to explain the observed  $3^{\circ}\text{K}$  radiation. Secondly, it is difficult to see how the radiation pressure can brake the contraction because, at the turning point the

mean free path is larger than the radius of the Universe. Finally, there are theorems (see Hawking (52)) which show that a homogeneous, isotropic collapsing universe will never bounce unless it has some negative energy density fields, and in this cosmology there are none. This model will be discussed later in the light of experimental evidence.

The 'big-bang' model of the Universe was proposed by Gamow (53) and explains naturally the  $3^{\circ}\text{K}$  radiation - see Penzias and Wilson (54), Field et.al. (55) as the relic radiation of the initial explosion. In its original form, it is a non-charge symmetric theory and perhaps provides the strongest support for the view that the Universe does not contain equal amounts of matter and antimatter. The incompatibility of the big-bang theory and charge symmetry was shown by Zeldovich (56) and Chiu (57), because the  $\gamma$ -radiation in the observable Universe is  $10^8$  times less than predicted on a charge-symmetric basis.

A number of attempts have been made recently to avoid this radiation catastrophe. Harrison (58) has suggested that in the early stages of condensation of the Universe, there were spatial fluctuations in the Baryon number,  $N$ . As annihilations occur, the inhomogeneity is amplified because the overall Baryon number must be conserved, but in order to separate large regions of matter and antimatter by this means one has to find a non-statistical origin for these fluctuations. Omnes (59) makes some drastic assumptions in order to achieve the separation, and his assumptions are criticised by Steigman (51). In particular,



Omnes requires the nucleon-antinucleon scattering at energies,  $E$  given by  $100 \text{ MeV} < E < 1 \text{ GeV}$  to be essentially elastic, but experimental evidence by Ekspong et.al. (60) and Cork et.al. (61) as well as phenomenological theory - see Koba (62) - show that at short range, the antinucleons attract the nucleons rather than repel them.

At the present time, there is no satisfactory theory for separation of matter and antimatter in the early stages of the big-bang e.g.  $t < 10^{-3}$  secs from creation and until a satisfactory mechanism is found, one must assume that the initial conditions were asymmetric. In order to satisfy the charge-symmetry law, one would then have to argue that there is an ensemble of metagalaxies, some are charge symmetric and characterized by  $10^8$  times more radiation than ours, while the observable metagalaxy developed out of one of the non-symmetric initial metagalaxies.

Another popular cosmological theory is the steady-state theory advocated by Hoyle (63) and Burbidge (64) in which it is assumed that creation of particle-antiparticle pairs is continuous. The Universe was more or less the same in previous epochs as it is now, and will be in the future epochs. The creation of particle-antiparticle pairs is a consequence of conservation of Baryon number, and Steigman (51) discusses the consequence of the expected creation rate,  $q$  given by

$$\frac{dn_{\pm}}{dt} = q - 3 H_0 n_{\pm} - \sigma v n_{+} n_{-}$$

rate of change  
of density  
within the  
galaxy

creation  
rate per  
unit ~~volume~~  
volume

effect of  
expansion of  
Universe  
on the  
density

loss rate of particles  
due to annihilation  
- if perfect mixing.

$\sigma$  = cross-section for annihilation

$H_0$  = Hubble constant

$n_{\pm}$  = densities of antimatter and matter

in relation to  $\gamma$ -ray astronomy.

He shows that for this steady-state model  $\frac{dn_{\pm}}{dt} = 0$  and if lifetime of Universe,  $t \gg$  Annihilation lifetime,  $\tau$  a steady-state sets in where the annihilation rate balances the creation rate, and, for the galaxy

$$q < 10^{-26} \text{ cm}^{-3} \text{ s}^{-1}$$

when the  $\gamma$ -ray flux limits are taken into account. If the antimatter had been created in our own galaxy, there should have been  $10^4$  more  $\gamma$ -radiation than has been observed. This problem could be solved if one assumed that antimatter is created in antimatter regions and matter in predominantly matter regions - but this would be equivalent to a new law in physics, i.e. non-local conservation of Baryon number.

Hoyle (65) has recently proposed another possibility. He assumes, that the pair-creation would take place in the galactic centre where matter is most dense and where the annihilation  $\gamma$ -radiation would be absorbed, Jelley (66) before it could escape.

This review of present cosmological theories indicates that the presence of significant amounts of antimatter within our own galaxy would be embarrassing for the 'big-bang' cosmologists, and would favour the steady-state model. It has been shown that the present gamma-ray astronomy results impose severe limitations on the presence of antimatter in the Universe, provided one assumes that the absorption of annihilation  $\gamma$ 's is negligible.

## CHAPTER 2. - THE DETECTOR

### 2.1. Description of Apparatus

The detectors used in the two balloon flights were almost identical, and had the following features.

A schematic diagram of the detector is shown in Fig.2. Two plastic scintillator disks (Nuclear Enterprises, type NE102A) were used to define the geometry of the telescope. The disks were ~~50~~50 cm in diameter and 0.32 cm in thickness. The upper disk was viewed by two photomultiplier tubes which were outside of the telescope's geometry. In order to secure uniform light collection, an integrating-sphere coated with a high reflectivity white paint was used. The lower disk was viewed by a single photomultiplier tube and the integrating-hemisphere gave a somewhat poorer resolution than the upper lightguide.

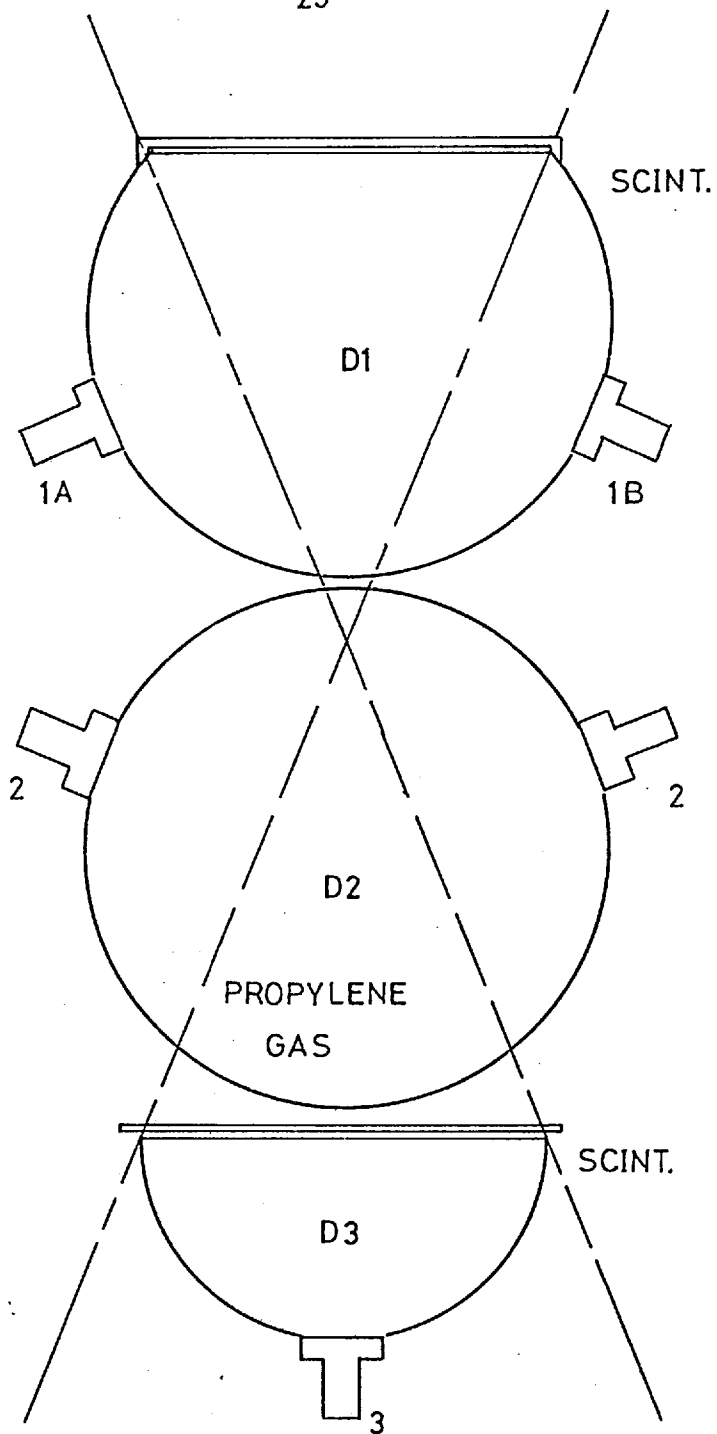
Only events which triggered all three p.m. tubes simultaneously were recorded, and hence, as the separation of the two scintillator disks was 140 cm, the geometrical factor of the telescope is given by

$$G = \frac{S_1 S_2}{l^2}$$
$$= 200 \text{ cm}^2 \text{ ster.}$$

$S_1$  = Area of top disk  
 $S_2$  = Area of bottom disk  
 $l$  = separation

(Heristchi (67))

The Cerenkov element was a spherical aluminium tank which contained



scale  
1 cm = 10 cm.

FIG. 2 SCHEMATIC DIAGRAM OF DETECTOR

propylene gas,  $C_3H_6$  at a pressure of 4.8 atmospheres (N.T.P.).

The walls of the tank were coated with the high reflectivity paint, and as the Cerenkov light was viewed by two p.m. tubes outside of the telescope geometry, the tank acted as its own integrating sphere.

The Cerenkov threshold rigidity for nuclei with  $A/Z = 2$  was set at 18.6 GV. The outputs from the two p.m. tubes were added together.

The detector also consisted of a Hall Probe Magnetometer which enabled the orientation of the telescope to be defined to better than  $\pm 3^\circ$  of arc. On the second detector, a sun sensor was also added in order to remove the  $180^\circ$  ambiguity associated with the Hall Probe output.

The complete detector was suspended at a zenith angle of  $50^\circ$  to the vertical, and some degree of temperature stabilization was achieved by using a partially blackened polystyrene-foam cover.

#### 2.1.1. Electronics

When a coincidence between the three scintillators occurred, the pulse heights of the outputs of the three scintillator elements and the Cerenkov element were each analysed by a 127 channel logarithmic pulse height analyser. If the Cerenkov pulse exceeded a predetermined value, a low gain amplifier was switched in circuit. The pulse height analyser (PHA) outputs were each stored in a seven-bit shift register

in coded form (due to the nature of the feedback elements of the shift-register) ready for read-out. The digitised outputs of these PHA's together with a flag (which indicated the gain in the Cerenkov channel) were telemetered to the ground station via a 136 Mhz frequency-modulation transmitter. A certain amount of noise immunity was built into the system by arranging for the 'zero' binary state to initiate a 4 millisecc pulse train and the 'one' binary state to initiate a 8 millisecc pulse train, that is, the (28+1) logic levels stored in the shift registers were sequentially transmitted as 29 pulse trains of differing widths.

The detector has an effective dead time of 0.50 seconds while the pulse height information of a coincidence event is transmitted. As will be seen later, this instrumental dead time is unimportant for flight II because of the low flux of the heavy ions in the cosmic radiation, but for flight I, it represents a 10% correction factor to the 'apparent' heavy nucleiflux values.

The block diagram of the electronic housekeeping circuits is shown in Fig. 3. During the whole of the flights, an Olland on board recorded the temperature and pressure of the detector. The pressure was also recorded by a Baroswitch as a safety measure. The on-off coding of the Olland and Baroswitch altered the frequency of a subcarrier

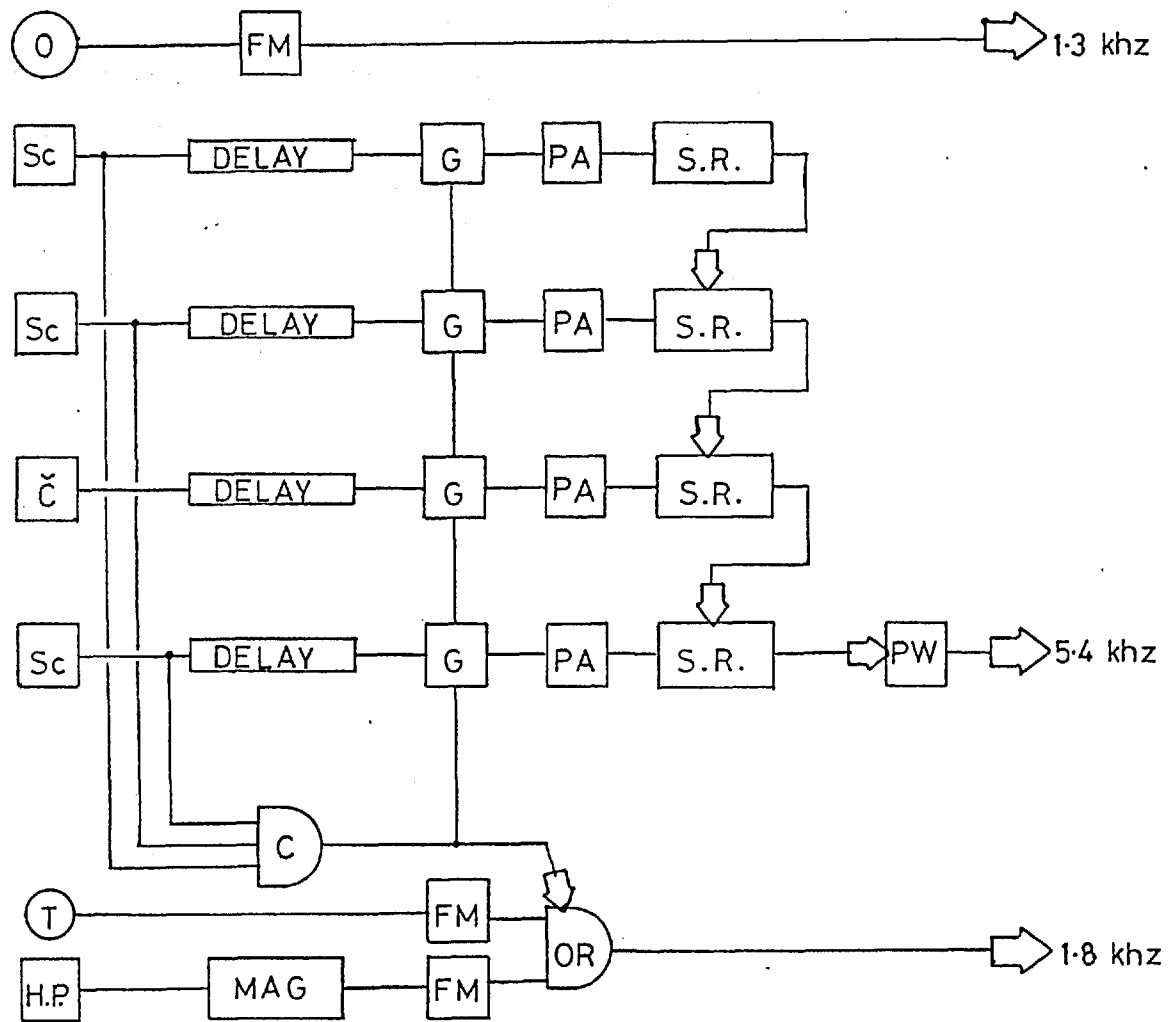


FIG. 3 BLOCK DIAGRAM OF DETECTOR ELECTRONICS



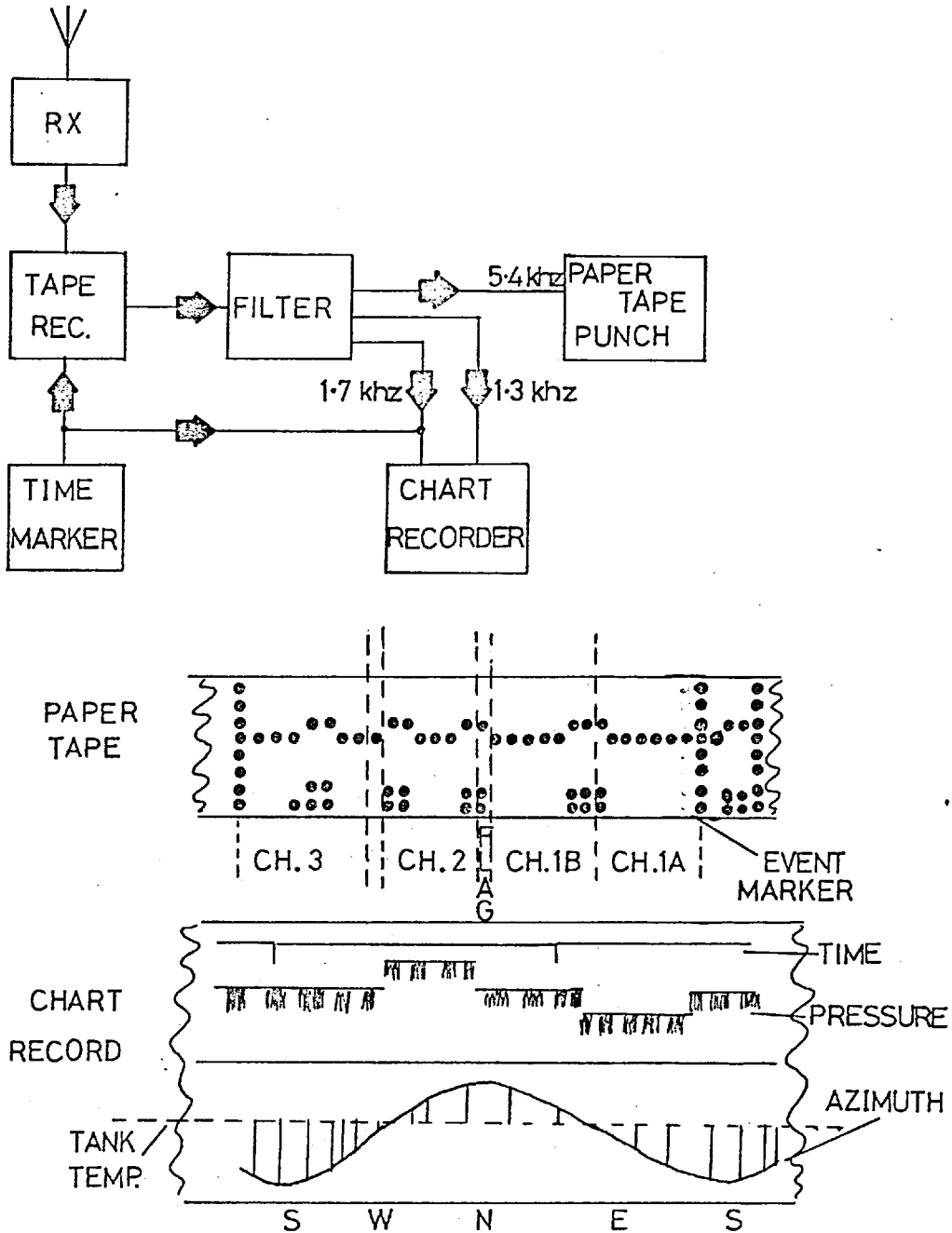


FIG. 4 SCHEMATIC DIAGRAM OF INFORMATION RETRIEVAL

oscillator in discrete steps. The output from the Magnetometer, in the form of a slowly varying subcarrier frequency, was continuously monitored, except during the 0.5 seconds when the PHA information was read-out. During this time, the frequency of this subcarrier was determined by a thermistor strapped to the Cerenkov tank. In this way, it was possible to monitor the temperature of the propylene gas, whenever an event occurred.

#### 2.1.2. Ground Equipment.

The telemetered barometer and magnetometer channels were recorded by a multipen recorder, together with 1 minute timing signals generated in the ground station. The telemetered PHA information was recorded on a FACIT high-speed paper tape punch, and every so often the event information on the paper tape was correlated with the orientational information on the chart record. As an extra safety measure, all the basic telemetered signals were recorded onto magnetic tapes in case extra analysis of the data was required at a later stage.

Fig. 4 illustrates how the information was recovered.

Automatic timing devices detached the detector from the balloon at dusk, and the detector returned to earth by parachute. The propylene gas was released from the tank at the instant that the detector was detached from the balloon. The first flight ended at 1821 E.A.T. ; however, the signal from the second detector was lost before cut-down.

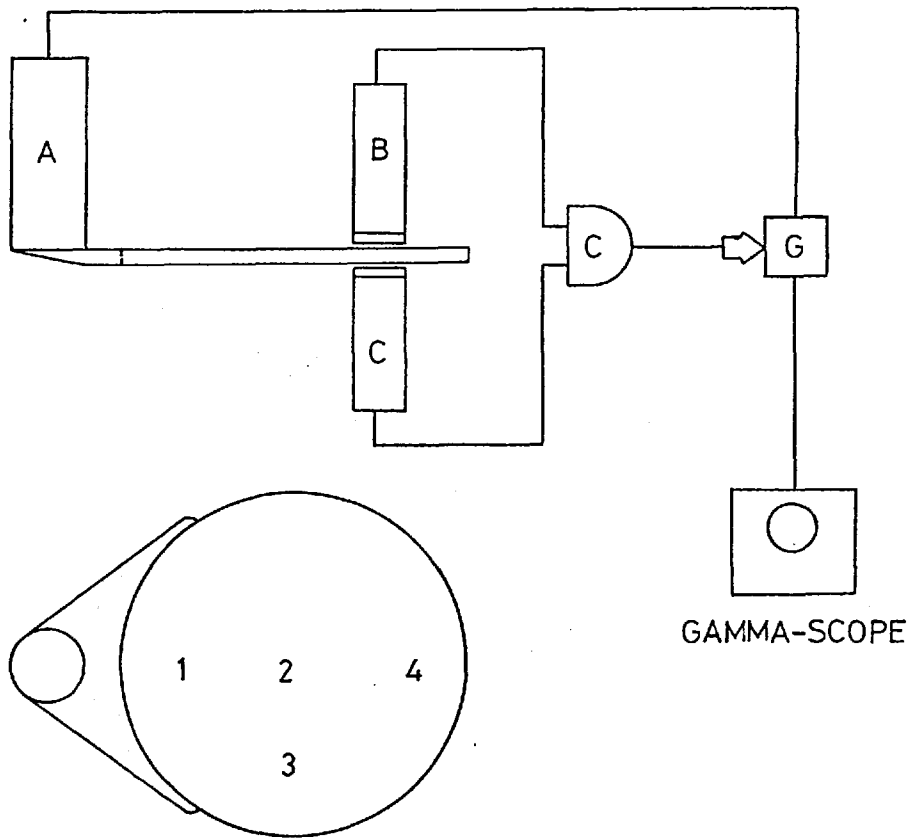


FIG. 5 LIGHT OUTPUT TEST OF SCINTILLATOR DISK

## 2.2. Scintillator Elements

### 2.2.1. Design Criteria and Calibration

A scintillator element is a fluorescent substance, i.e. a substance capable of emitting light when traversed by an ionizing particle.

From a consideration of the energy lost by a particle of charge  $Z$  it can be shown that, if the particle travels at relativistic speeds, the light output  $L$  from the scintillator

$$L \propto Z^2$$

This relationship holds for small  $Z$ , but for large  $Z$  see later.

The general aim of the experiment was to record as many heavy nuclei as possible and hence, as these nuclei represent about 1% of the total primary cosmic radiation, the collection area of the scintillator disks had to be as large as possible. It was hoped initially that a simple, direct optical coupling between the pm tube and the scintillator via a plastic lightguide would give adequate light collection from any part of the disk. However, the results of the simple experiment shown schematically in Fig. 5 indicated that this method was unsatisfactory.

A 1" scintillator disk was glued to the face of pm tube, B and another to C. These pm tubes were placed one above the other, but

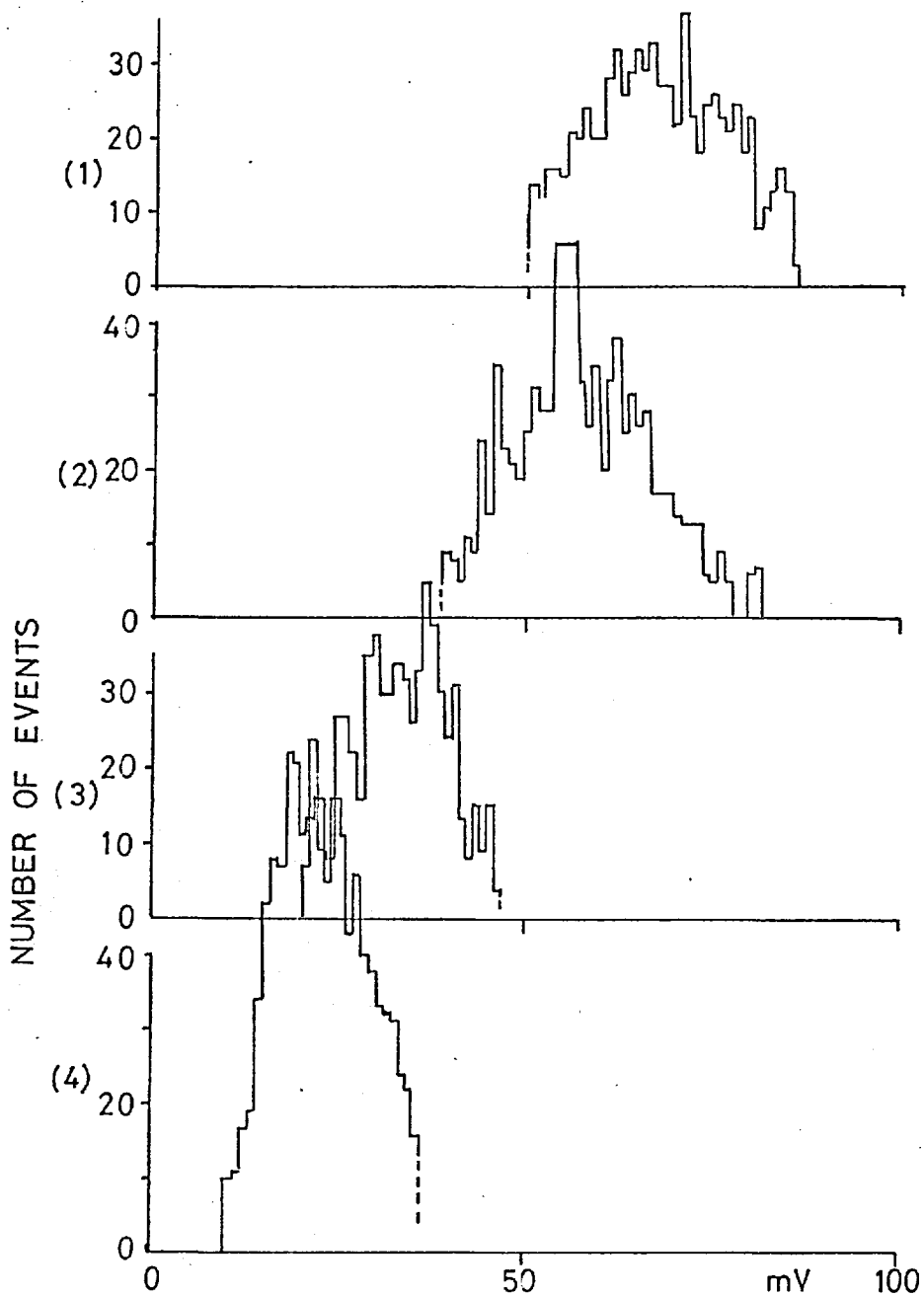


FIG. 6 COMPARISON OF PULSE HEIGHTS FROM SCINTILLATOR DISKS

slightly separated so that the 6" diameter scintillator disk - to which pm tube A was attached via the perspex lightguide - could be moved between them. Light collection was enhanced by using a 2" pm tube for A, and also by wrapping the large scintillator and light guide in silver foil. When B and C recorded a coincidence event, the pulse height was recorded by the  $\gamma$ -scope. The results are shown in Fig. 6. This shows the distribution of pulse heights for 4 different sets of events, i.e. it can be seen that the mean pulse height produced by mesons passing through the scintillator close to the pm tube is twice the size of the pulse from the same type of mesons which pass through the far side of the disk. Crabb (68) also reaches the same conclusions.

The second method adopted and eventually used was the integrating sphere principle of light collection. If the area of the sphere is large compared to the collecting area of the pm tubes, no matter at which point light is generated in the scintillator (so long as the photons leave the scintillator in the same way, and undergo numerous reflections from the walls) the light collection efficiency should be the same. The efficiency is determined by the coefficient of diffuse reflectance of the coating of the sphere (69). Most of the commercially available paints with a high reflectance use Titanium Oxide as a

pigment, but unfortunately this pigment exhibits an absorption of light below a wavelength,  $\lambda \approx 4000 \text{ \AA}$ . As a paint was also required for the Cerenkov tank, and as most of the Cerenkov light is transmitted with a wavelength

$$\lambda_c \approx 4000 \text{ \AA}$$

much time was spent experimenting with pigments and binders suggested by Dubbs (70). All samples prepared were tested on a Beckman Spectrophotometer and their coefficient of diffuse reflectance was compared with the accepted standard - freshly prepared powdered magnesium oxide - over a wavelength range

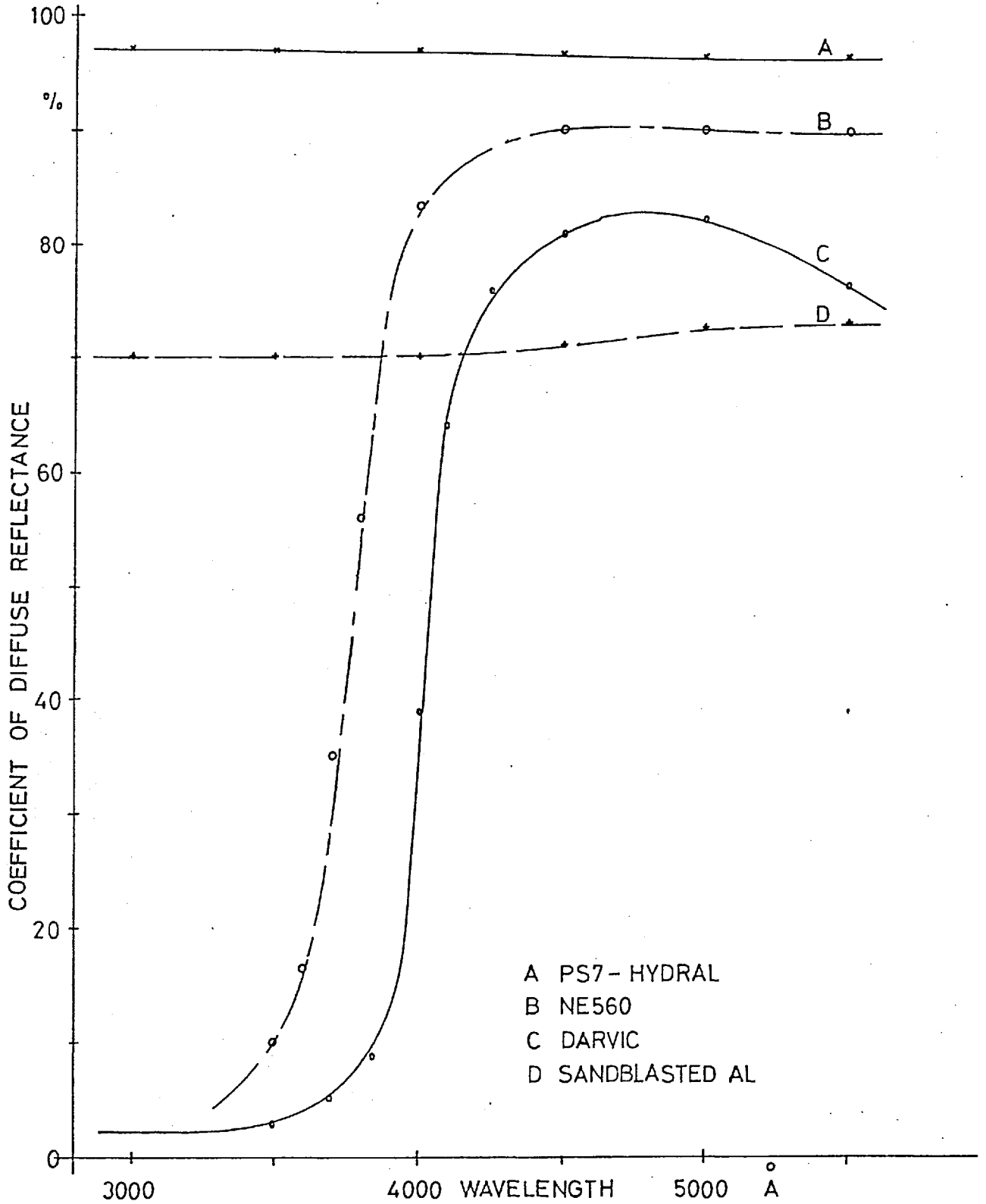
$$3000 < \lambda < 7000 \text{ \AA} .$$

In Fig. 7 the spectrographs of different surfaces are compared.

The best pigment and binder were found to be calcined aluminium hydroxide - Hydral 710 and potassium silicate (PS7) in distilled water. Fig. 8A shows an electron micrograph of the pigment particles and Fig. 8B shows the coefficient of diffuse reflectance of the paint. It can be seen that the coefficient

$$C \approx 96 (\pm 1) \%$$

over the entire range of interest.



A PS7-HYDRAL  
B NE560  
C DARVIC  
D SANDBLASTED AL

FIG. 7 SPECTROGRAPHS OF DIFFERENT SURFACES





BARIUM SULPHATE

FIG. 8A ELECTRON MICROGRAPH OF PIGMENTS 1.8 mm = 1 micron



ALUMINIUM HYDROXIDE

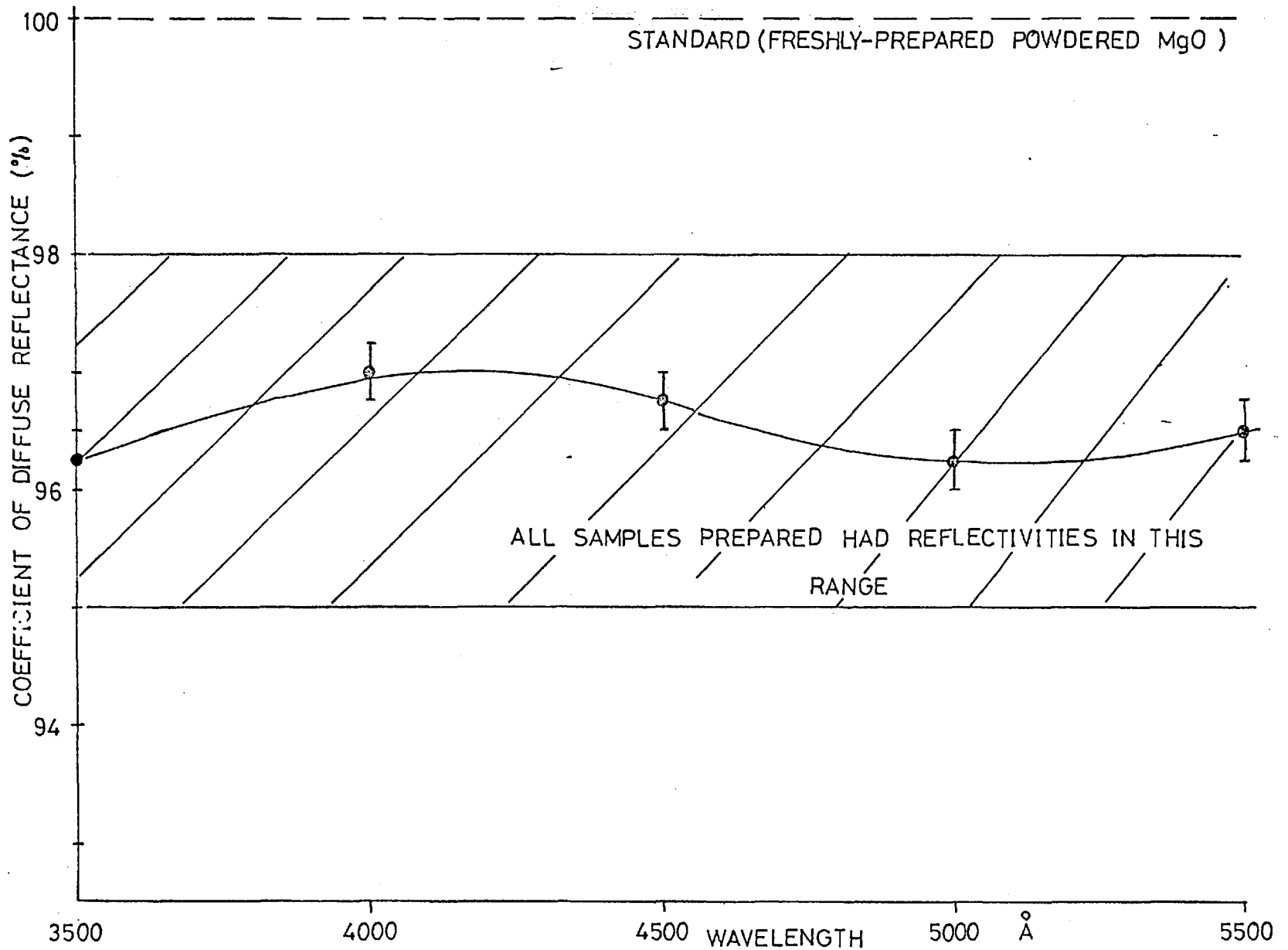


FIG. 8B DIFFUSE REFLECTANCE OF PS7-HYDRAL PAINT

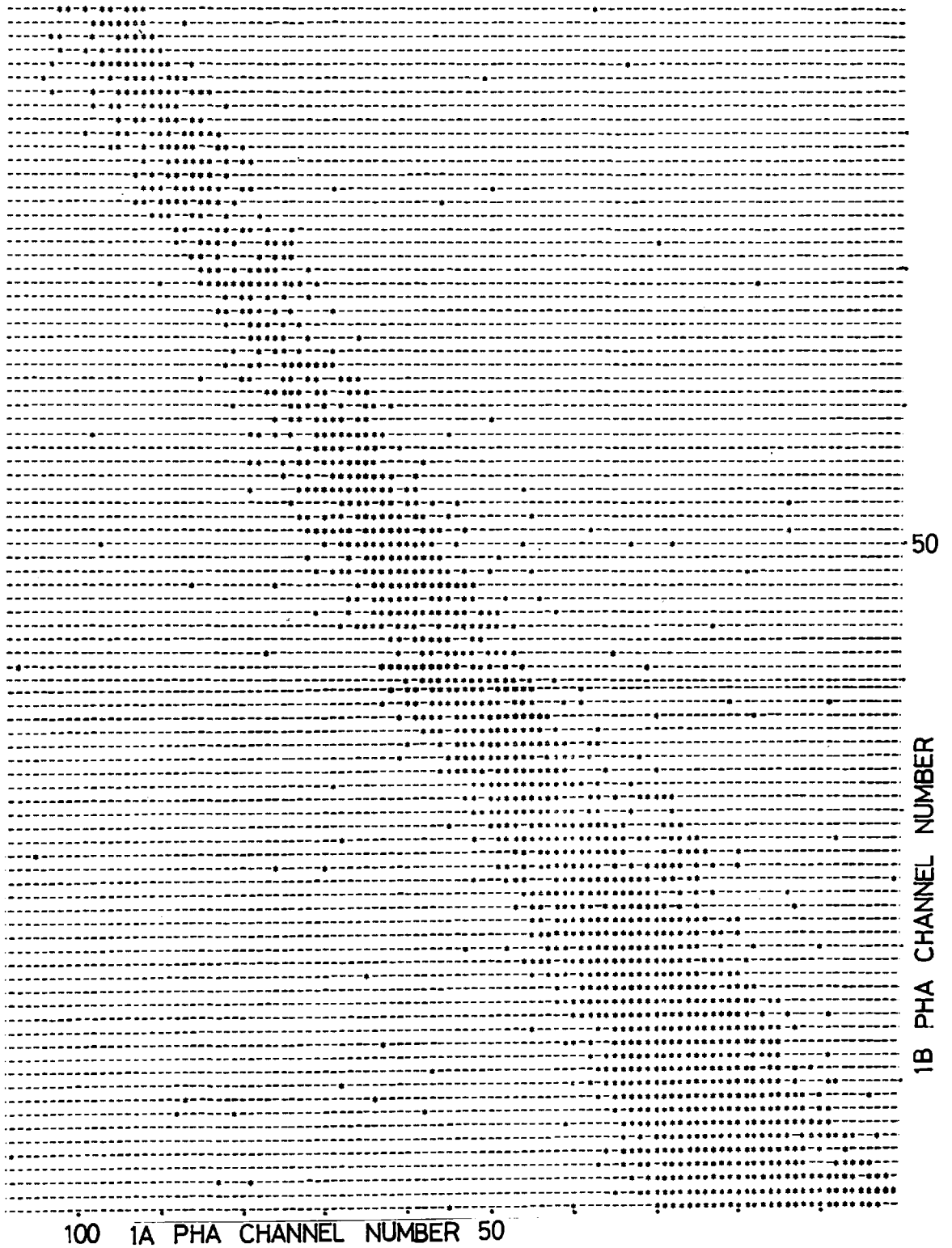


FIG 8C COMPUTER OUTPUT ILLUSTRATES UNIFORMITY OF LIGHT COLLECTION IN TOP SCINTILLATOR

### 2.2.2. Uniformity of Light Collection

Once the photons emerge from the scintillator disk, the only sources of nonuniformity of light collection are:

(a) direct impact of the photons on the pm tube photocathode as compared to photon collection after many reflections off of the spherical walls;

(b) irregularities in the tank coating which produce 'black spots' i.e. preferred directions of scatter.

The contribution of (b) to the non-uniformity is considered negligible because of the visual inspection of the coatings and the assumption that the net light collection is due to multiple reflections.

Although the effect of (a) is difficult to assess theoretically, the in-flight results indicate that the non-uniformity in the top scintillator is small. By comparing the outputs of channels 1A and 1B, the spread of events about the minimum ionizing line is small as shown in Fig. 8C and there are very few events for which the output in one of the top channels is significantly different to that in the other channel. Although the geometry of the bottom scintillator light guide is slightly different to the top light guide - and there is the added possibility of a charged particle passing through the bottom p.m. tube face (estimated 3% prob.) - the non-uniformity of light collection is not considered serious.

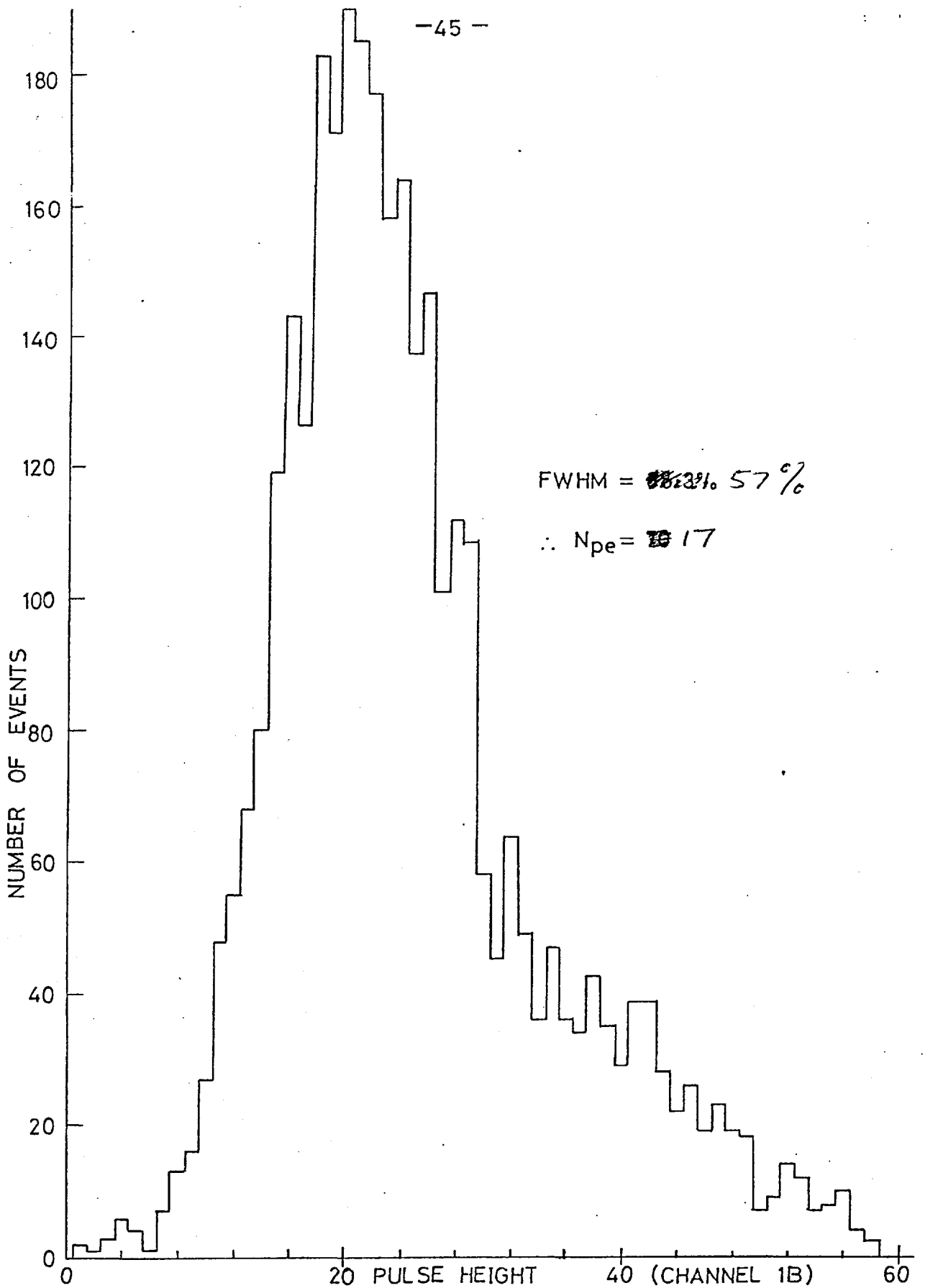


FIG. 8D PULSE HEIGHT DISTRIBUTION FOR SEA-LEVEL MESONS

### 2.2.3. Efficiency of Scintillator Elements

An estimate of the efficiency of the scintillator light collection system can be deduced from the sea-level  $\mu$ -meson calibration curves.

The mean number of photoelectrons produced at the pm tube photocathode is

$$\bar{N}_{pe} = c_p q_p \bar{N}_i \quad \text{where}$$

$c_p$  = mean photon collection efficiency

$q_p$  = mean quantum efficiency of pm tube

$\bar{N}_i$  = mean number of photons produced.

For the scintillator NE102A, the energy loss is  $\sim 1.8 \text{ MeV/grm.cm}^{-2}$  for a unit-charge, minimum ionizing particle (Crispen and Hayman - 1964 Proc. Phys. Soc. 83, p.1051). As one photon is released for approximately every 140 eV of ionisation energy deposited (Barnaby and Bartoh - 1961, Proc. Phys. Soc., 76, p.750), the total photon yield for both top and bottom scintillators is  $\sim 4250$  photons. The mean quantum efficiency of the photomultiplier tubes was 10% and so the number of photoelectrons expected is related to the light collection efficiency figure by

$$N_{pe} \sim 425 c_p$$

The light collection efficiency for the bottom scintillator

element was somewhat poorer than for the top scintillator. This was indicated by a lower mean number of photoelectrons produced by sea level  $\mu$ -mesons, and in the flight, by a poorer resolution of individual charge groups.

On a typical sea-level run with one of the detectors, the mean number of photoelectrons produced was  $\sim$  ~~40~~<sup>35</sup> p.e. for the top scintillator and ~~20~~<sup>20</sup> p.e. for the bottom scintillator. A  $\mu$ -meson sea level distribution is shown in Fig. 8D.

#### 2.2.4. Preflight Gain Setting

In order that the detector was not saturated by an excessive counting rate when at altitude, it was necessary to adjust the scintillator channel gains so that the minimum detectable charge was,  $Z = 3$ .

The gain setting procedure was as follows:

(i) The position of the meson peak was determined for each of the PHA outputs.

(ii) A pulsed photodiode was used as an artificial light source which gave a well defined peak in all PHA outputs. The dropper resistors to the pm tubes were varied, and their effect on the photodiode pulse height was recorded. See Fig. 9.

(iii) On the assumption that the light output from the lithium nuclei would be nine times greater than that for the  $\mu$ -meson, the

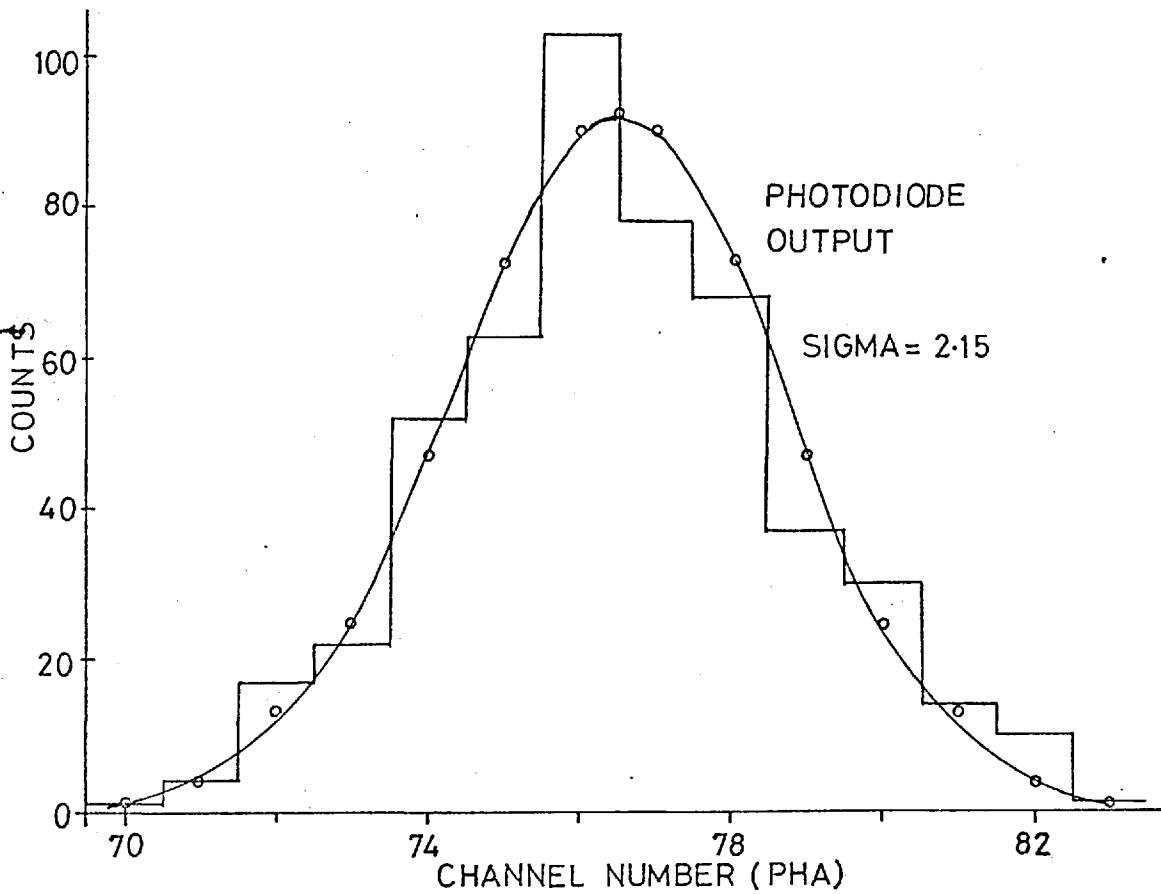
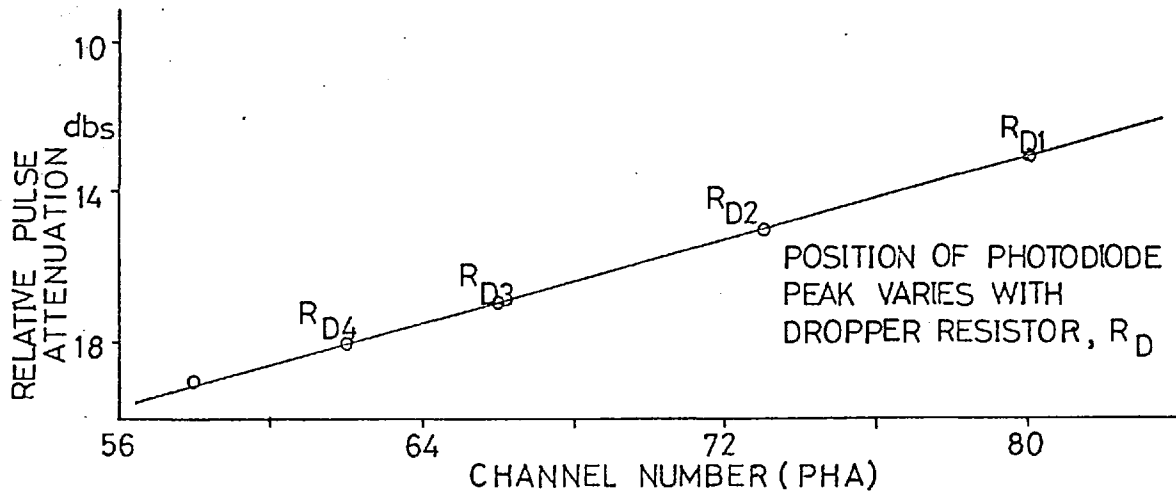


FIG. 9 PREFLIGHT CALIBRATION OF CERENKOV



appropriate dropper resistor required for reducing the gain by nine times was deduced from (ii).

(iv) Finally, a decision had to be made on the best position for the lithium group, i.e. the PHA channel number. One obvious criterion is that the iron group should be located at the highest channel numbers, say 120. According to the simple theory, the ratio of the light outputs, L, should be related by

$$\frac{L_{Fe}}{L_{Li}} = \left( \frac{Z_{Fe}}{Z_{Li}} \right)^2$$

but according to Webber (72) this relationship does not hold, and the ratio

$$\frac{L_{Fe}}{L_{Li}} \Big|_{\text{exp}}^t \approx 10$$

It was decided to follow this experimental value, and this meant that if lithium were located in PHA channel 20, then the iron group would be expected in PHA channels 115 → 120. It will be seen later that the results obtained differ with those of Webber.

### 2.3. Gas Cerenkov

#### 2.3.1. Design Criteria

When a very energetic charged particle passes through a material with a velocity,  $\beta$  which is greater than the velocity of light in that material, a characteristic radiation, called Cerenkov radiation, is emitted. The Russian theoreticians Frank and Tamm (73) developed the theory behind the radiation and they established that it was emitted in a well-defined cone about the trajectory of the incident particle. The half-opening angle of this cone,  $\theta$  is given by

$$\cos \theta = \frac{1}{\beta n}$$

$\beta$  = velocity of charged particle  
 $n$  = refractive index of material.

Hence there are physical limits to the particle velocities which can cause the emission of this light.

1) ...  $\frac{1}{n} < \beta < c$

The lower limit

2) ...  $\beta_T = 1/n$

is called the threshold velocity, and the corresponding kinetic energy of the incoming particle is called the threshold energy.

$$3) \dots E_T = A \left[ m_o \gamma_T c^2 - m_o c^2 \right]$$

A = atomic mass number

$m_o$  = mass of proton

$$\gamma_T = \frac{1}{\sqrt{1 - \beta_T^2}}$$

The physics of the experiment requires the Cerenkov threshold energy to be

$$E_T \approx 10 \text{ GeV/nucleon}$$

and so the refractive index of the Cerenkov medium has to be close to unity. Hence a gas Cerenkov must be used (instead of liquid or organic Cerenkov).

The main disadvantage of a gas device is the extremely low light yield (74). It was thought impractical to attempt to focus the light from a large gas device and so the integrating sphere technique of light collection was adopted instead. The maximum amount of light is emitted at a wavelength

$$\lambda_c \approx 4000 \text{ \AA}$$

and although the glass windows of the pm tubes absorb some of the light at these wavelengths, the calibration tests showed that adequate light collection was achieved without the need for quartz window tubes.

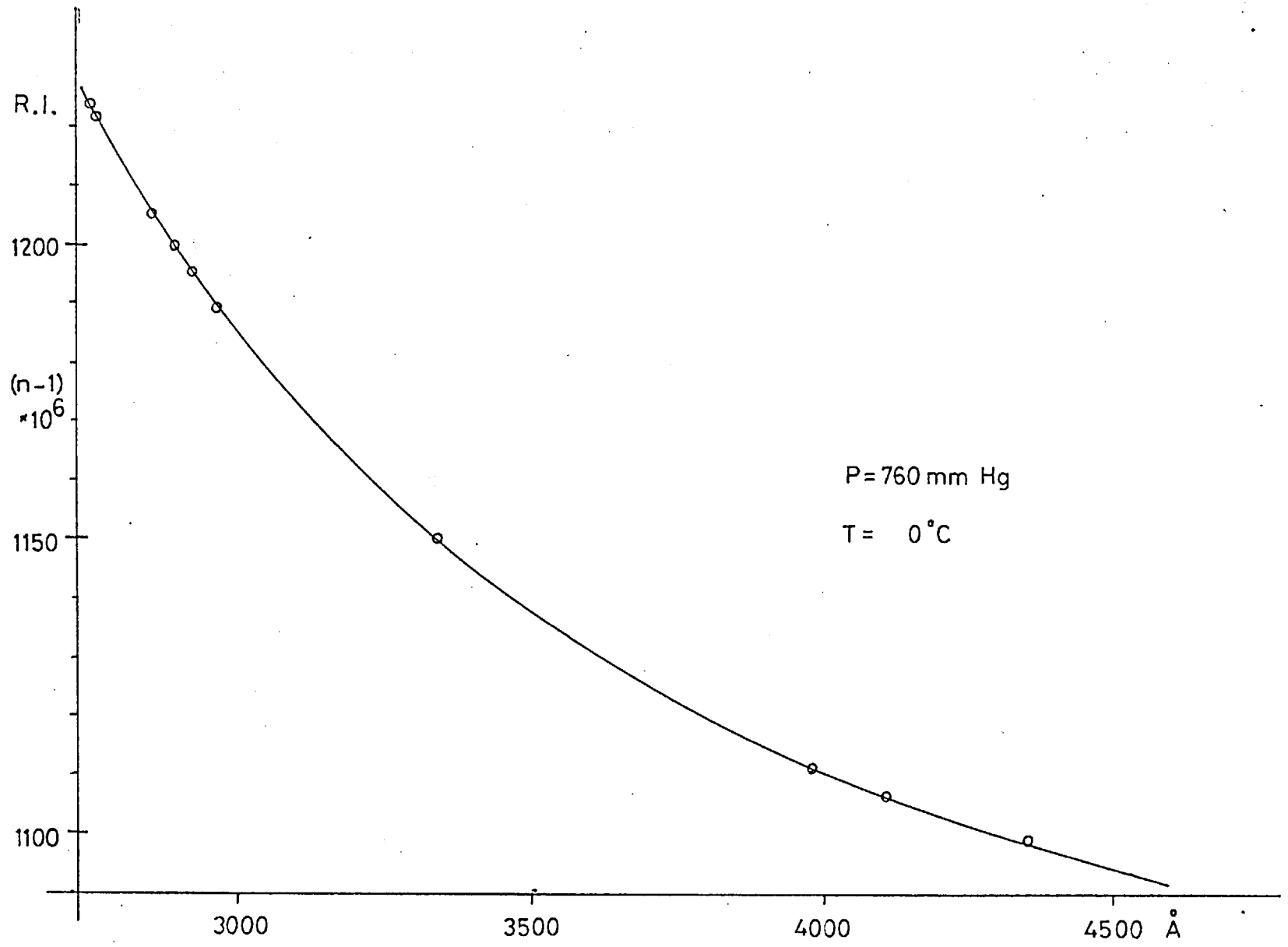


**FIG. 10** VARIATION OF REFRACTIVE INDEX WITH WAVELENGTH

One advantage of gas Cerenkov is the ability ~~to be able~~ to adjust the refractive index by altering the pressure, p:

$$4) \dots \quad \eta \propto P \quad \eta = (n-1)$$

The refractive index of propylene at N.T.P. given by Landort and Bernstein (at a wavelength of 4000 Å) is

$$n = 1.0011$$

i.e.  $\eta = 1.1 \times 10^{-3}$

The variation of refractive index with wavelength is shown in Fig.10.

The required refractive index for a threshold energy of 10 GeV/nucleon is

$$\eta_T = 5.3 \times 10^{-3}$$

Hence, from (4), the required gas pressure is 4.8 atmosphere for propylene.

In order to determine the pulse height expected from the Cerenkov the pm tube quantum efficiency,  $\delta(\lambda)$  must be known. The quantum efficiency is defined as the probability that a photoelectron will be produced by a photon of wavelength,  $\lambda$ . The photoelectron yield,  $Y_{pe}(\beta)$  is defined by

$$Y_{pe}(\beta) = \int_{\lambda} \delta(\lambda) \cdot \frac{dN(\beta)}{d\lambda} d\lambda$$

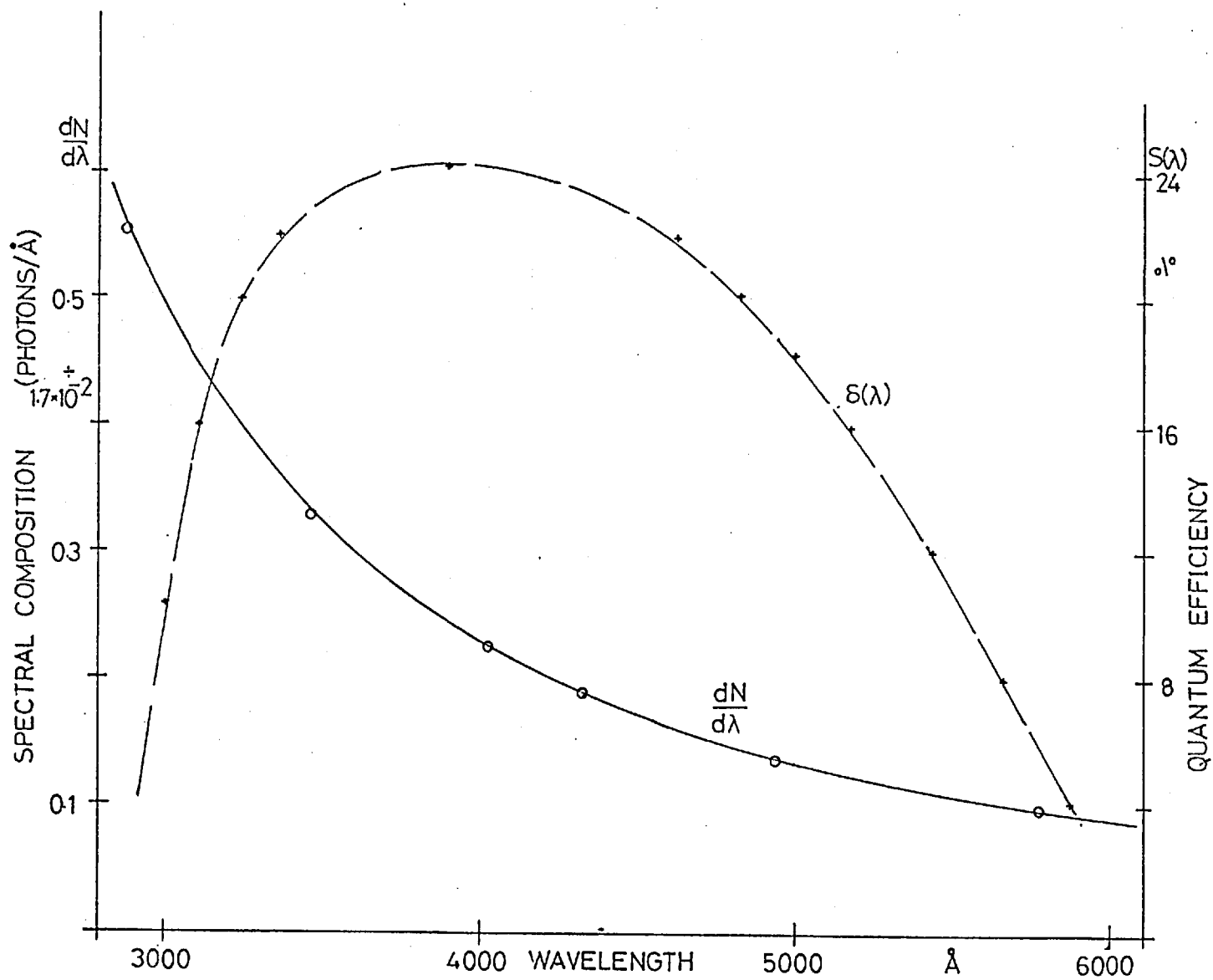


FIG. 11 VARIATION OF QUANTUM EFFICIENCY AND SPECTRAL COMPOSITION WITH WAVELENGTH.

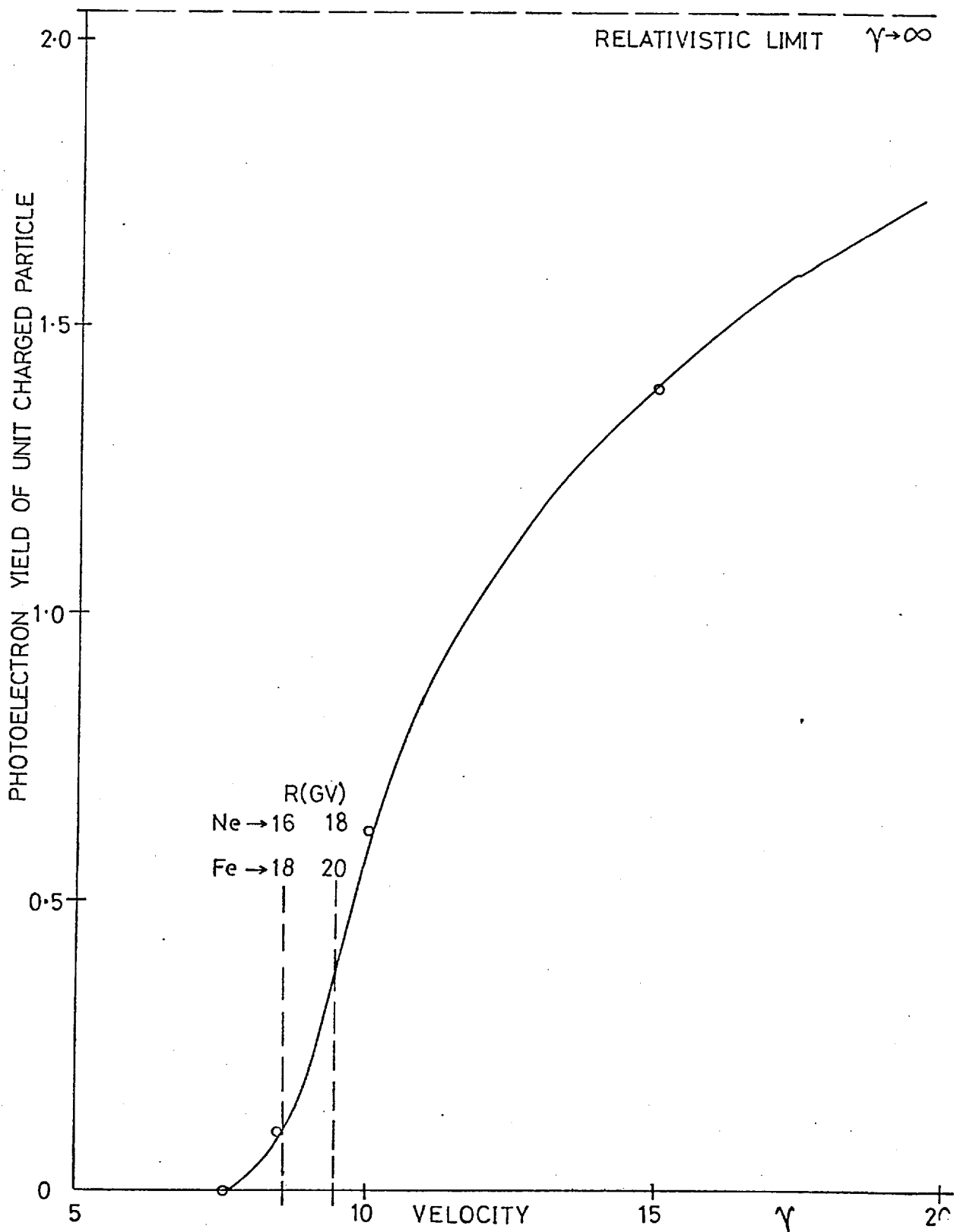


FIG. 12 CERENKOV PHOTOELECTRON YIELD AS A FUNCTION OF VELOCITY

The ratio ( $dN/d\lambda$ ) is the theoretical spectral composition of the Cerenkov radiation

$$\frac{dN}{d\lambda} = \frac{2\pi Z^2}{137} \left(1 - \frac{1}{\beta^2 n^2}\right) \cdot \frac{1}{\lambda^2} \cdot f(\beta) \text{ photon/\AA.cm path.}$$

where  $f(\beta)$  depends upon dispersion in the media.

In Fig. 11 the quantum efficiency and the spectral compositions for a particular velocity,  $\beta$  are shown.

The photoelectron yield (proportional to the pulse height) has been evaluated for a number of velocities,  $\beta$  and is shown plotted against  $\gamma = (1 - \beta^2)^{-\frac{1}{2}}$  in Fig. 12.

### 2.3.2. Preflight Calibration

The Cerenkov device was tested at sea-level by filling the tank with distilled water and monitoring the pulse height for sea-level  $\mu$ -mesons.

The relationship between the light output for the water-filled tank and the propylene gas-filled tank is shown below for different paint reflectivities, R

		$N_{pe}$		
		R=85%	R=90%	R=95%
<u>Water</u>				
$\beta \rightarrow 1$ muons		19	28	45
<u>Propylene</u>				
threshold <del>neon</del> <sup>carbon</sup> nuclei	6		8	13.5
28.5 GV	" "	30	40	67
$\beta \rightarrow 1$	" "	60	80	135



All these figures are based on the assumption of 10% photo-cathode efficiency. The water test indicated that the coefficient of diffuse reflectivity was indeed 95%. In Fig. 13, the Cerenkov output during the water test is shown. The fwhm (full width at half maximum) value was used to test the theoretical prediction of light output.

Denoting,

$$\text{fwhm} = \Delta v \quad (\text{in channel numbers})$$

and the position of the peak,  $v$ , the number of photoelectrons which produced the mean peak is given by

$$N_{pe} \sim \left( \frac{2.36}{\Delta v/v} \right)^2 = 33 \quad \text{for Fig.13.}$$

### 2.3.3. Efficiency of Cerenkov

In the determination of the upper limit to anti-nuclei, the gas Cerenkov device is used, in effect, as an anticoincidence counter - see Chapter 7.

It is necessary, therefore, to assess the probability that an ordinary nuclei with a rigidity,  $R_C$  - the geomagnetic threshold rigidity should not produce an output in the gas Cerenkov whose threshold,  $R_C$  is less than  $R_G$ . If such a relativistic nucleus did

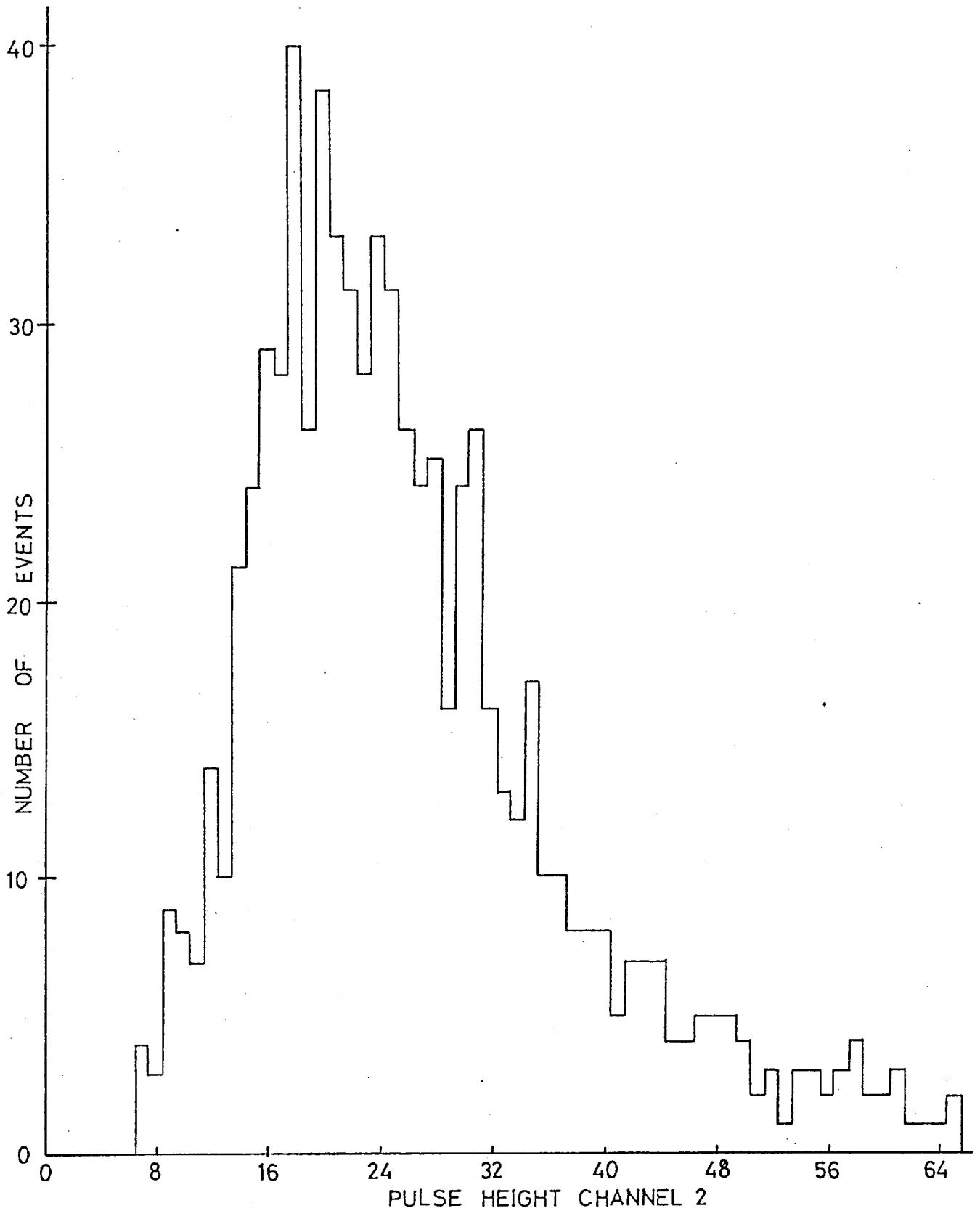


FIG. 13 MESON PULSE HEIGHT DISTRIBUTION

not produce an output, it would look like an antinucleus.

In Fig.49 it is clear that, if the search for antinuclei is restricted to the azimuthal range  $E (\pm 45^\circ)$  then, the minimum rigidity nucleus which could be detected is  $R \sim 19.5$  GV (corresponding to incoming zenith of  $30^\circ$ ). Referring to Fig. 12, if the incoming nucleus has a ratio  $A/Z \approx 2$  then the estimated number of photoelectrons produced by a 19.5 GV primary is

$$N_{pe} \Big|_Z \approx 0.4 Z^2$$

For an incoming lithium nucleus,  $Z = 3$ ,  $N_{pe} \sim 3.6$ . For gaussian statistics the standard deviation,  $\sigma = \sqrt{3.6} = 1.9$

Probability of not seeing 1 photoelectron is  $\approx 17.06\%$ .

This represents the worst possible case. It is clear that for the higher  $Z$  nuclei, this probability will be negligible, i.e. for the carbon nucleus, the probability of 1 photoelectron or less is  $\approx 0.04\%$ .

The effective geometrical factor for these low rigidity particles is much smaller than the total geometrical factor  $G_T$  of the telescope, i.e. typically  $\sim G_T/20$ . Hence the estimated efficiency of the detector in the discrimination of particles and antiparticles is estimated to be dependent upon the charge of the primary, being  $\sim 99.5\%$  for lithium nuclei and better than 99.99% for nuclei heavier than carbon.

#### 2.3.4. Scintillation Light in Gas Tank

When a charged particle traverses a gas, it may emit light due to ionisation or recombination processes. Although no explicit test of the magnitude of this spurious light in the Cerenkov tank was conducted before the flight it is possible to place an upper limit on the amount of unwanted light from the in-flight data. See section 3.2.6.

Jelley (Proc. Theor. Phys., Vol.IX, p.61) puts the limit to ionisation and recombination light in propane (for singly charged particles) as

$$\frac{dW}{dl} < 8 \times 10^{-3} \text{ eV/cm}$$

The 'spurious' light output for propane is negligible compared to the Cerenkov light output, and it is to be expected to be negligible for propylene too.

#### 2.4. Hall-Probe Magnetometer

##### 2.4.1. Description

The azimuthal orientation of the balloon payloads was continuously monitored by a magnetometer which utilised the Hall effect in semiconductor materials. Until recently the Hall effect magnetic field probe (H.E.P.) was unsuitable for measurements of magnetic field strengths of the same order as the Earth's field, i.e. 0.3 gauss,

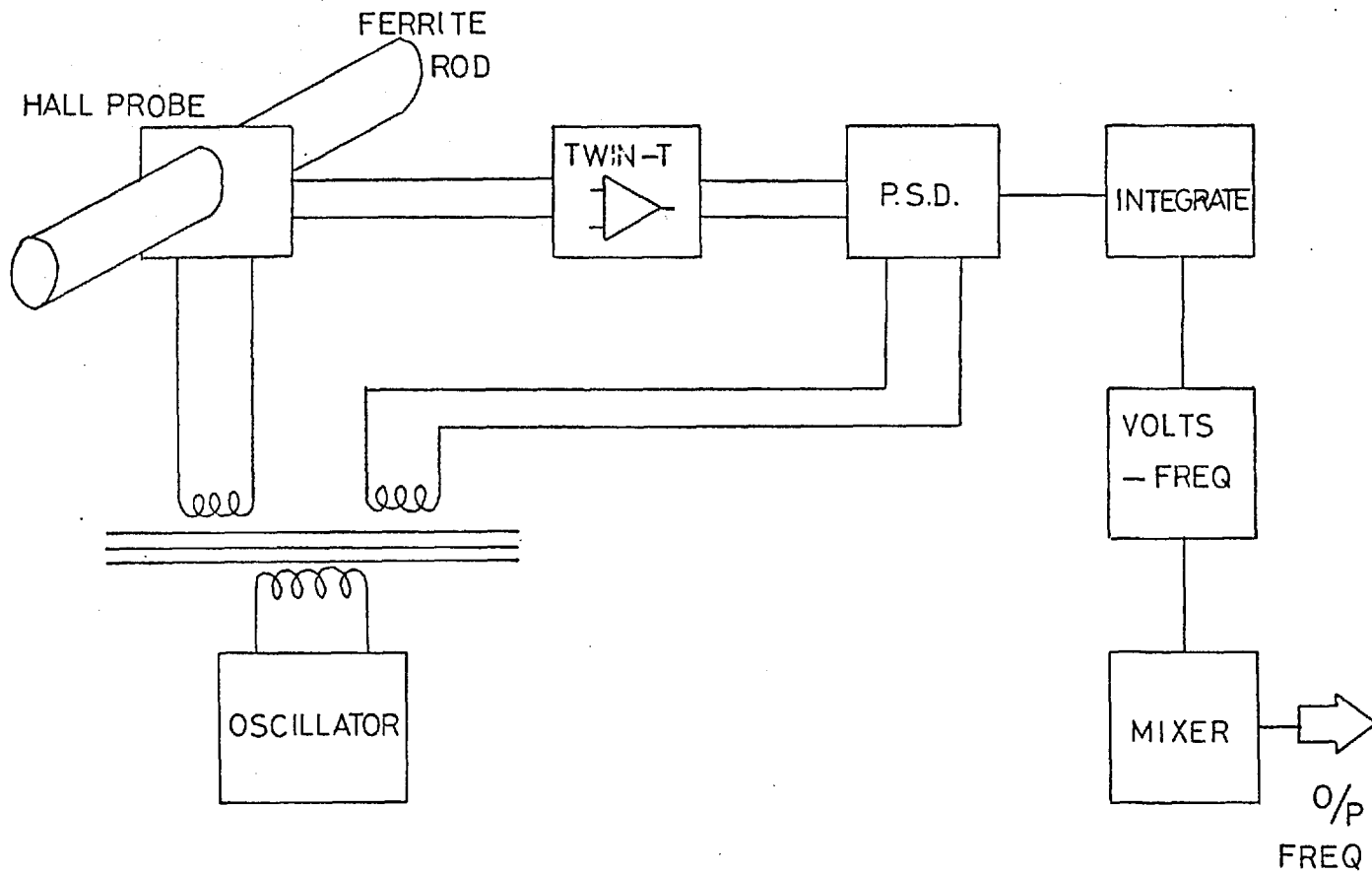


**FIG. 14** BLOCK DIAGRAM OF MAGNETOMETER

because of the poor sensitivity as compared to fluxgate-type magnetometers. The H.E.P. is still inferior for precision magnetometry, but in the balloon flights, an azimuthal sensitivity of  $\delta\theta < 3^\circ$  was achieved and this was more than adequate.

The magnetometer is shown in block form in Fig. 14.

The master oscillator is a multivibrator circuit which works at a frequency of  $f_o = 1500$  hz. The output of this circuit feeds into the primary of a transformer. One secondary winding of this transformer supplies the control current,  $i_{H.P.}$  for the Hall effect sensor, and the other secondary winding goes to the phase-sensitive detector.

The output from the H.E.P. is also a square wave of frequency,  $f_o$ , but the amplitude of this signal is proportional to the component of the magnetic field perpendicular to the 'face' of the H.E.P. The reason for this square-wave input to the H.E.P. is that it is easier to detect small variations in an a.c. signal than a d.c. signal, and the noise immunity is better.

The ferrite rods are placed perpendicular to the 'face' of the Hall Probe and their effect is to improve the signal to noise ratio of the system by a factor of 100. See Appendix A(1).

The detailed electronic circuitry is shown in Fig. 15.

The square wave output from the H.E.P. is selectively amplified by a TWIN-T feedback amplifier. This stage provides most of the noise

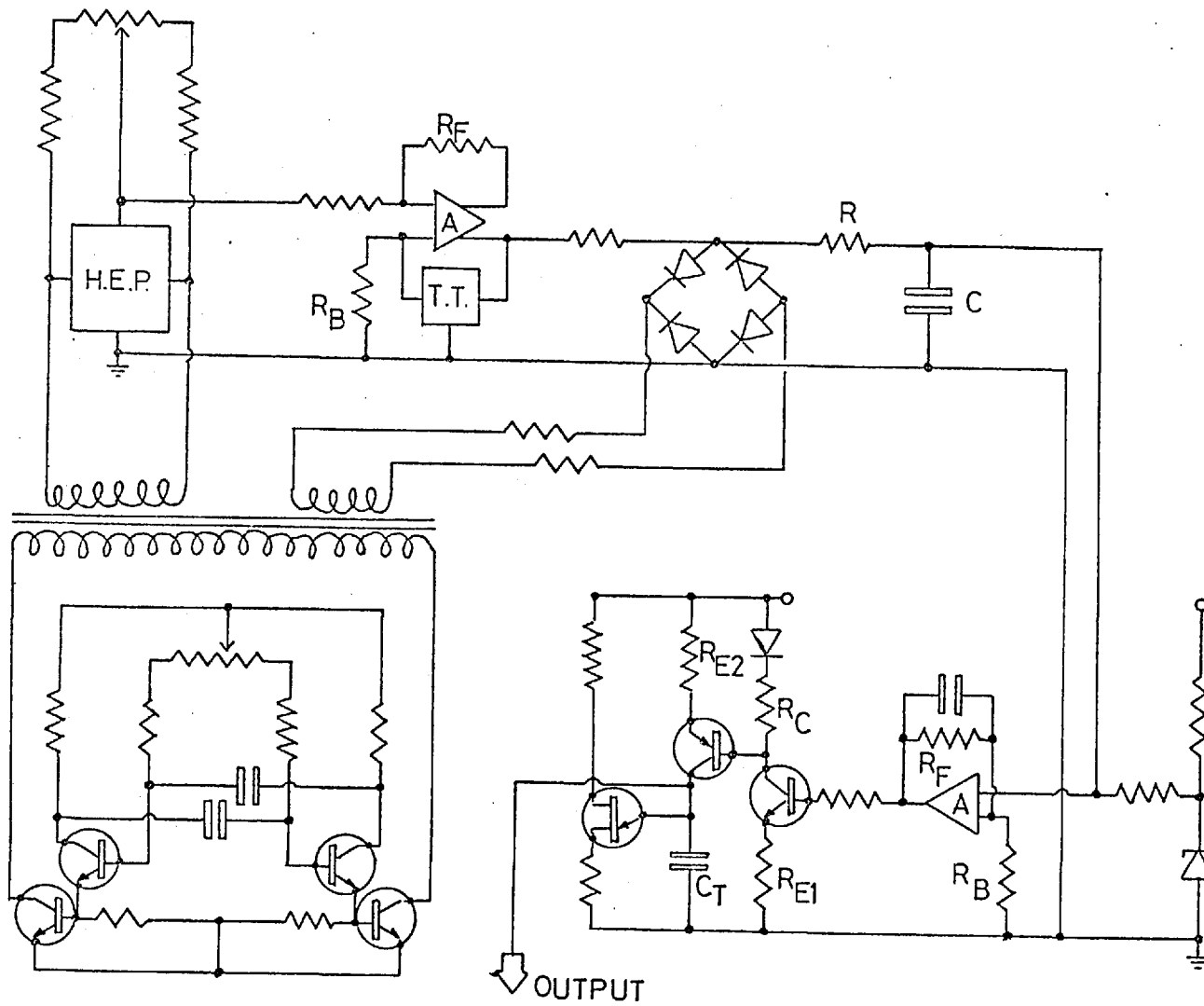


FIG. 15 MAGNETOMETER ELECTRONICS

immunity because the feedback components are chosen so that only a narrow band of frequencies,  $f_c \pm \Delta f$  are amplified. The circuit is adjusted until

$$f_c = f_o$$

After amplification, the signal goes into one side of a diode-bridge, the other side of which is fed by the secondary winding from the oscillator. This stage acts like a simple phase-sensitive detector. It only passes signals which are in-phase with the output square-wave from the oscillator. The phases are adjusted throughout the circuit so that the required Hall Probe signal is passed. Hence, this stage adds more noise immunity because it is a selective phase-filter whereas the TWIN-T cct. is a selective frequency filter.

The rectified signal is integrated by a simple RC network which effectively demodulates the H.E.P. signal. The output from the integrator is a mean d.c. level which varies in sympathy with the variation in the magnetic field strength perpendicular to the H.E.P.

The final circuit converts the d.c. level to a variable output frequency suitable for telemetering. The response of the overall cct. must ensure that the maximum change in magnetic field strength does not swing the output frequency outside the limits of the telemetry filters. The overall response of the magnetometer is discussed in Appendix A(ii) together with the detailed electronic ccts.



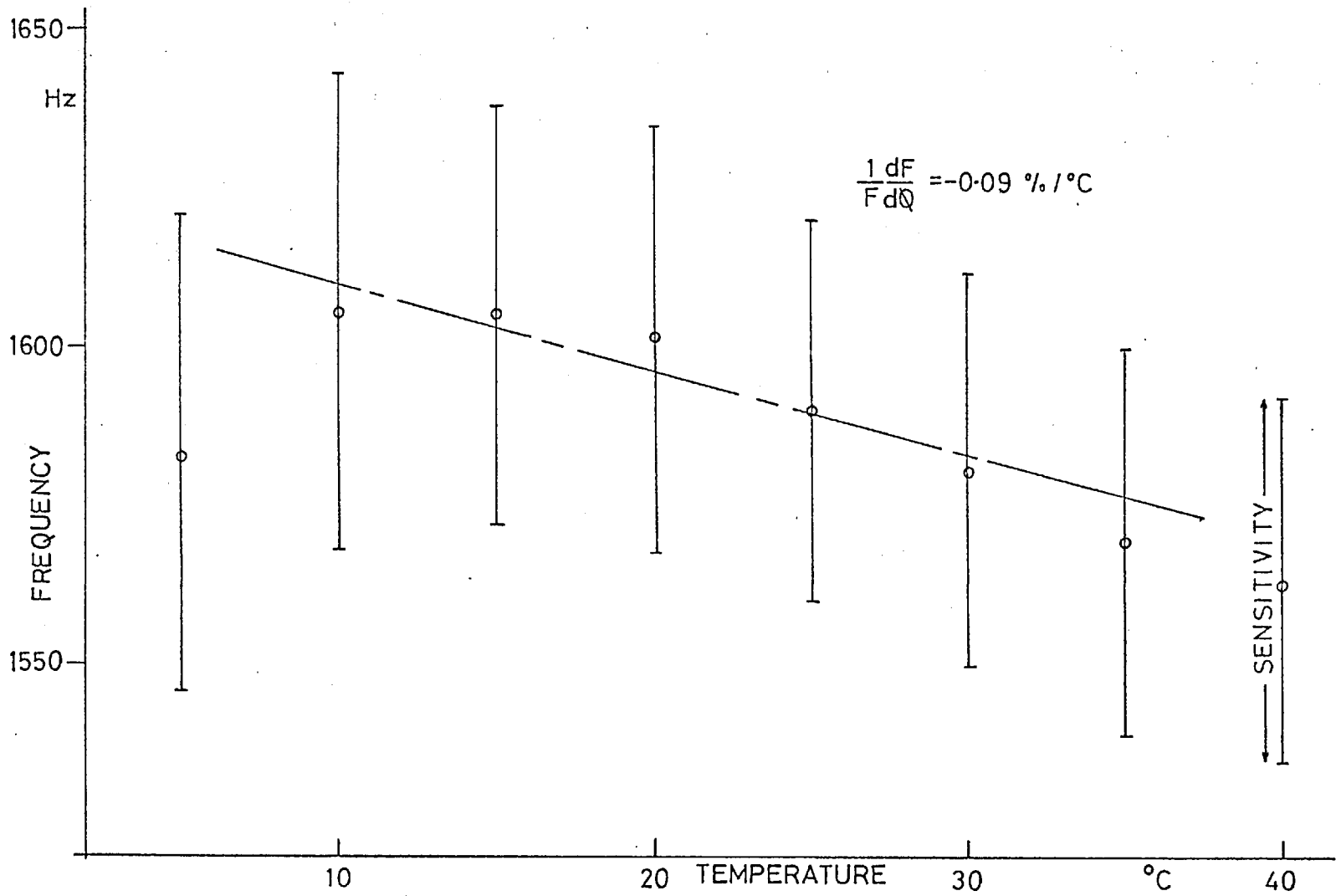


FIG. 16 TEMPERATURE STABILITY OF THE MAGNETOMETER

### 2.4.2. Calibration

The usefulness of the magnetometer for balloon flights depends upon its stability to variation in both line voltages and temperature, and its linearity of response, that is, how closely it follows the relationship

$$f_o = k_1 + k_2 \sin \theta_A \quad \theta_A = \text{azimuth angle}$$

The temperature coefficient of the whole cct is shown in Fig. 16. This was the best that could be achieved, and was adequate for the two balloon flights because the temperature of the detector was controlled to  $20(+10)^{\circ}\text{C}$ , and it can be seen that, in this region, the temperature coefficient of the centre frequency,  $f_c$  is

$$\frac{1}{f_c} \frac{\partial f_c}{\partial \theta} = - 0.09 \text{ \%}/^{\circ}\text{C}$$

The temperature effect manifested itself as a variation in the centre frequency,  $k_1$  and the sensitivity of the magnetometer denoted by the length of the bars in Fig. 16, remained essentially constant. This behaviour was verified during the actual flights.

Note that, due to the method of measurement of the azimuthal angles during flight, this temperature effect does not introduce any error to the determination of the azimuths. See section 2.4.4.

The line voltage coefficient was found, during testing, to be

$$\frac{1}{f_c} \frac{\partial f_c}{\partial V_L} = 1.0 \text{ \%/volt}$$

However, the variation in the line voltages from the stabilised low voltage power supplies would only be of the order of  $dV_L < 50$  mVolts. For this variation in voltage, the variation in the output frequency is

$$\frac{df_c}{f_c} = 0.05 \%$$

which is negligible.

Note also that this effect does not introduce any error to the determination of azimuths.

During testing of the circuits, the output frequency  $f_o$  was plotted against azimuthal angle,  $\theta_A$ , and the response is shown in Fig. 17. The output follows a sin law dependence very closely, the mean deviation at any point on the most sensitive part of the response is  $\pm 1$  hz which corresponds to an error of  $2^\circ$  of arc in the determination of azimuth.

During preflight tests, it was established that the maxima and minima of the responses did correspond to magnetic North and South, as given by a compass. Hirstmonceaux have no record of any magnetic anomalies at Kampala, and so it was assumed that the orientation given by the magnetometer at altitude would be the correct one.

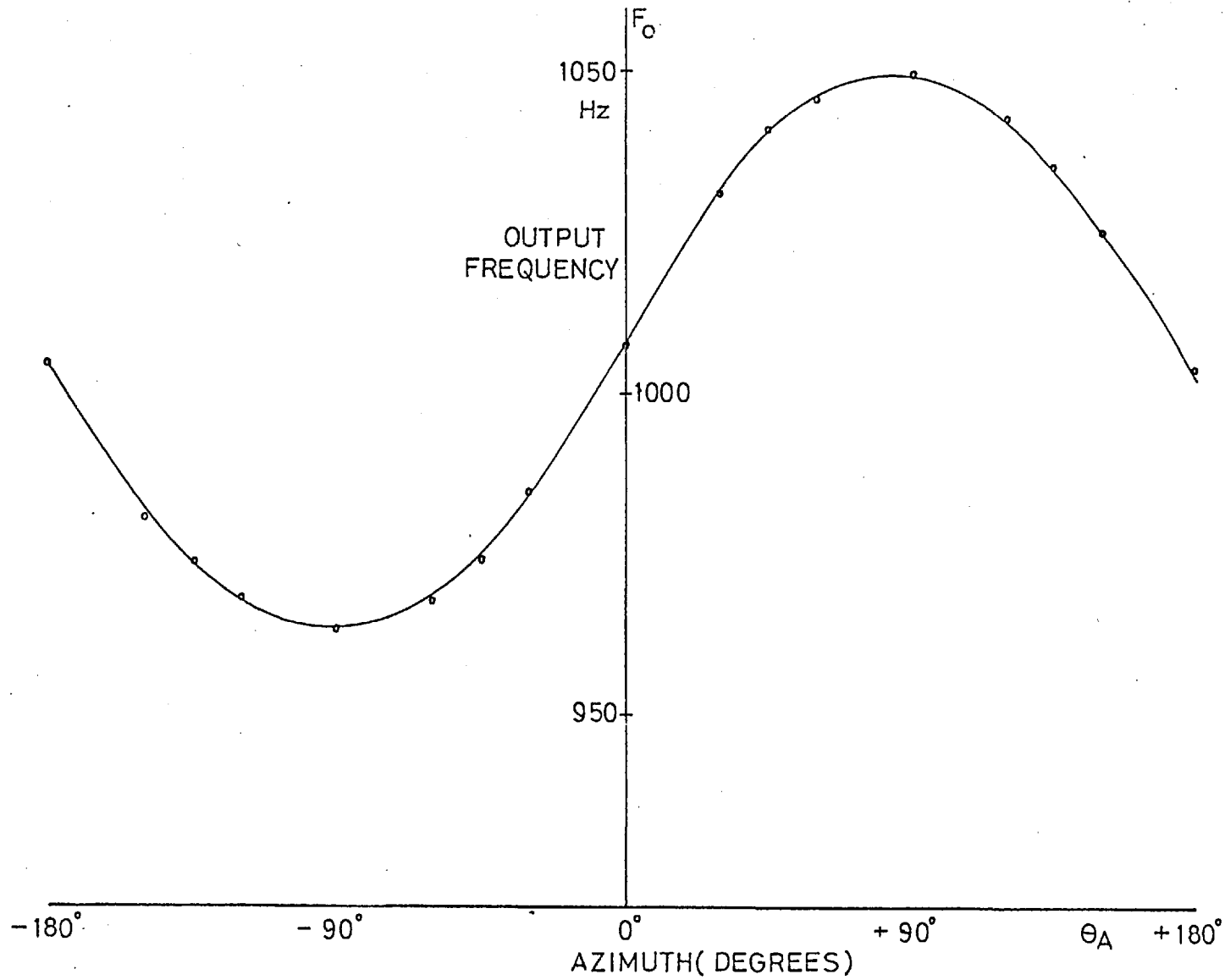


FIG. 17 MAGNETOMETER AZIMUTHAL RESPONSE.

The only other source of angular error, besides any intrinsic non-linearity of the response, would be due to nutation, that is, a swinging of the detector in a vertical plane. Inspection of the magnetometer output for the duration of the flight fails to reveal a large angular swing, because of the near-constancy of the frequency separation of the maxima and minima.

$$\text{If } \frac{\Delta f_o}{f_o} < 5\%$$

$$\text{then, } \Delta \theta_z < \pm 10^\circ \text{ of arc} \quad \theta_z \text{ is zenith angle}$$

With this criterion, it is possible to deduce a maximum possible angular error due to nutation. If  $\theta_N$  is the nutation angle, and  $\theta_A$  is the azimuthal angle, the error in estimating the azimuth is

$$\epsilon_\theta = \cos^{-1} \left| \cos \theta_N \cos \theta_A \right| - \theta_A$$

This function is plotted in Fig. 18. The interesting feature is that there is no error in the determination of due East and due West, because for these orientations,  $\cos \theta_A \equiv 0$

#### 2.4.3. Limitations

The one obvious limitation of the Hall Effect sensor is that its output is ambiguous.

The output frequency,  $f_{OUT}$  is related to the azimuthal

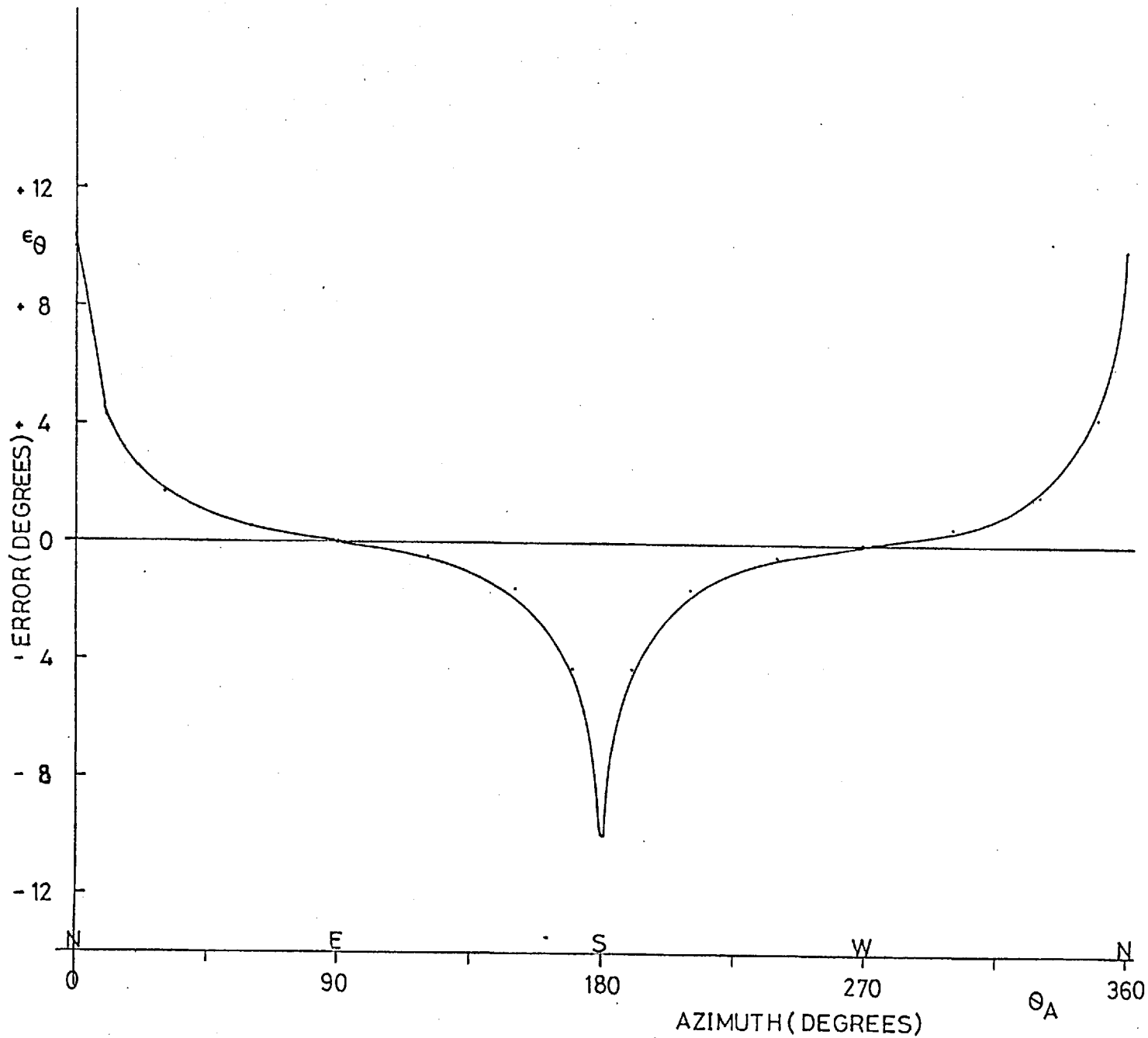


FIG 18 POSITIONING ERROR FOR TILT OF 10°

orientation,  $\theta_A$  by

$$f_{OUT} = k_1 \sin \theta_A + k_2$$

but,

$$\sin \theta_A \equiv \sin (\pi - \theta_A)$$

for  $0 < \theta_A < \pi/2$ ,

and there will be the same frequency output for the different absolute orientations.

The ambiguity can be eliminated either

(a) by a sun sensor - as in flight II

or (b) by the use of another H.E.P. sensor which is placed perpendicular to the first.

The advantage of employing the second H.E.P. sensor is twofold. Firstly, it does not depend upon the sun being within the field of view of the sunsensor and secondly, the sensitivity, or orientational accuracy of the combination is independent of the orientation whereas for a single H.E.P. magnetometer the orientational accuracy,

$\frac{\partial f_{OUT}}{\partial \theta_A}$  varies a great deal over the complete range of azimuths:

$$\frac{\partial f_{OUT}}{\partial \theta_A} \approx \pm 1.0 \text{ degree/hz} \quad \text{for } \theta_A \approx 0^\circ \text{ and } \theta_A \approx 180^\circ$$
$$\frac{\partial f_{OUT}}{\partial \theta_A} \approx \pm 10.0 \text{ degree/hz} \quad \text{for } \theta_A \approx 90^\circ \text{ and } \theta_A \approx 270^\circ$$

In the first flight, the inherent ambiguity in the azimuthal orientation was resolved by sampling the high counting rates over long, uninterrupted records. The East-West assymetry results in a difference of counting rates,  $\frac{R_W}{R_E} \approx 2 / 1$  and hence, if the

East-West crossovers are slow, the statistics on the counting rates are good enough to indicate the correct orientation.

#### 2.4.4. Determination of Azimuth

In order to determine the upper limit to the flux of antinuclei in the cosmic radiation, it is necessary to study the events within azimuthal intervals - say  $\pm 11^\circ$  intervals (See Chapter 7).

The method adapted to determine these intervals was to

(a) Scan over several cross-overs, and determine the maximum frequency,  $f_{\max}$  and the minimum frequency,  $f_{\min}$ .

(b) Define the zero degree crossover (due East) and the  $180^\circ$  crossover (due West) by

$$\frac{(f_{\max} - f_{\min})}{2}$$

(c) Define the  $45^\circ$  points from the crossovers as

$$\frac{(f_{\max} - f_{\min})}{2} \sin 45^\circ$$

i.e. assume the response to follow a perfect sin law.



(d) Similarly, to define the  $\theta_A$  points as

$$\frac{(f_{\max} - f_{\min})}{2} \sin \theta_A$$

This technique can only be adapted when the detector is free to rotate, and rotates with a period of the order of a few minutes.

### 2.5. Pulse Height Analysers

The pulse height analysers (PHA) consisted of an intrinsically high-Q choke which was damped down to a stable  $Q = 30$  and followed by a discriminator. A coincidence pulse opened the f.e.t. gates to the PHA's and the phototube pulse from the delay line was amplified and excited the choke. The choke and parallel capacitance formed a resonant circuit whose natural frequency was  $\sim 30$  khz. When the choke was excited, the circuit produced a wavetrain whose frequency was 30 khz and whose amplitude decayed exponentially. The rate of decay was determined by the circuit Q value. The number of oscillations whose amplitude exceeded a preset discriminator level were clipped and 'counted' by a shift register.

The number of pulses fed into the shift register depended on the size of the exciting-pulse and the Q-factor, according to the relationship

$$N_p = \frac{Q}{\pi} \log_e V_i/V$$

Any possible input to the PHA during counting and telemetry was inhibited. After all the pulses for an event had been counted, the states of the shift register were clocked out at a frequency of 60 hz. As there were (28+1) bits of information to be clocked out, the effective deadtime of the detector was 0.48 secs. The relevance of this deadtime is discussed in Section 3.2.5.

#### Calibration and Stability

All tests on the PHA's were conducted with a high-level Hewlett-Packard pulse generator and a quality Marconi attenuator which attenuated the output pulse in decibel steps. This provided a convenient method of calibration because the attenuation was proportional to the logarithm of the voltage and also the number of pulses outputted from the PHA was proportional to the logarithm of the voltage. Hence, if the PHA electronics were distortion-free, the plot of output to attenuation (dbs) should be linear.

The PHA's were extensively tested for both linearity and stability against line voltage variation and temperature. A graph which is representative of the temperature stability achieved is shown in Fig. 19.

As an extra check, in-flight calibration was employed to monitor the stability of the PHA's. This is discussed in the following chapter.

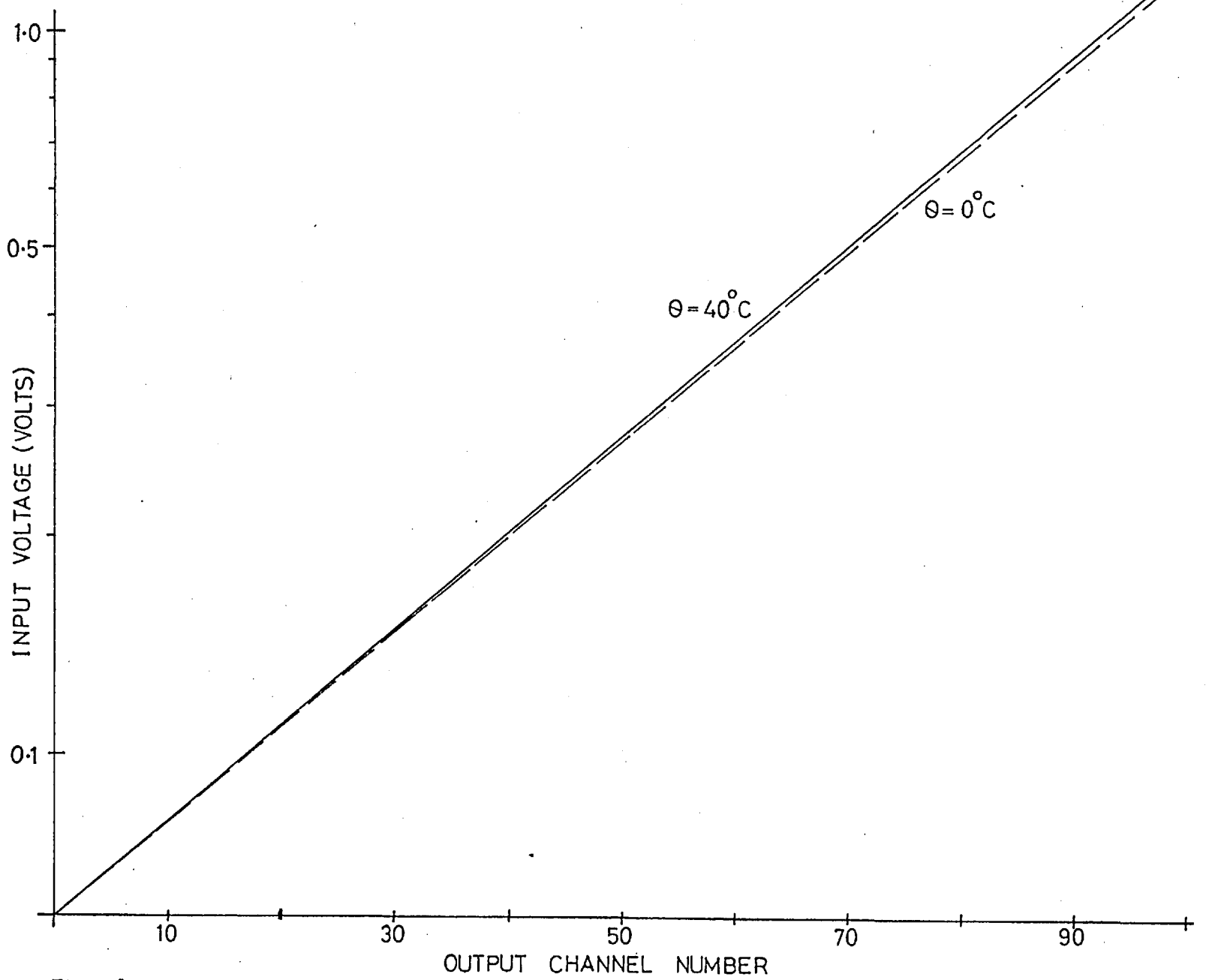


FIG.19 TEMPERATURE STABILITY OF PHA CIRCUITS

## CHAPTER 3. - BALLOON FLIGHTS AND DATA ANALYSIS

### 3.1. Balloon Flights

The first flight took place on May 13th, 1970 at Kampala. The balloon reached a float altitude of 5 millibars, i.e.  $5.5 \text{ gm.cm}^{-2}$  residual atmosphere and its altitude remained essentially constant ( $\pm 0.5 \text{ gm.cm}^{-2}$ ) until cut-down at 1820 E.A.T.

The second flight took place on June 1st, 1970 at Kampala and reached the same altitude as for flight I. However, the altitude slowly changed during the course of the flight, as shown in Fig. 20B. As a result, when the data for both flights are combined, only the first 4 hours data for Flight II has been considered. The signal from this flight was lost at 1900 E.A.T. before cut-down.

The balloons used were 450,000 cu.ft. WINZEN balloons. The residual pressure was monitored by an Olland and also a baroswitch device, and the readings of both instruments agreed to within  $0.5 \text{ gm.cm}^{-2}$ .

The temperature profile during both flights is shown in Fig. 20A. Temperature stability was achieved by partially blackening the polystyrene foam covering of the detector. This box had 75% blackening on the sides and 100% top and bottom. It is clear that the temperature of the complete detector was extremely stable until after sunset, when there was no heat transfer into the box. The thermistor monitoring the

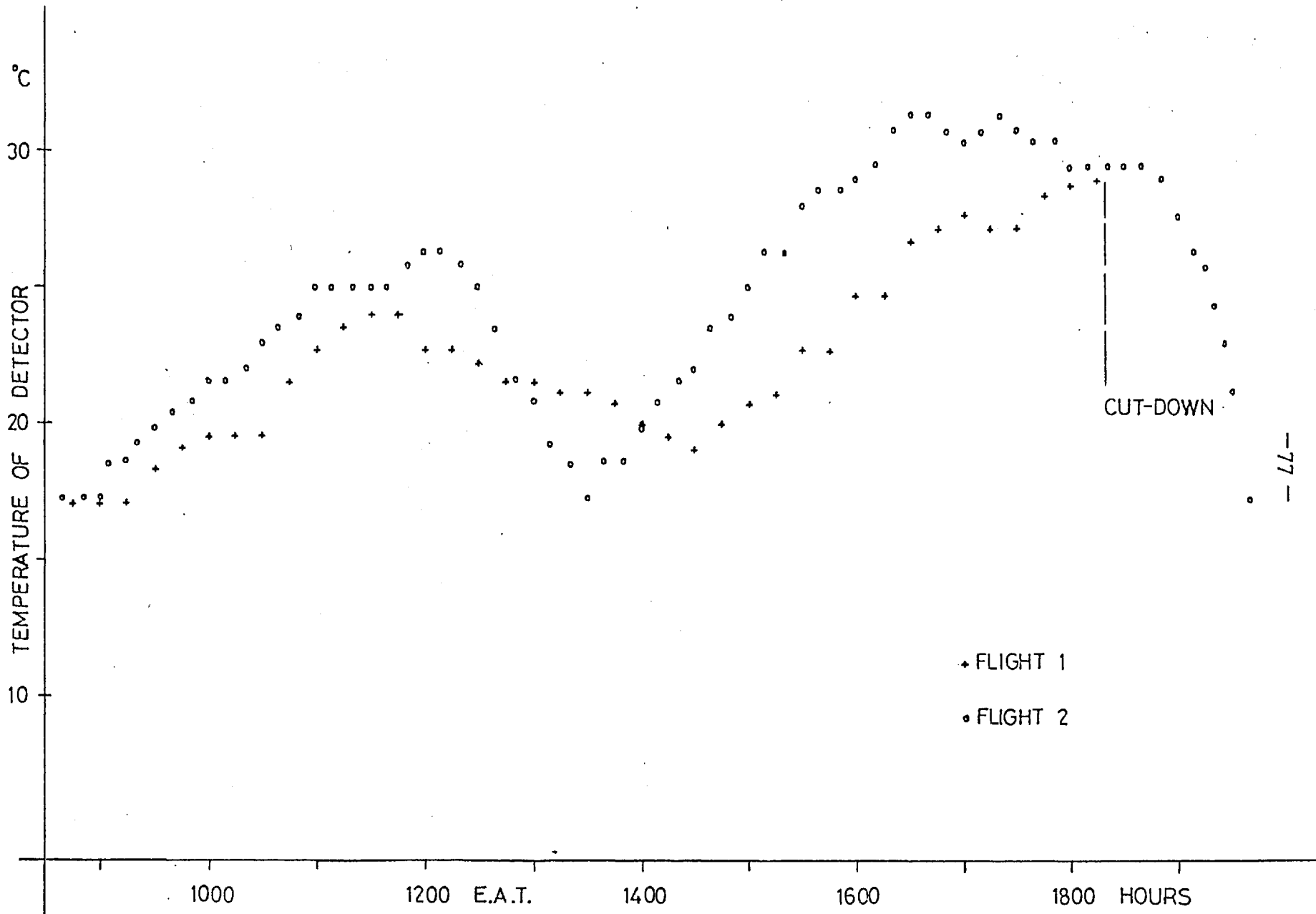


FIG. 20A TEMPERATURE-TIME PROFILE FOR BOTH FLIGHTS

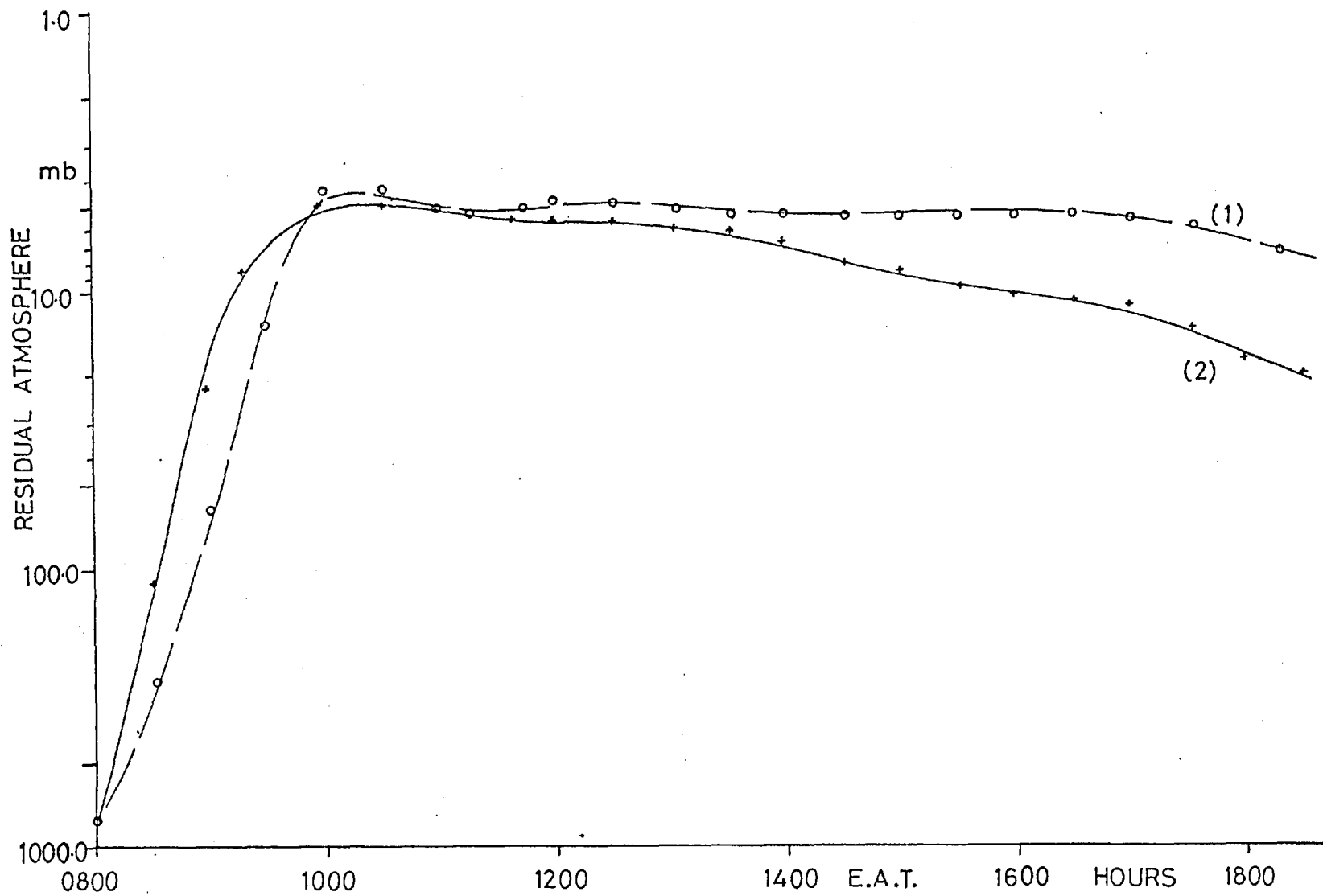


FIG. 20 B ALTITUDE-TIME PROFILE FOR BOTH FLIGHTS

temperature of the gas tank, showed a slow rise in temperature during the flights. Hence the gas was well away from its freezing point of  $-5^{\circ}\text{C}$ . The temperature of the tank, and therefore gas, was  $20^{\circ}(+3^{\circ})\text{C}$  for each flight.

### 3.2. Data Analysis

#### 3.2.1. Raw Data

During both flights, the bulk of the data was recorded in a form suitable for computer processing. All the pulse-height information was on 8-hole punched paper tape and the orientational data and event ~~data~~<sup>blip</sup> were simultaneously monitored on a 2 channel pen chart-recorder, together with a 1 minute and 5 minute time-marker generated in the receiving station. In order that the event and orientational information might be unambiguously correlated, marks were made on both the chart record and the paper tape output at frequent intervals during the course of the flight. As the chart-recorder also monitored the pressure and temperature of the detector, these marks served to correlate all the event parameters to the time markers which were numbered according to local (East African) time.

#### 3.2.2. In-Flight Calibration

Before the flights, the PHA's had been extensively temperature tested and checked for linearity, but it was necessary to be able to check as much of the electronics as possible during the course of the flights,

eventhough the temperature of the detector, as a whole, was temperature stable.

The in-flight calibration was achieved by means of a standard two-pulse generator and associated timer. A 20 minute timer was developed which triggered the pulse generator. The generator produced first a large pulse which gave a PHA output in channel 120 and a half second later produced a small pulse which gave an output in channel 20. Both pulses had a low-temperature-coefficient zener diode as a voltage reference. During both flights, all PHA channels showed a net channel change at the high level of

$$\Delta \text{Ch. no.} < 1$$

and so a correction to the preflight calibration curves when interpreting the data was unnecessary. Note, only the scintillator channels were checked, not the Cerenkov channel, but as all the scintillator channels behaved in the same way, there was no reason to believe that the identical Cerenkov PHA circuits would be different.

### 3.2.3. Correlation of Events with Azimuth

For Flight I, the output from the Hall Probe was the only indication of the orientation, and so, although North and South were known, East and West were ambiguous. By studying the counting rates for an East or West crossover over a long stretch of clear magnetometer output it was possible to assign the direction unambiguously, because the expected counting rate when West-pointing is twice the expected



rate when East-pointing, - see Chapter 7.

Fortunately, for Flight I, the gains of the scintillator channels had been set incorrectly, so that as well as the heavy nuclei,  $Z > 3$ , a lot of background and part of the alpha spectrum was recorded also. Although the spurious background events, e.g. slow protons - discussed in Chapter 4 - are azimuthally independent of the primary cosmic radiation, the flux of alphas seen was sufficiently high to show a higher  $\vec{W}$  counting rate than  $\vec{E}$  counting rate.

For Flight II, this procedure was unnecessary because the sun-sensor removed the ambiguity, but as a check, the integrated  $\vec{W}$  flux was compared to the integrated  $\vec{E}$  flux and the ratio for  $Z > 3$  was

$$\frac{N_{\vec{W}}}{N_{\vec{E}}} \sim 2.$$

#### 3.2.4. Scintillator and Cerenkov Response to Heavy Nuclei

A computer programme was developed to accept the punched paper tape and decode the Johnson logic raw data. The computer outputted the event information in punched card form with a (chronological) event number, 3 bits of scintillator pulse height information and the Cerenkov pulse height together with a flag which indicated the high gain mode or low gain mode of the Cerenkov channel amplifiers.

The programme was extended to plot out 2 dimensional graphs comparing (a) 1A and 1B scintillator outputs (top scintillator)

(b) 1A and 3 scintillator outputs (top and bottom)

(c) 1A and 2 (low gain) scintillator and Cerenkov outputs respectively.

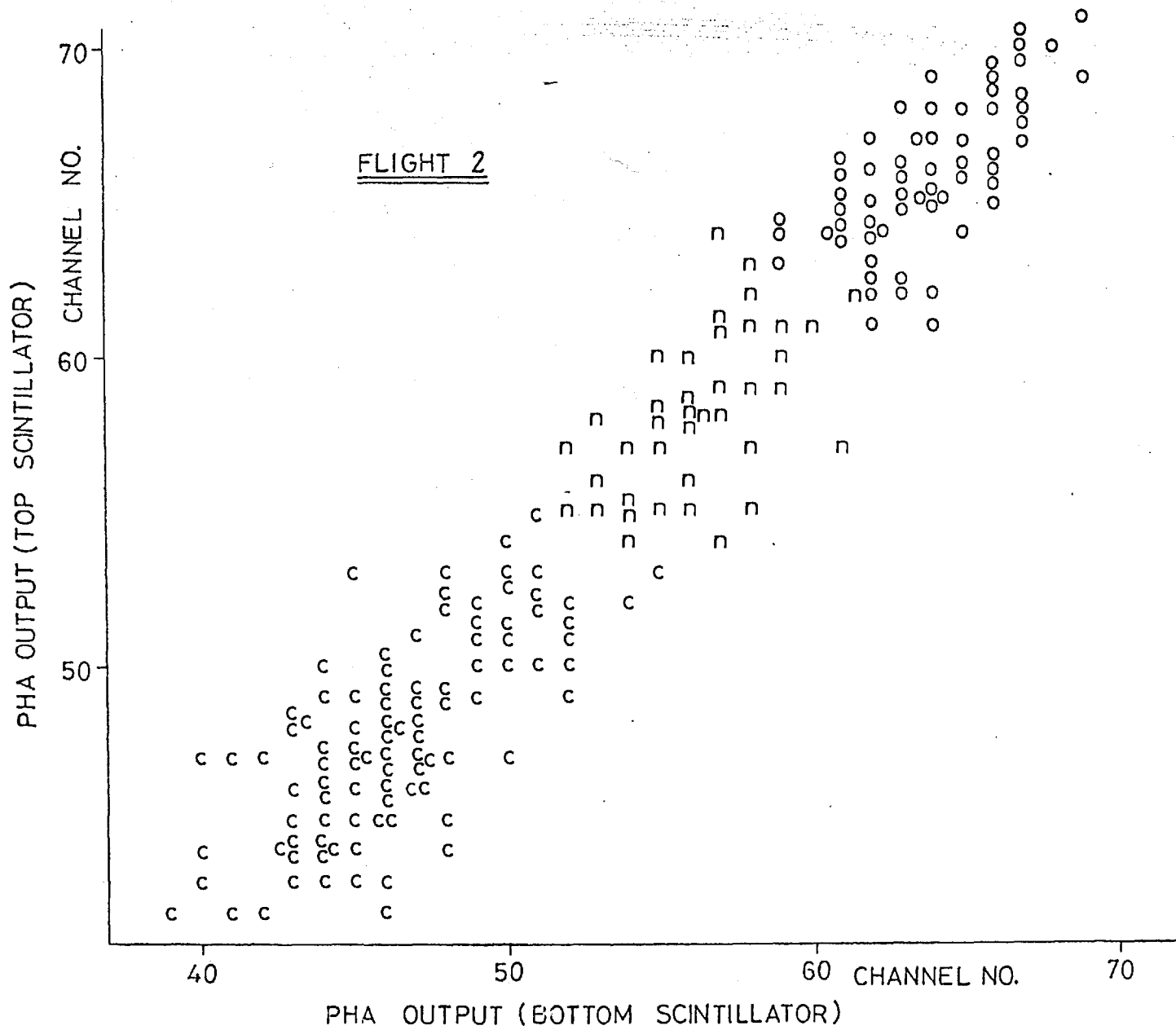


FIG. 21 A HEAVY NUCLEI GROUP (CARBON, NITROGEN OXYGEN)

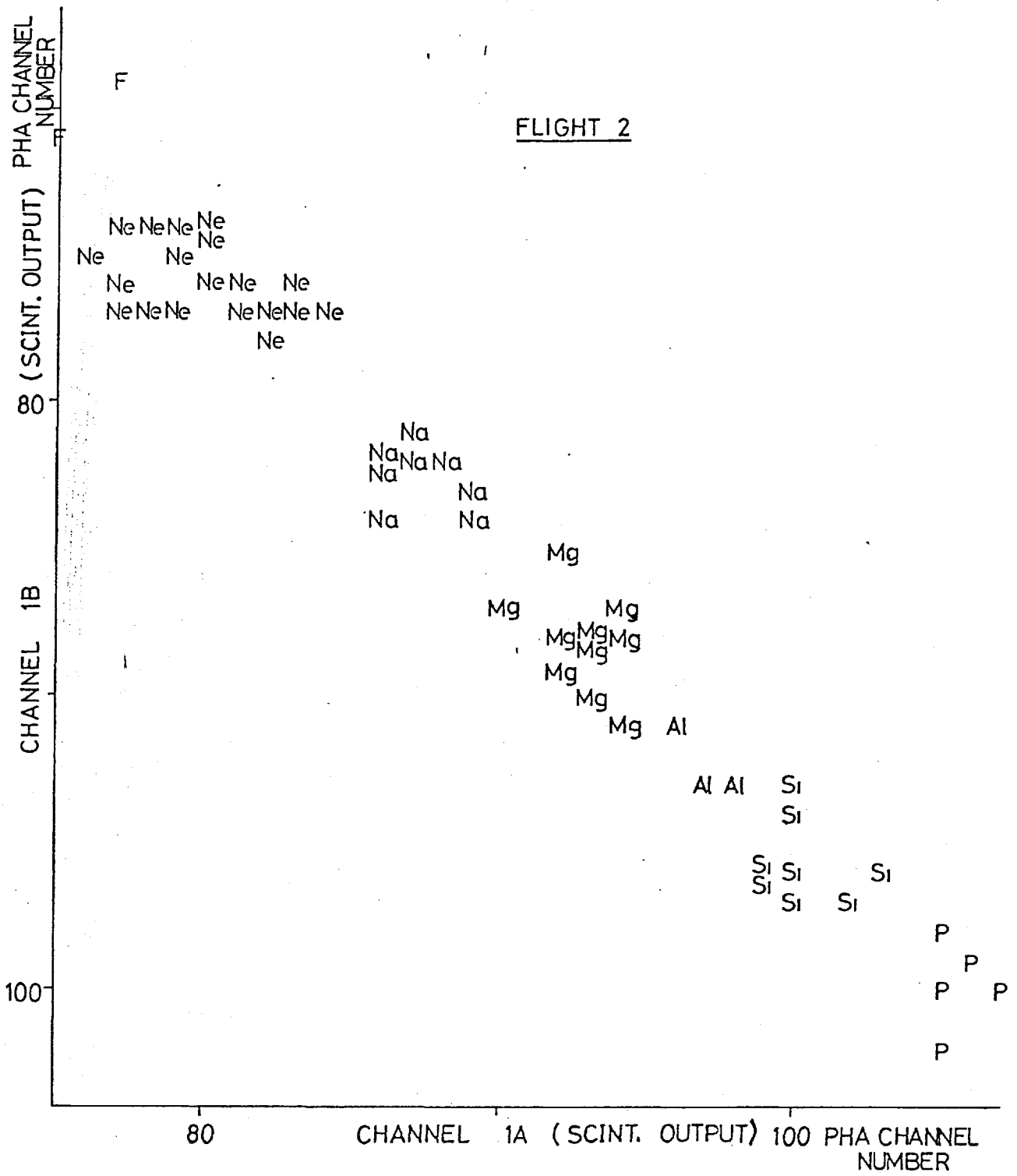


FIG. 21 B HEAVY-NUCLEI GROUPS

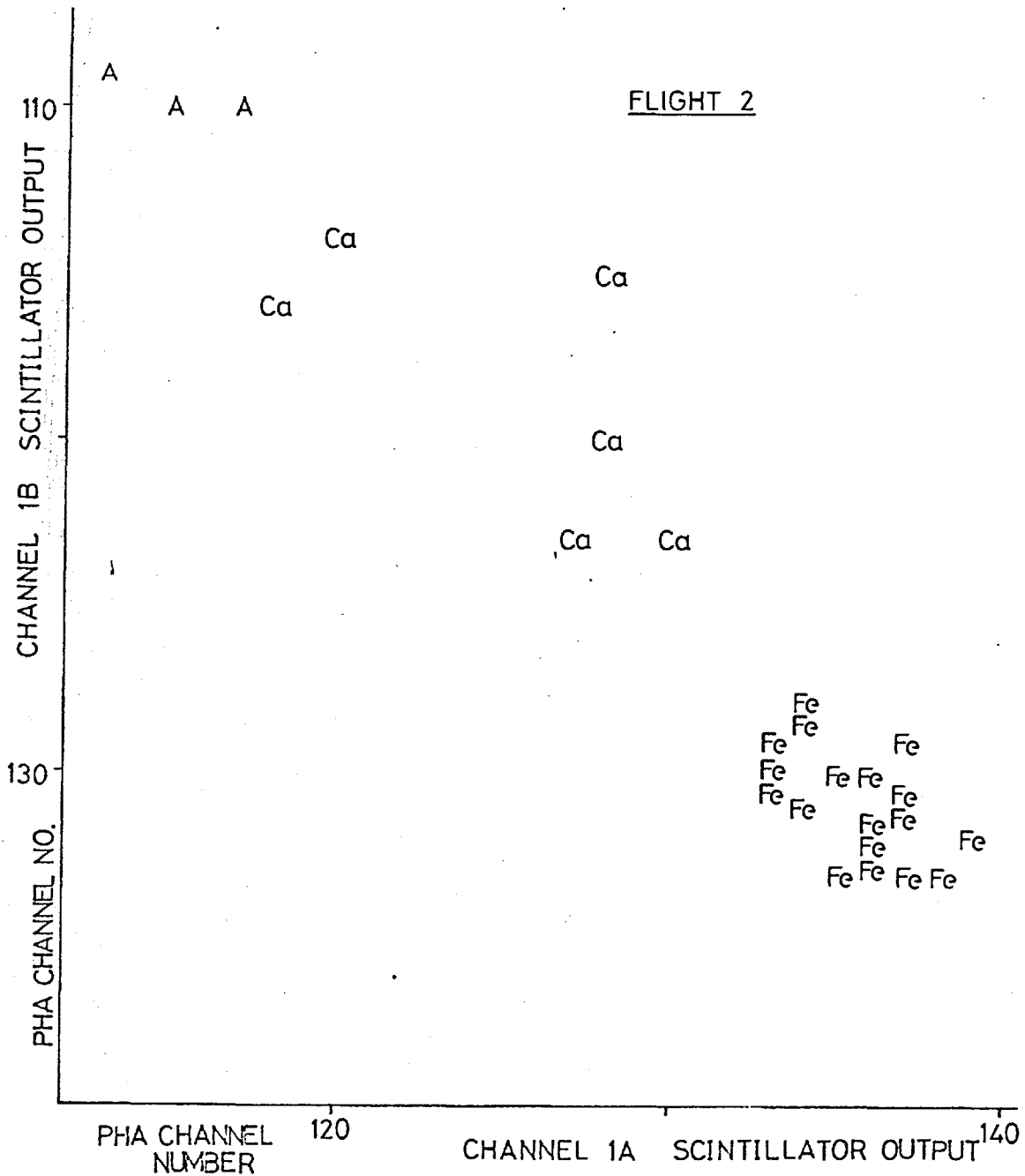


FIG. 21 C HEAVY-NUCLEI GROUPS

In the graphs, or 'crossplots', the events belonging to a particular charge group could be seen as a cluster of points, i.e. high density region. Typical crossplots are shown in Fig. 21A, 21B and 21C. The most abundant nuclear species heavier than helium are carbon and oxygen nuclei and hence, it was possible to locate these species at a glance. As the gain setting for Flight I was incorrect, it was not possible to check that the relative positions of the 'supposed' carbon and oxygen groups occurred where expected on the basis of the preflight mu-meson calibration, but for Flight II it was verified that the expected and experimental scintillator outputs tallied. (As an independent check, the expected relativistic-limit outputs from the Cerenkov device tallied with the experimental values.)

The iron group nuclei also stood out as a well-defined group of events, characterised by very high Cerenkov outputs.

Using the well-defined carbon and oxygen and iron groups as indicators, it was possible to interpolate and unambiguously identify the charge groups up to  $Z = 14$  as shown on Fig. 21B, except that lithium, in particular, and beryllium were difficult to resolve from the background events. On the assumption that the lower charge groups give a scintillator output which is proportional to the square of the charge (subsequently proven) and that no saturation effects were present in either the scintillator or the electronics it was attempted to fit

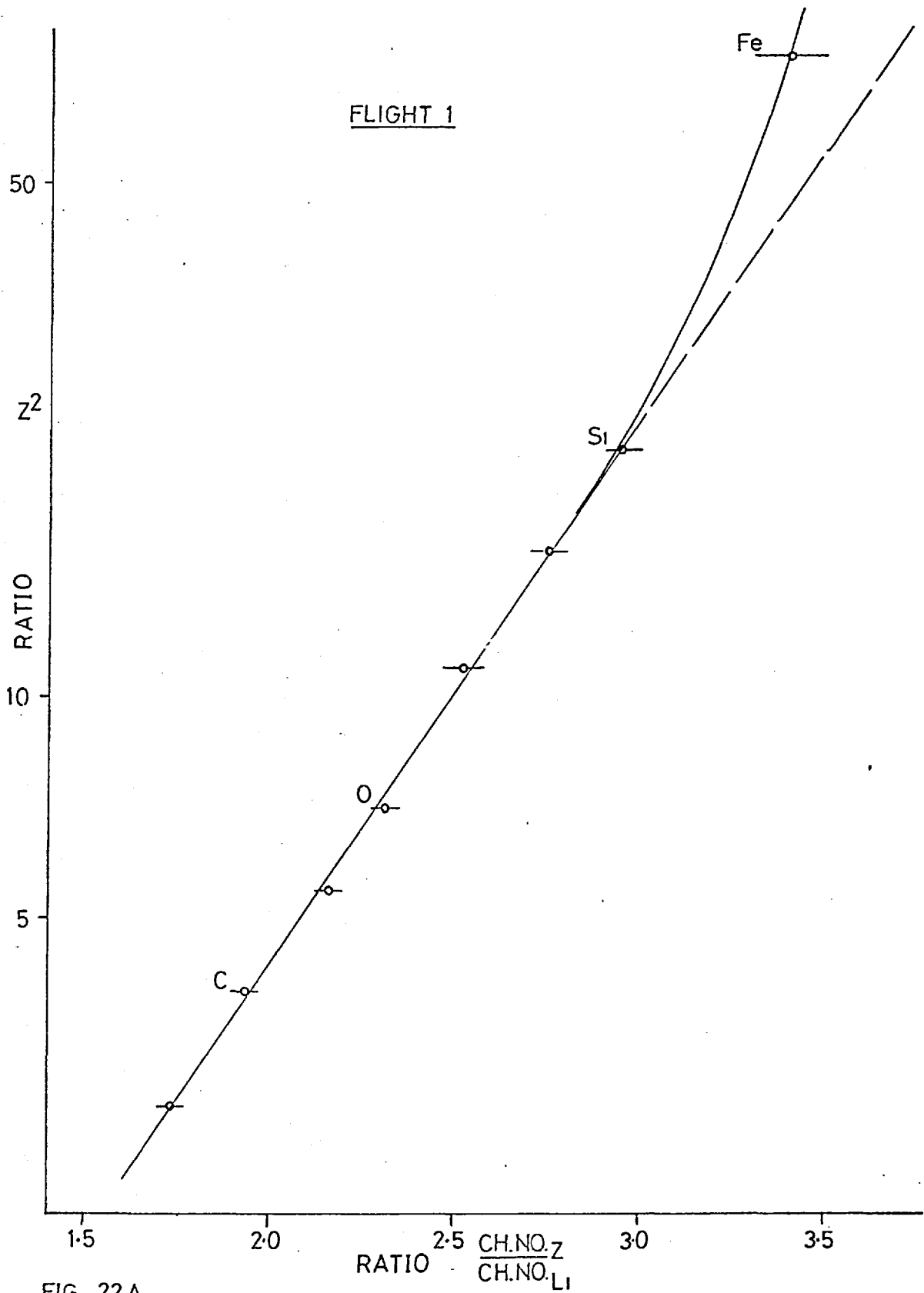


FIG. 22A  
SCINTILLATOR RESPONSE TO HEAVY NUCLEI

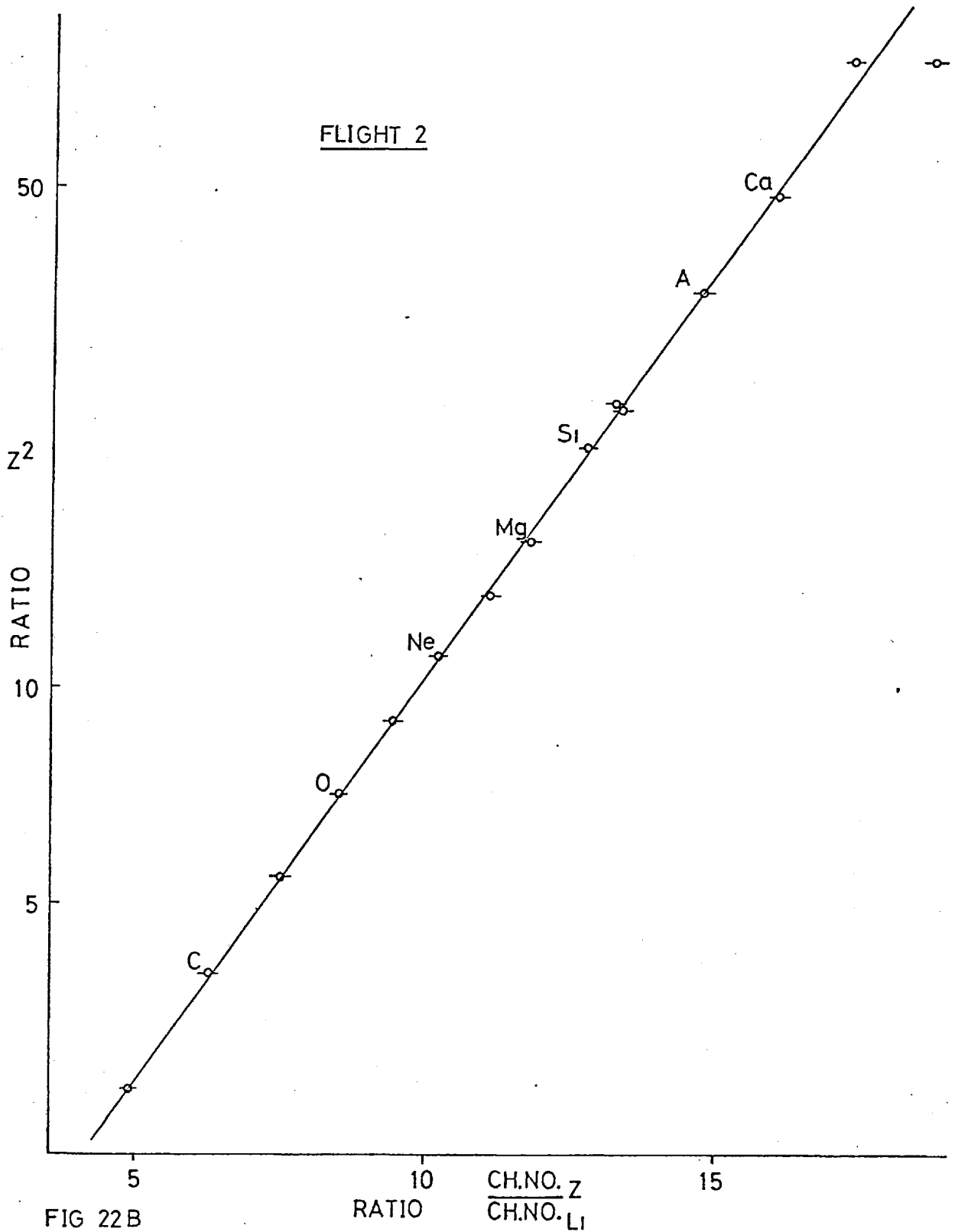


FIG 22 B  
SCINTILLATOR RESPONSE TO HEAVY NUCLEI

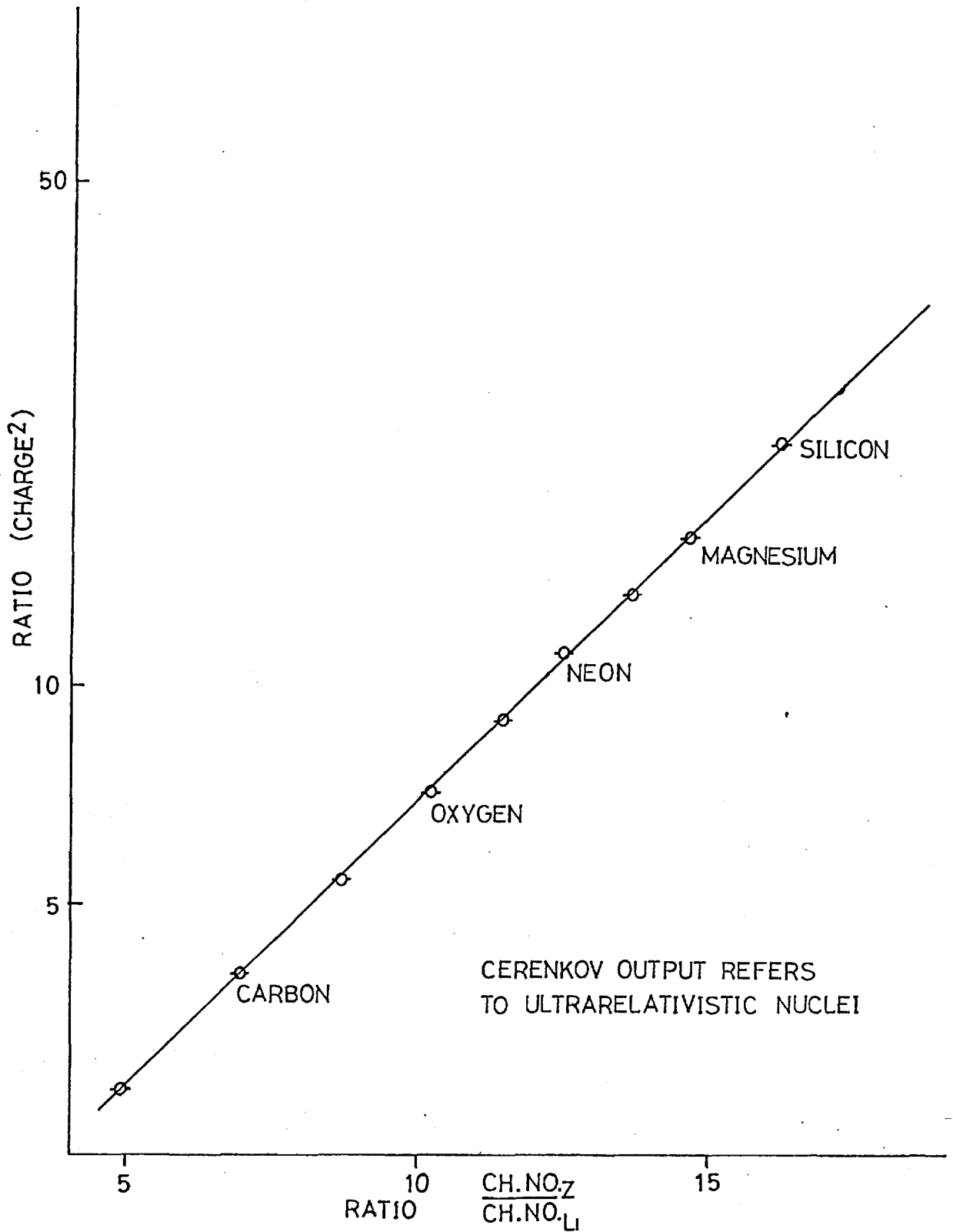


FIG. 23 ILLUSTRATION OF LINEARITY OF GAS CERENKOV OUTPUT UP TO SILICON (Z=14)



the heavier nuclei to this relationship. The result is shown for Flight I in Fig. 22A and for Flight II in Fig. 22B.

The most likely interpretation in these different results is that for Flight I, the electronic amplifiers saturated for the iron group, because the scintillator gains had been set too high, and the logarithmic amplifiers recycled for the iron nuclei. This means that the effective iron group channel number was 150  $\rightarrow$  155, and the linearity of the amplifiers prior to the flight had only been checked up to channel number 140.

For Flight II, the gains were lower so that the iron group appeared around channel numbers 135  $\rightarrow$  140 (see Fig. 21C) and to within the errors, the position of the iron group is consistent with a  $Z^2$  dependence. This conclusion is inconsistent with that of von Rosenvinge and Webber (71) who have presented evidence for a non  $Z^2$  dependence of the scintillator outputs for large charge groups.

In Fig. 23 it is clear that the prediction that the Cerenkov output at relativistic speeds is a function of  $Z^2$  is upheld to the highest Z recorded. Unfortunately the iron group completely saturated the low gain Cerenkov.

Having established the position of the charge groups, it was possible to establish the charge of a particular event which occurred between the highest density parts of a particular crossplot by the locations in the other two crossplots. For charge  $5 < Z < 14$ , the

estimated error in determining the charge is  $\Delta Z < 0.5$  units of charge. The derived charge spectra are treated in Chapter 6.

The rigidity spectra of the dominant species and the charge groups are discussed more fully in Chapter 5. Briefly, it was possible to derive the 10.5, 18 and 28 GV integral flux points from the charge group counting rates due West, due North or South and due East respectively. The spectra were extended up to 36 GV by analysing the Cerenkov outputs of those events belonging to the same charge group.

Using the preflight calibration curves for the Cerenkov device, the number of events with PHA outputs greater than a specific PHA output was converted into the number of events with velocities greater than a certain velocity,  $\gamma$ . Choosing a suitable ratio ( $A/Z$ ) for each species, the number of events exceeding a rigidity,  $R$  could be derived:

$$R = (A/Z) m_0 \gamma c^2 \text{ GV}$$

For a rigidity,  $R \sim 36$  GV, the velocity  $\gamma \approx 18$  and for this value of  $\gamma$ , the PHA output was  $\sim 10$  channels from the ultrarelativistic limit,  $\gamma \rightarrow \infty$ . it would have been extremely difficult to estimate the integral flux values beyond,  $R \sim 36$  GV.

One useful check on each method adopted for calculating the integral rigidity spectra was the 18 GV flux value and also the 28 GV flux value, because these values could be obtained from both the orientational information and the Cerenkov information.

Finally, the derivation of the upper limit to antinuclei is discussed in detail in Chapter 7, but briefly, this required a search for apparent relativistic nuclei events (deduced from the scintillator crossplots) with zero Cerenkov outputs which were recorded when the detector was eastpointing (correlation of event nuclei with magnetometer blip). Although a few such events were recorded for  $3 < Z < 5$  nuclei, there is a natural explanation for these in terms of background which is discussed in the following chapter.

#### 3.2.5. Dead-Time Correction

In the first flight, incorrect gain settings resulted in a high counting rate due to the presence of albedo protons, nuclear interactions in the detector and primary alphas.

Whenever an event triggered the scintillator elements the PHA information was coded and transmitted to the ground station. The time taken for the transmission of the information was 0.5 secs, and hence the detector could not respond to consecutive events unless the time interval between them was,  $\tau > 0.5$  secs.

As an average counting rate of 1 every 25 seconds had been anticipated, this dead time was considered unimportant, however for flight I the average counting rate was 1 every 6 seconds and the dead time must be taken into account in the derivation of the absolute fluxes of the heavy nuclei.

The average correction to the exposure time at altitude is

$$\begin{aligned} & - (N_T \times \text{Dead Time } (\tau)) \quad \text{where } N_T \text{ is the total} \\ & \hspace{15em} \text{number of counts} \\ & = - \frac{5338 \times 0.5}{60} \text{ mins} \\ & = - 44.5 \text{ mins} \end{aligned}$$

As the total time at altitude was 515 minutes, the effective exposure time for the heavy nuclei is

$$\tau_{\text{exp}} = 470.5 \text{ mins}$$

In order to derive the integral rigidity spectrum for each charge group, it is necessary to compute the flux values while pointing West ( $\pm 45^\circ$ ) and also East ( $\pm 45^\circ$ ). As there are more events recorded when West-pointing, it is essential to derive the correction to the exposure time for each quadrant separately.

WEST-QUADRANT W( $\pm 45^\circ$ )

Total number of events recorded	1191
Dead Time	9.9 mins
Total time west-pointing	103 mins
Effective exposure time	93.1 mins

EAST-QUADRANT E( $\pm 45^\circ$ )

Total number of events recorded	814
Dead time	6.8 mins
Total time east-pointing	107 mins
Effective exposure time	100.2 mins

These effective exposure times were used to compute the flux values.

### 3.2.6. Ionization and Recombination Light in Gas Cerenkov

It is possible to place an upper limit to the ratio of scintillation light (via ionisation and recombination processes) to Cerenkov light in the propylene gas by using the in-flight data. As discussed later in Chapter 4, subrelativistic protons and alpha particles are capable of depositing as much energy, in the form of ionisation energy, as heavier, relativistic nuclei in either top or bottom scintillator disks (and hence the gas). However, unlike these relativistic nuclei, they are unable to produce Cerenkov light in the propylene gas.

In figure 27, alpha particles in the splash albedo flux with an energy,  $E_{\alpha} \sim 200 \text{ MeV/n}$  deposit the same amount of energy in the top scintillator as a relativistic boron nucleus, and the same amount of energy in the bottom scintillator as a relativistic neon nucleus. One would expect these particles to deposit approximately the same amount of ionisation energy in the propylene gas as a relativistic oxygen nucleus. If one assumes that all albedo alphas have been assigned correctly, less than 1 photoelectron is produced due to scintillation light alone, in the propylene. However, the mean number of photoelectrons due to Cerenkov light for a relativistic oxygen nucleus is  $\sim 1/85$ . To a rough approximation

$$\frac{S}{C} \Big|_{\substack{\text{propylene} \\ \text{gas}}} < \frac{1}{85}$$

i.e. it is negligible.

## Chapter 4 - BACKGROUND EFFECTS IN THE DETECTOR

### 4.1. Discussion of Background

Two distinct types of background events are present with this detector.

Firstly, high energy ( $E > 10^{12}$  eV) protons can interact in the material surrounding the detector, or in the detector itself. The disrupted nucleus gives rise to many secondary products which produce an 'event' characterised by a large Cerenkov output. These events are discussed in section 4.2.

Secondly, splash and reentrant proton and alpha particle albedo are recorded. These 'events' are characterised by a zero Cerenkov output because the particles in question have subrelativistic energies. As an event with a zero Cerenkov output whilst the detector is Eastpointing could be an antinucleus, it is necessary to identify all albedo events. By comparing the outputs from the top and bottom scintillators, the albedo particles are unambiguously defined and in section 4.3. the derivation of the albedo energy spectra is described.

It is also possible that with such a large detector, spurious 'events' might be synthesised by the chance coincidence of a number of particles traversing the different detector elements. It is easy to show, however, that the chance coincidence rate is negligible.

The chance coincidence rate of pm tube noise pulses is small because a 3-fold coincidence is required. The expected rate

$$R_{cc} = 3 N_1 N_2 N_3 \tau^2 / \text{sec}$$

$N_1$  = singles rate for tube 1A

$N_2$  = singles rate for tube 1B

$N_3$  = singles rate for tube 3.

The time,  $\tau$  is the length of time that the coincidence electronic 'gate' is active,

$$\tau \approx 200 \times 10^{-9} \text{ secs.}$$

The singles rates for each tube were approximately 5000/min.

Substituting, the expected rate becomes

$$R_{cc} \approx 7 \times 10^{-11} / \text{sec.}$$

The chance rate will be greater if one considers an  $\alpha$ -particle traversing two detector elements and another particle traversing the third element. The rate of this 2-fold coincidence is

$$R = 2 A_j \alpha j_p A_f \tau / \text{sec}$$

$j_\alpha$  = alpha flux/cm<sup>2</sup> ster. sec

$A_\alpha$  = solid angle accessible to alphas

$j_p$  = particle flux/cm<sup>2</sup> ster. sec.

$A_p$  = " " " " " particles

$\tau = 200 \times 10^{-9} \text{ sec.}$

Even if the whole area of the gas tank is accessible to the particle flux, the rate is

$$R \approx 2 j_\alpha \cdot 200 j_p \cdot 2\pi \cdot 10^4 \cdot 200 \cdot 10^{-9} / \text{sec}$$

$$\approx j_\alpha j_p$$

But, as the alpha flux is  $j_\alpha < 10^{-5} / \text{cm}^2 \text{ster. sec.}$  and the total cosmic ray flux is  $\sim$  few particles/ $\text{cm}^2 \text{ster. sec.}$  even the 2-fold rate is negligible.

#### 4.2. Jets

A high energy primary,  $E_p > 100 \text{ GeV/n}$  when it interacts with a nucleus in some material, disrupts the nucleus and produces three types of secondary particles (see ref. (75)),

(i) A number,  $n_s$ , of minimum ionizing 'shower' particles. The particles correspond to protons of energy greater than 500 MeV and pions of energy greater than 80 MeV. Fowler (76) showed that the majority of these shower particles are pions. These particles emerge from the interaction volume within a narrow cone of angles about the axis of the primary particle.

(ii) Protons of energy,  $E_p$ , where

$$25 < E_p < 250 \text{ MeV.}$$

These protons are not ejected isotropically from the interaction, but are collimated in the forward direction. The most probable value of the angle of ejection is  $40^\circ \rightarrow 50^\circ$ , and decreases as the energy of the primary increases.

(iii) Low energy protons and nuclear fragments,

$$E \approx \text{few MeV}$$

whose range in any material is extremely short.



The spurious high output Cerenkov events (see Table 1A) could be explained by the nuclear interactions of the primary proton flux in the styrofoam cover and aluminium of the detector such that

(a) the number of shower particles  $n_s = n_\pi > 4$ .

(b) a number of slow protons traverse top and bottom scintillators (see Fig. 24).

One test of this theory is whether or not the expected flux of such events is large enough. The number of shower particles can be represented as a function of the primary energy,  $E_p$ , by

$$n_\pi = 2.1 E_p^{\frac{1}{4}} \quad (\text{see Fig. 25})$$

There is some doubt as to whether the functional relationship,  $n_\pi(E_p)$  at energies  $E_p > 10^3$  GeV/n is  $E_p^{\frac{1}{4}}$ ,  $E_p^{\frac{1}{2}}$  or  $\log E_p$ . The equation above gives the qualitative relationship, at least - Rotelli (77); Spergel (78); Hillas (79).

In order that

$$\bar{n}_\pi > 4$$

we require that

$$E_p \gtrsim 500 \text{ GeV.}$$

(As the fluctuation in the number of pions is quite large, see Fig. 26, this is a very loose lower limit.)

Taking the integral proton flux as

$$j_p (> E_p) \approx 10^{-3} \text{ p/cm}^2 \text{ ster. sec.}$$

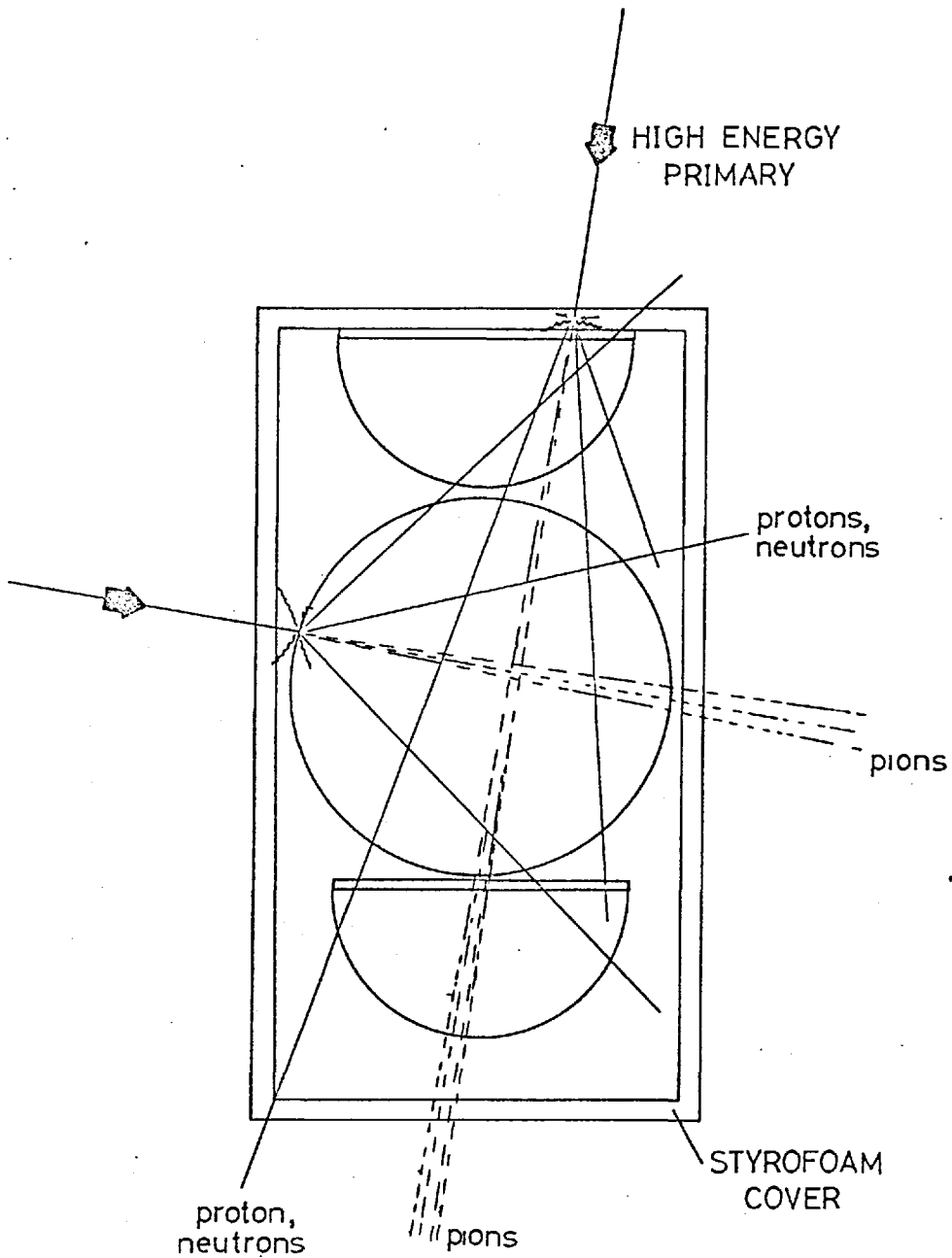


FIG. 24 SCHEMATIC DIAGRAM OF POSSIBLE NUCLEAR INTERACTIONS

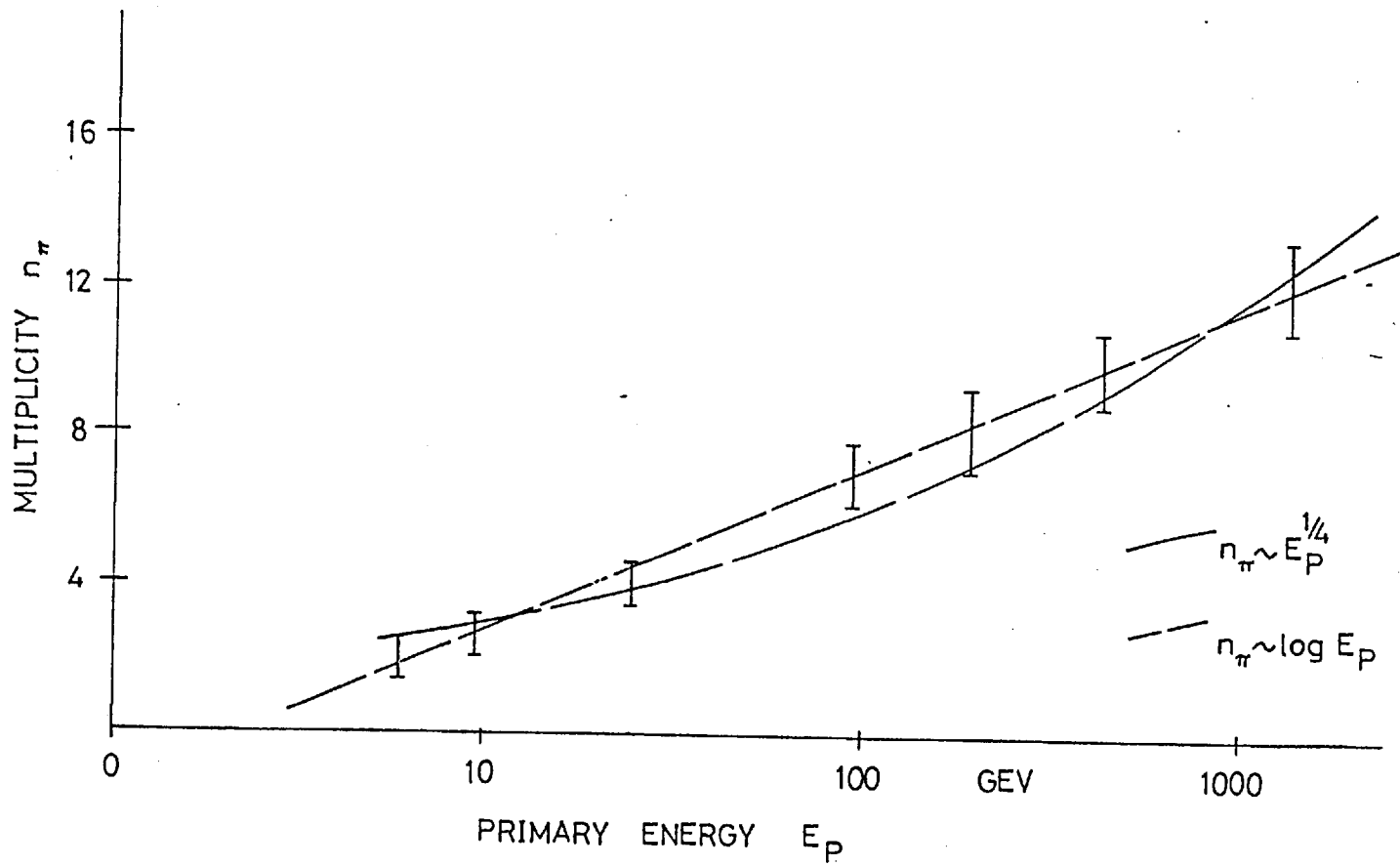


FIG. 25 ENERGY DEPENDENCE OF PION MULTIPLICITY

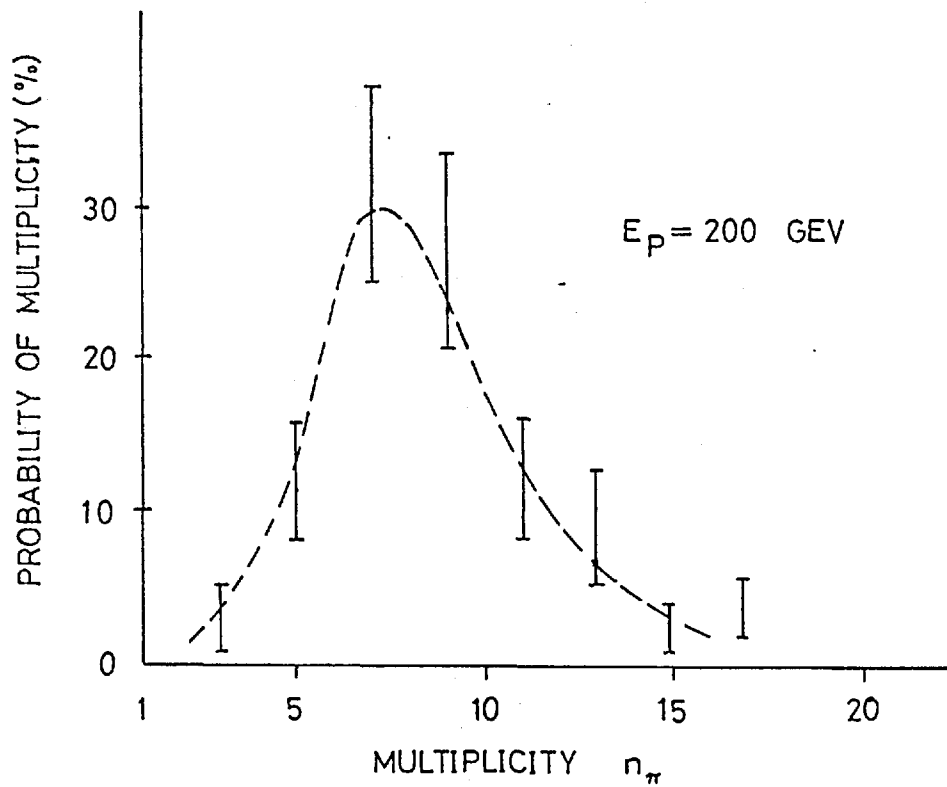


FIG. 26 PROBABILITY DISTRIBUTION OF PION MULTIPLICITY

Interaction mean free path,  $\lambda_p \approx 100 \text{ gm/cm}^2$ .

Maximum amount of material in which interaction could occur,

$$x \approx 1 \text{ gm/cm}^2$$

Solid angle of arrival,  $G$ ,  $\approx$  Geometrical factor of telescope

$$\approx 200 \text{ cm}^2 \text{ ster.}$$

Expected interaction rate

$$N = j_p \cdot G \left( 1 - \exp\left(-\frac{x_{\text{atmos}}}{\lambda_p}\right) \right) \cdot \exp\left(-\frac{x}{\lambda_p}\right)$$

As the residual atmosphere is small, to a good approximation

$$N = 10^{-3} \cdot 200 \cdot \frac{1}{100} \text{ events/sec.}$$

$$\approx 0.002/\text{sec.}$$

The observed mean rate was 0.02/sec as shown in Table 1A. (If the effective collecting area is taken to be the area of the tank and the effective solid angle  $\pi$  steradians, the expected rate becomes 0.3/sec.)

#### 4.3. Albedo

The term albedo is given to particles which are generated by nuclear collisions of the primary cosmic rays in the earth's atmosphere. 'Splash' albedo is the name given to upward-moving secondaries and 're-entrant' is the name given to downward-moving secondaries. It has

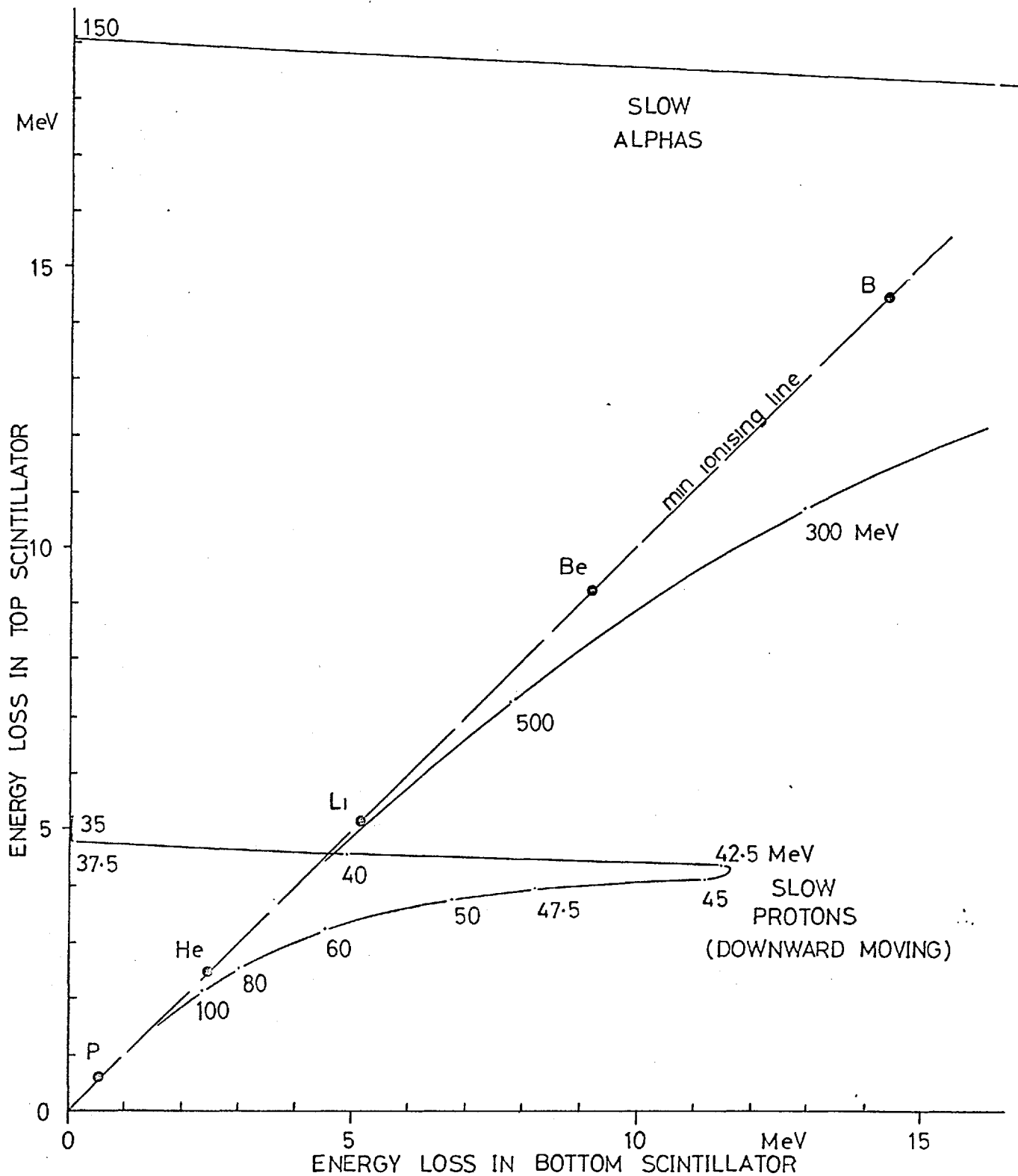


FIG. 27 COMPARISON OF ENERGY LOSSES IN TOP AND BOTTOM SCINTILLATORS

been established (80) that when albedo is produced at a certain latitude,  $\lambda_L$  in, say the Northern Hemisphere, its trajectory will closely follow the magnetic field line intersecting the earth at that latitude. This splash albedo will look like a re-entrant albedo particle in the Southern Hemisphere at its conjugal point at latitude  $\lambda_L$ . However, when these albedo are produced in the equatorial regions such that  $\lambda_L < 30^\circ$  it can be shown (Webber (81)) from Stormer theory that they tend to form a diffuse background, being re-entrant at any longitude within this latitude belt.

Daniel and Stephens(82) used the East-West asymmetry to attempt to measure the positron-electron ratio in the primary cosmic rays. However, the known presence of albedo electrons at balloon altitudes makes this measurement difficult because a re-entrant electron recorded coming in from due West at the equator is indistinguishable from a primary positron.

The main components of this albedo background are slow protons and electrons. The energy losses of a slow proton and a slow  $\alpha$ -particle in the top and bottom scintillators have been computed using the data in the UCRL range-energy curves, and the results are shown in Fig. 27. The energy losses of relativistic nuclei are also shown, for comparison. It can be seen that confusion between slow protons and relativistic nuclei can only arise for proton energies,  $E_p$  in a well-defined range

$$38 < E_p < 42 \text{ MeV.}$$

and even then, the protons can only be confused with lithium nuclei. It can be seen that slow alpha particles can cause confusion with beryllium relativistic nuclei for alpha energies,  $E_{\alpha}$  given by

$$500 < E_{\alpha} < 300 \text{ MeV}$$

(The importance of this possible confusion is shown in Chapter 7, Section 7.1.2. These albedo particles are indistinguishable from relativistic antinuclei, and due to the relatively high flux of albedo protons, and high-energy albedo alphas they limit the sensitivity of the present detector to a ratio of antilithium to lithium or anti-beryllium to beryllium of a few percent.)

Also, the albedo alphas with energy,  $E_{\alpha}$  in the range  $155 < E_{\alpha} < 165 \text{ MeV}$  are indistinguishable from relativistic carbon nuclei, but the flux of alphas in this narrow energy range is negligible for the purpose of the present experiment.

#### 4.3.1. Splash and Re-entrant Proton Flux

Albedo particles have been shown to be valid progenitors of spurious antinuclei events with this type of detector. It was hoped to avoid most of these background counts by adjusting the gains and threshold of the scintillator channels so that only events with charge,  $Z > 3$  would be recorded. However, for FLIGHT I the gains in the scintillator channels were incorrect, and even some alpha events were recorded.



At first, it was thought that the large background extending from the alpha region to beryllium and beyond on the crossplot of the bottom scintillator, Ch. 3 and one of the top scintillator channels, Ch. 1A was due to the Landau-tail effect of the large alpha flux. However, this implied that the photoelectron collection efficiency was much poorer than had been assumed and also, as the detectors were physically identical, the effect should have been seen on the second flight - but it was not seen.

The alternative explanation, and the one which fits all the available facts, is that most of the background is due to slow protons. Further, by inspection of the crossplot of Ch. 3 and Ch. 1A shown in Fig. 28, it is possible to separate splash and re-entrant slow protons and to estimate the differential flux of both. Also shown on Fig. 28 is shift of origin due to different gain settings → explains lack of high counting rate for FLIGHT II.

Events for which

(i) Ch. 1A is small and Ch. 3 is large represent re-entrant albedo which are stopping in the bottom scintillator

(ii) Ch. 1A is large and Ch. 3 is small represent splash albedo which are stopping in the top scintillator and all these events give no output from the Cerenkov device.

If these events are part of the true primary alpha flux with

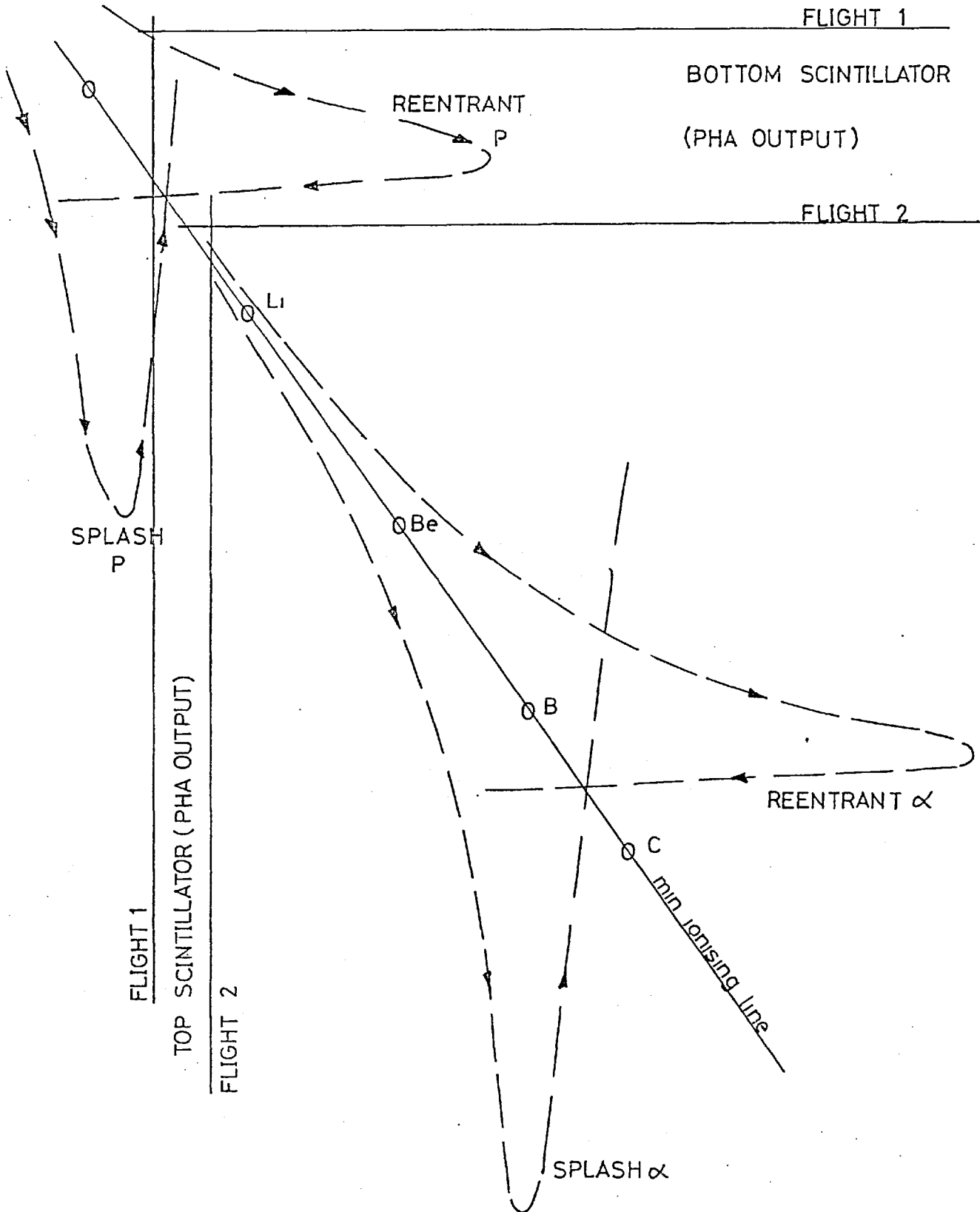


FIG. 28 SCHEMATIC DIAGRAM OF ALBEDO TRAJECTORIES IN THE SCINTILLATOR CROSSPLOT



(A) AZIMUTH DEPENDENCE OF NUCLEAR INTERACTION EVENTS

AZIMUTHAL ORIENTATION $\theta$	NUMBER OF EVENTS $N_{\theta}$	EXPOSURE TIME $T_{\theta}$ mins	RATE $R_{\theta}$ $\text{min}^{-1}$
NORTH	109	110	1.00 ( $\pm 0.10$ )
SOUTH	122	165	0.74 ( $\pm 0.07$ )
EAST	70	100	0.70 ( $\pm 0.09$ )
WEST	89	93	0.96 ( $\pm 0.10$ )

(B) AZIMUTH DEPENDENCE OF ZERO CERENKOV EVENTS

$\theta$	$N_{\theta}$	$T_{\theta}$ mins	$R_{\theta}$ $\text{min}^{-1}$
NORTH	380	110	3.46 ( $\pm 0.17$ )
SOUTH	356	165	2.17 ( $\pm 0.11$ )
EAST	229	100	2.29 ( $\pm 0.15$ )
WEST	400	93	4.30 ( $\pm 0.21$ )

TABLE 1

rigidity R such that

$$R_G < R < R_C$$

$R_G$  = geomagnetic threshold

$R_C$  = Cerenkov threshold rigidity.

there should be no events satisfying this criterion when the detector is eastpointing (unless the primary helium flux contains a significant proportion of antihelium). However, an investigation into the orientation of the detector when the zero-Cerenkov events were recorded indicated that these events were azimuthally independent. The counting rates are shown in Table 1. All these events for the eastpointing detector must be slow protons, and if these events are plotted as in Fig. 29, most of the points lie in the region of the graph where the trajectories of the slow protons is expected.

In Fig. 30 the estimated differential flux values of the splash and re-entrant proton albedo by inspection of the crossplots are compared to those given by Dev Verma (83).

#### Discussion of Slow Proton Results

In Fig. 30, it can be seen that the measurements of the splash and re-entrant proton albedo fluxes at Kampala in Uganda agree extremely well with the Dev Verma fluxes when allowance has been made for (a) ionization losses when extrapolated to top of the atmosphere (b) the different cut-off rigidities, i.e. 15 GV at Kampala and only 4.9 GV at Palestine in Texas.

This factor

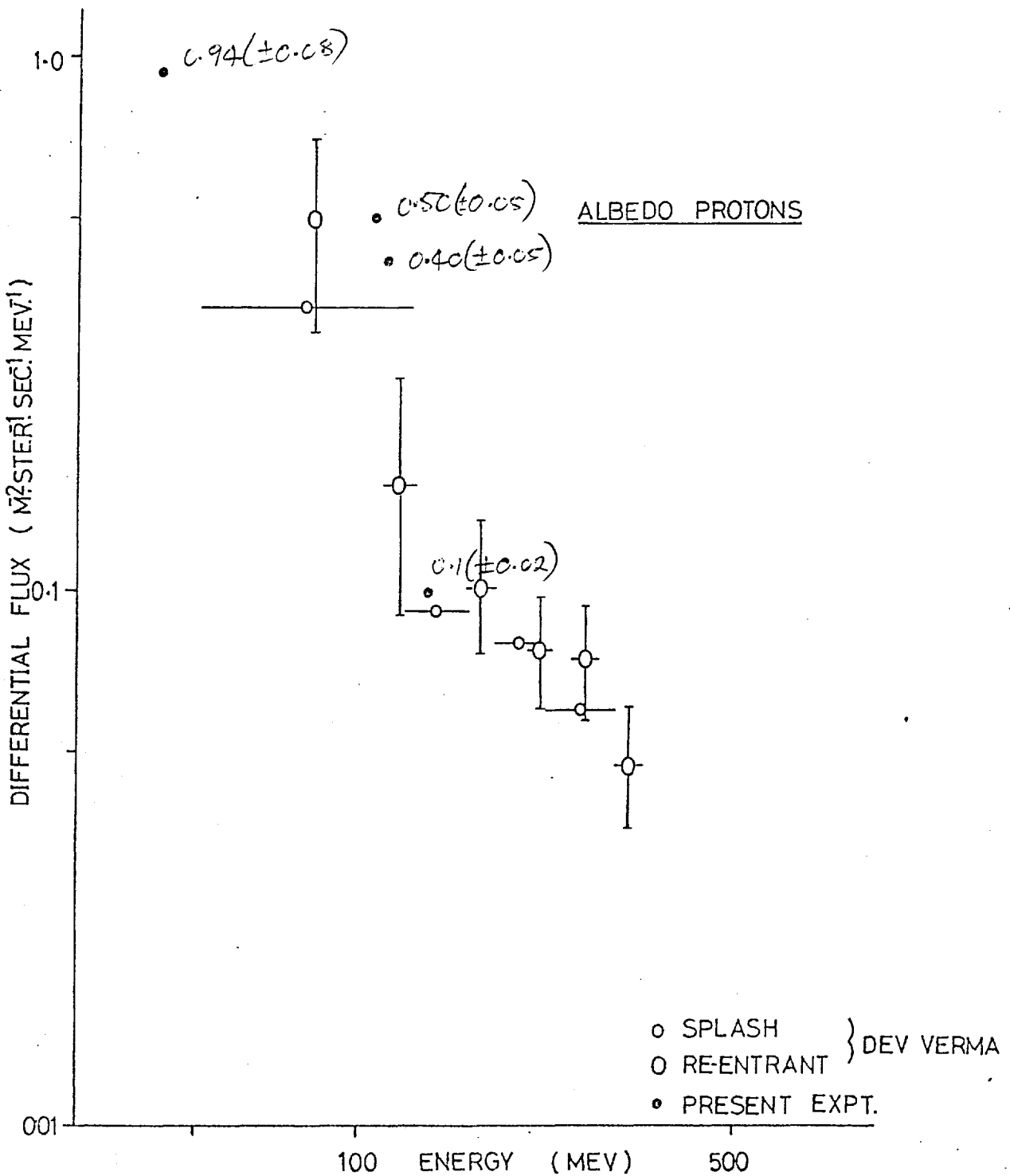


FIG. 30 DIFFERENTIAL FLUX OF ALBEDO PROTONS NORMALISED TO ZERO GRMS.CM<sup>-2</sup> RESIDUAL ATMOSPHERE AT PALESTINE, TEXAS.

$$\begin{aligned} j_{\text{KAMPALA}}(\text{albedo}) &= j_{\text{PALESTINE}}(\text{albedo}) \cdot \left(\frac{15}{5}\right)^{-1.5} \\ &= 0.2 j_{\text{PALESTINE}} \end{aligned}$$

reflects the fact that these are secondary particles produced by nuclear interaction in the atmosphere.

The excellent agreement lends credence to the assignation of most (if not all) of the events with zero Cerenkov in the background to slow protons.

#### Albedo Alphas

An estimate of the splash alpha albedo flux has been derived from a consideration of the zero Cerenkov events in the 'spallation' region of the Ch. 3 v. Ch. 1A crossplot. These results are discussed in the next section.

#### 4.4. Spallation in the Detector

When a heavy nucleus traverses a medium, there is a probability, the fragmentation probability, that it will fragment, or spall into lighter nuclei due to a nuclear interaction in that medium.

If the type of secondary produced is disregarded the total collision probability is embodied in the mean free path,  $\lambda_z$  which is defined as the distance the particle can travel in the medium before the probability of a collision is  $e^{-1}$ .

Cleghorn (84) has established that the effective crosssection for

an interaction is equivalent to the geometrical cross-section of the nucleus in question (at relativistic energies). Hence, reliable estimates of the fraction of nuclei, of charge  $Z$  which spall when traversing matter, say  $x$   $\text{gcm}^{-2}$  can be obtained from

$$\frac{N}{N_0} \Big|_Z = \exp(-x/\lambda_Z)$$

where  $\lambda_Z \propto Z^{-2/3}$

Spallation events in the detector are characterised by a larger output in channels 1A (or 1B) than in channel 3. Hence it is possible to select events which spalled during passage through the detector tanks. In order to obtain a statistically significant result, a detailed analysis of the effect of spallation on carbon, nitrogen and oxygen nuclei only can be attempted.

The initial spallation-assigned events and total number of events are shown in Table IIA. As the total amount of matter in the detector was

$$x_d = 2.5 \text{ gcm}^{-2},$$

the results implied an extremely short interaction mean free path

$$\lambda_{\text{C,N,O}} \approx 7.0 \text{ gcm}^{-2}, \text{ whereas the geometrical mean free path}$$

$$\lambda_{\text{THEORY}} \approx 28.0 \text{ gcm}^{-2} \text{ for carbon.}$$

This discrepancy can be explained in terms of a spurious background which occurs in the spallation region of the Ch. 1 versus Ch. 3 crossplot.



(A) INITIAL ASSIGNMENT OF EVENTS

ELEMENT	FLIGHT 1		FLIGHT 2	
	NUMBER SPALLED	TOTAL NUMBER	NUMBER SPALLED	TOTAL NUMBER
CARBON	71	202	25	103
NITROGEN	30	77	12	39
OXYGEN	44	147	7	61

(B) AZIMUTHAL DEPENDENCE OF FLUX VALUES - FLIGHT 1

ELEMENT	FLUX OF ZERO CERENKOV EVENTS IN SPALL. REGION				ESTIMATED TOTAL BACKGROUND
	$\bar{N}$	$\bar{S}$	$\bar{E}$	$\bar{W}$	
CARBON	0.049 <sup>(6)</sup>	0.033 <sup>(6)</sup>	0.056 <sup>(6)</sup>	0.077 <sup>(8)</sup>	22(±2)
NITROGEN	0.016 <sup>(2)</sup>	0.005 <sup>(1)</sup>	0.019 <sup>(2)</sup>	0.039 <sup>(4)</sup>	6(±1)
OXYGEN	0.033 <sup>(4)</sup>	0.011 <sup>(2)</sup>	0.009 <sup>(1)</sup>	0.029 <sup>(3)</sup>	6(±1)

( ) DENOTES NUMBER OF EVENTS

(C) FINAL ASSIGNMENT OF EVENTS

ELEMENT	FLIGHT 1		FLIGHT 2	
	NUMBER SPALLED	TOTAL NUMBER	NUMBER SPALLED	TOTAL NUMBER
CARBON	21(±2)	152	16(±2)	94
NITROGEN	10(±1)	57	5(±1)	32
OXYGEN	6(±1)	109	7(±1)	61

TABLE II

It is assumed that most of these events are due to the same physical processes discussed beforehand, namely,

- (i) Slow particles
- (ii) Nuclear interactions in detector.

Instead of slow protons traversing the whole detector, these slow particles must be splash albedo alphas. The events are characterised by a zero Cerenkov output. The nuclear interactions are considered to be those in which non-relativistic alpha fragments and protons trigger the scintillators, and pions traverse the Cerenkov tank.

#### Selection Criterion

As these nuclear interaction events are indistinguishable from spallation products, it is necessary to assume an arbitrary selection criterion. The criterion assumed here is that, as there are more apparent spallation events per unit time for flight I than for flight II, it is sensible to think that more spurious events were introduced by the incorrect gain setting, i.e. most of the spurious background must be events with a low output in Channel 3.

It is improbable that a nuclear interaction in the detector could produce a zero Cerenkov event (see section 7.1.2.) and all the zero Cerenkov events will be considered to be either

- (a) slow alpha albedo flux ( $j_\alpha$ )
- or (b) true fragmentation of primary, ( $j_F$ )  $10 < R_{\text{prim}} < 18$  GV.

Another possible effect is the fragmentation of a primary of rigidity,

R > 18 GV into a secondary, of rigidity R < 18 GV in that part of the detector before the Cerenkov device. This is discussed more fully in section 7.1.2.

It is possible to obtain an estimate of the slow alpha albedo by considering the East-West fluxes, i.e.

$$j_{\vec{W}} (\text{zero C; spalln.}) = j_{\alpha} + j_F$$

$$j_{\vec{E}} (\text{zero C; spalln.}) = j_{\alpha} \approx j_{\vec{N}} = j_{\vec{S}}$$

The azimuthal dependence of the events with a zero Cerenkov output and in the spallation region is given in Table IIB. In this table, the 'estimated total background',  $N_{EST}$ , is the number of previously assigned events now considered to be due to slow alphas.

$$N_{EST} \sim 4 N_{EAST}$$

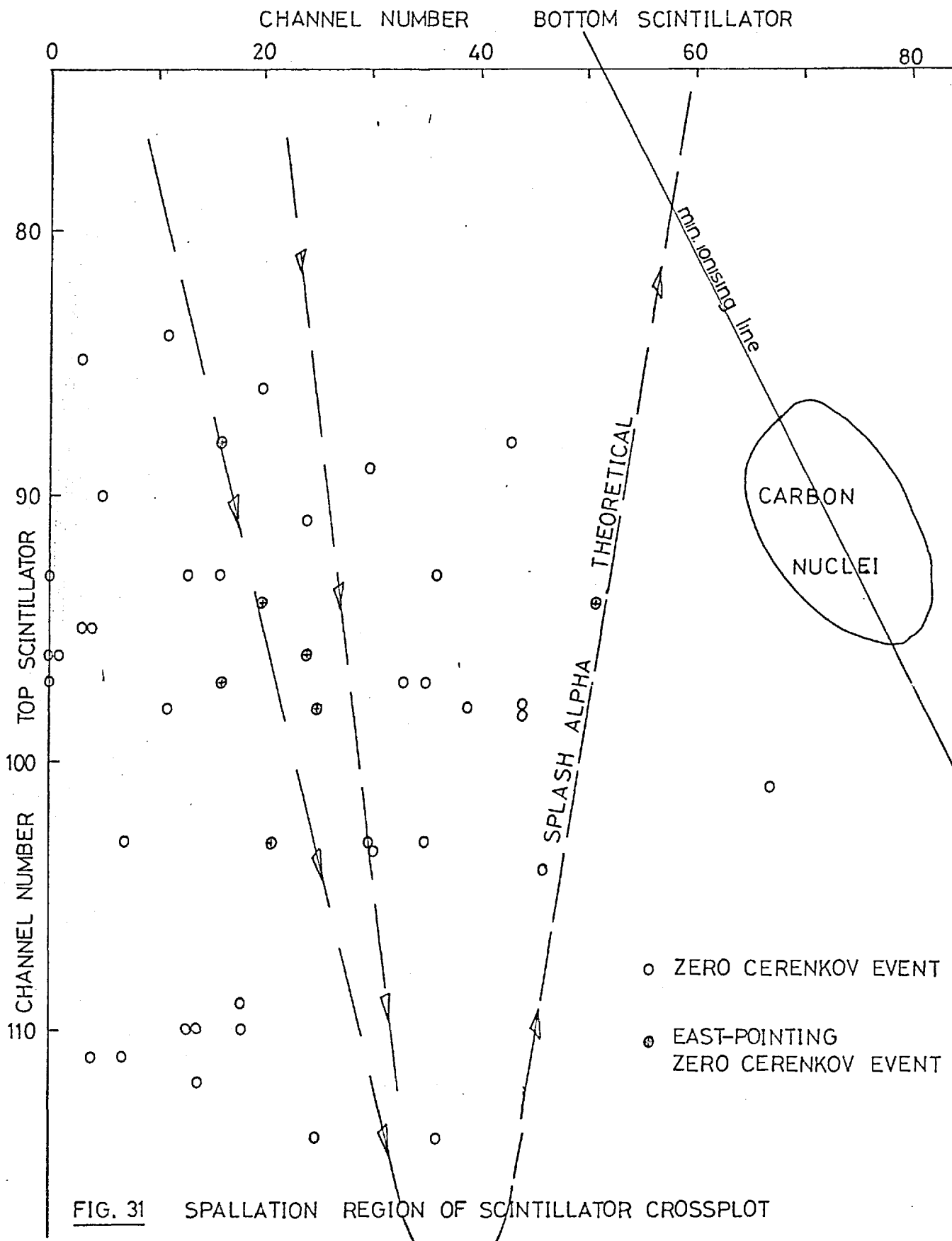
The estimated flux of nuclei in the rigidity range  $10 < R < 18$  GV which did fragment is

$$j_F = j_{\vec{W}} - j_{\vec{E}}$$

By using the value of  $j_F$ , it is possible to improve the estimate of the mean-free-path of the M-nuclei.

$$\text{FLIGHT I} \quad \lambda_{CNO} \approx 2.5 \times \frac{308}{37} = 21.0 \text{ (+ } \overset{4.0}{\cancel{2.0}} \text{) grm.cm}^{-2}$$

$$\text{FLIGHT II} \quad \lambda_{CNO} \approx 2.5 \times \frac{187}{24} = 19.5 \text{ (+ } \underline{2.0} \text{) grm.cm}^{-2}$$



These estimates are in reasonable agreement with the theoretical mean free path,  $\lambda_{\text{CNO}} \sim 28 \text{ grm.cm}^{-2}$ . The final number of spallation events are shown in Table IIC.

4.4.1.

Splash Albedo - Differential Flux Values

(i) 160 < E<sub>α</sub> < 170 MeV

$$N_{\alpha} = 6 \pm 2 \quad \tau = 515 \text{ min.}$$

$$\begin{aligned} \frac{dj_{\alpha}}{dE_{\alpha}} \Big|_{\text{splash}} &= \frac{6}{515} \times \frac{10^4}{60 \times 200} \times \frac{1}{10} \text{ m}^{-2} \text{ ster}^{-1} \text{ sec}^{-1} \text{ MeV}^{-1} \\ &= 0.00097 (\pm 0.0003) \text{ p/m}^2 \text{ ster. sec. MeV} \end{aligned}$$

$$\begin{aligned} \text{i.e. approx. } \frac{dj_{\alpha}}{dE_{\alpha}} \Big|_{\text{splash}} (160 < E_{\alpha} < 170 \text{ MeV}) &= 10^{-3} \text{ m}^{-2} \text{ ster}^{-1} \text{ sec}^{-1} \text{ MeV}^{-1} \\ &(\pm 0.3 \times 10^{-3}) \end{aligned}$$

(ii) 180 < E<sub>α</sub> < 300 MeV

$$N_{\alpha} = 28 \pm 5 \quad \tau = 515 \text{ min.}$$

$$\frac{dj_{\alpha}}{dE_{\alpha}} \Big|_{\text{splash}} (180 < E_{\alpha} < 300 \text{ MeV}) = 0.377 (\pm 0.067) \times 10^{-3} \text{ m}^{-2} \text{ ster}^{-1} \text{ sec}^{-1} \text{ MeV}^{-1}$$

These flux values, although tentative, should be correct to within an order of magnitude. The differential flux values were derived from the distribution of zero Cerenkov events in the Ch. 3, Ch 1A crossplot shown in Fig. 31.

## Chapter 5. - RIGIDITY SPECTRA OF HEAVY NUCLEI

"...time has come when the experimental data begins to interfere rather strongly with all hypotheses. It is a happy situation."

Yash Pal

### 5.1. Derivation of Spectral Exponents

The integral rigidity spectra of the predominant nuclear species and charge groups are shown in figures 33 → 39 inclusive. The data points derived by the present experiment have been extrapolated to the top of the atmosphere - see section 6.1. and are compared with the extensive measurements of Von Rosenvinge and Webber (90).

The data points for the integral spectra were derived in one of two different ways:

(i) The variation of geomagnetic threshold rigidity  $R_G$  with azimuth  $\theta_A$  is shown in figure 32. By correlating each event with the orientation of the telescope axis, it was possible to obtain the flux of particles with rigidity,  $R > R_G$ . The events were split into quadrants, and it follows that

$$j_{\text{WEST}}(Z_i) = \frac{N_{\text{WEST}}}{\Delta T_{\text{WEST}}} = j(Z_i; R > 10.5 \text{ GV})$$

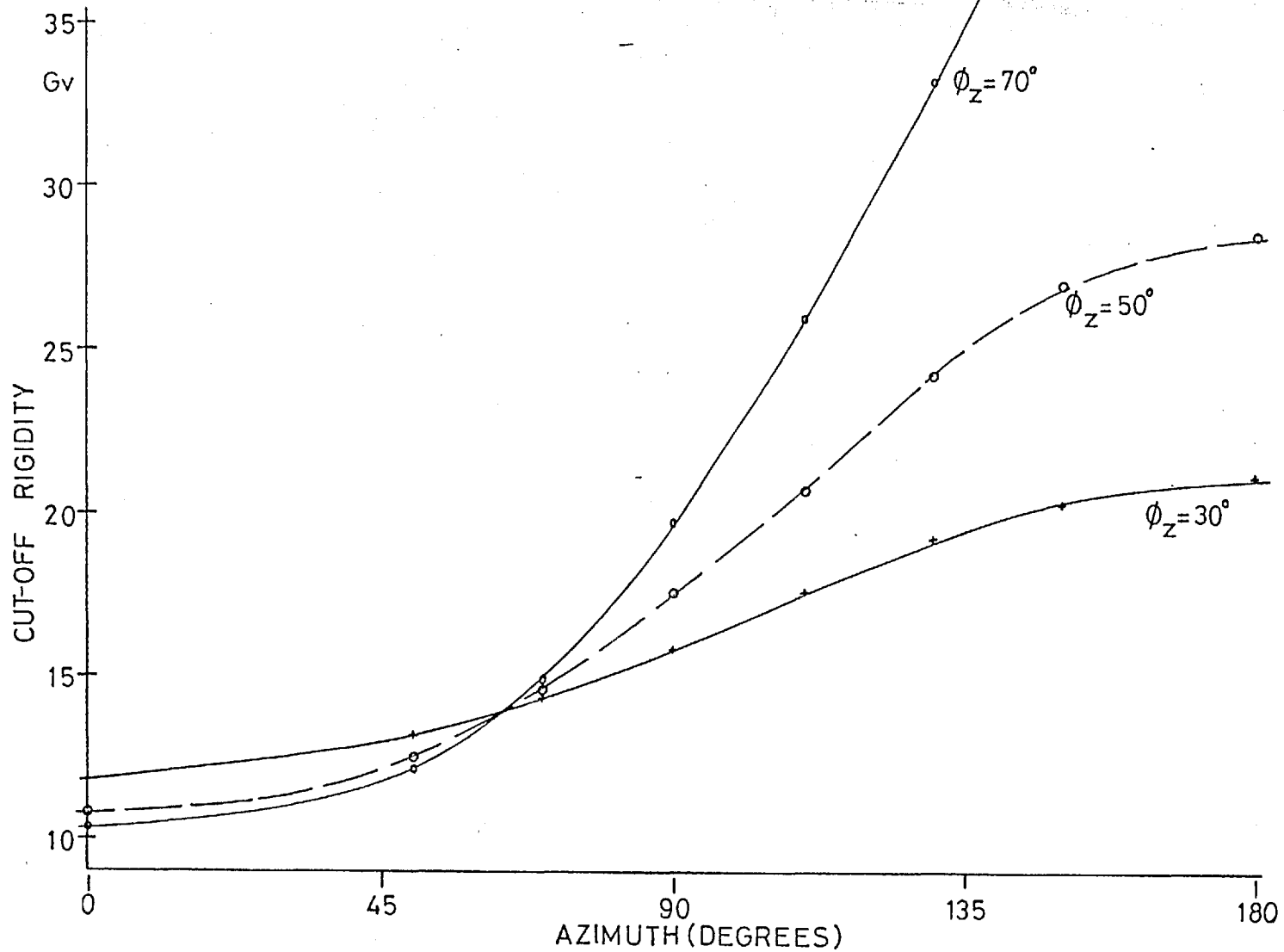


FIG. 32 VARIATION OF GEOMAGNETIC THRESHOLD RIGIDITY WITH AZIMUTH AND ZENITH ANGLES

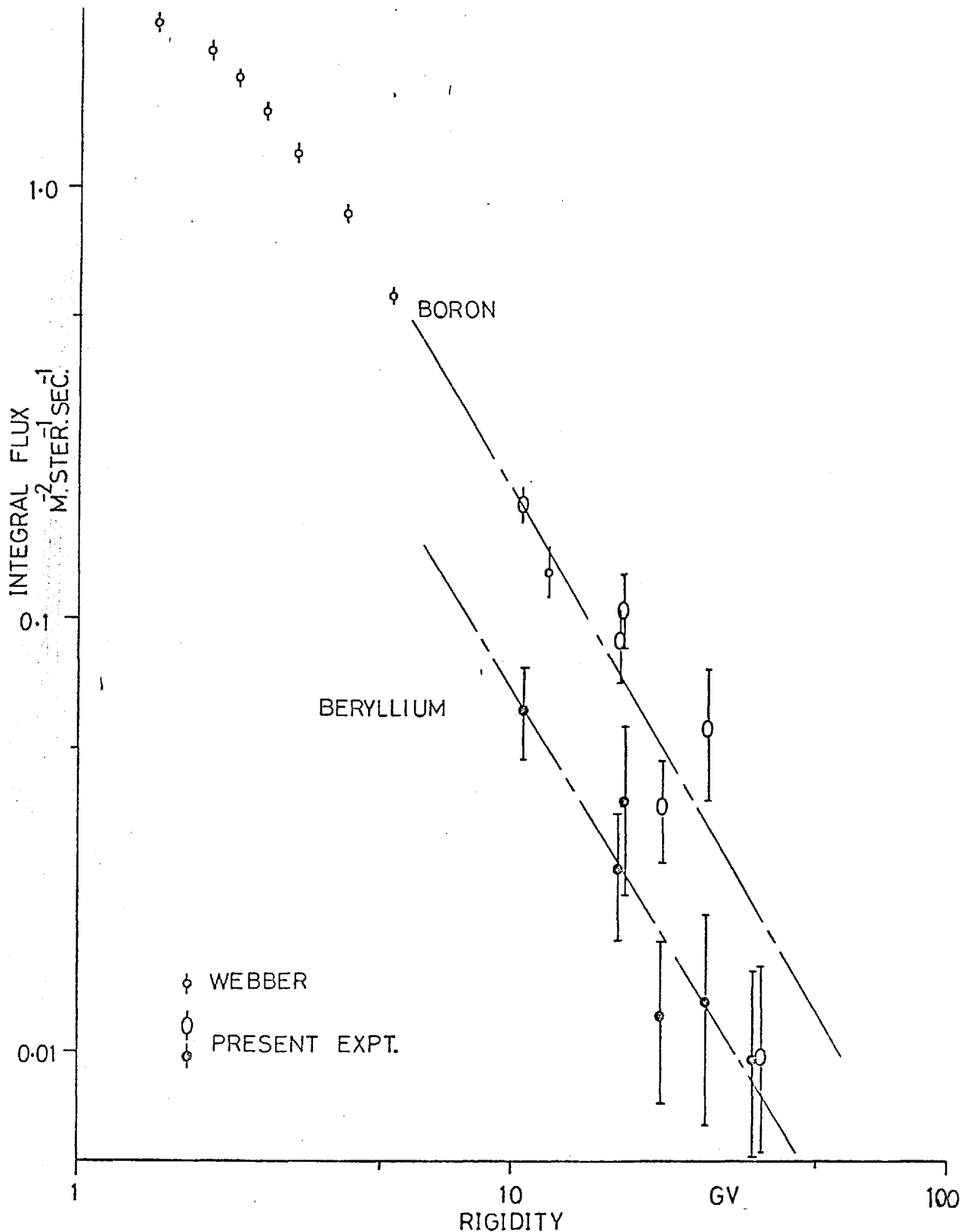


FIG 33 INTEGRAL RIGIDITY SPECTRUM OF BORON AND BERYLLIUM NUCLEI(AT TOP OF ATMOSPHERE)



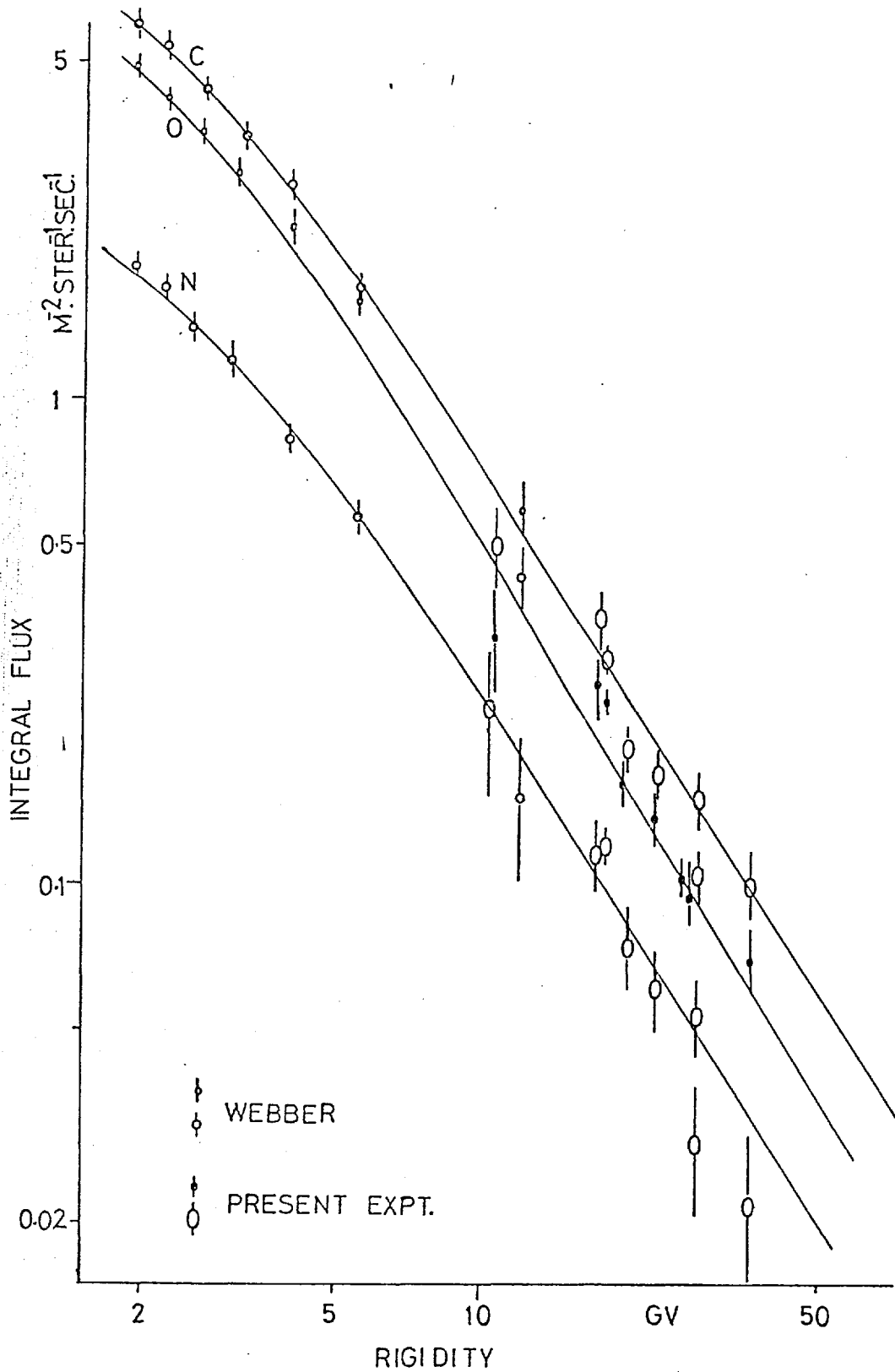


FIG 34 INTEGRAL RIGIDITY SPECTRUM OF CARBON NITROGEN AND OXYGEN(TOP OF ATMOSPHERE)

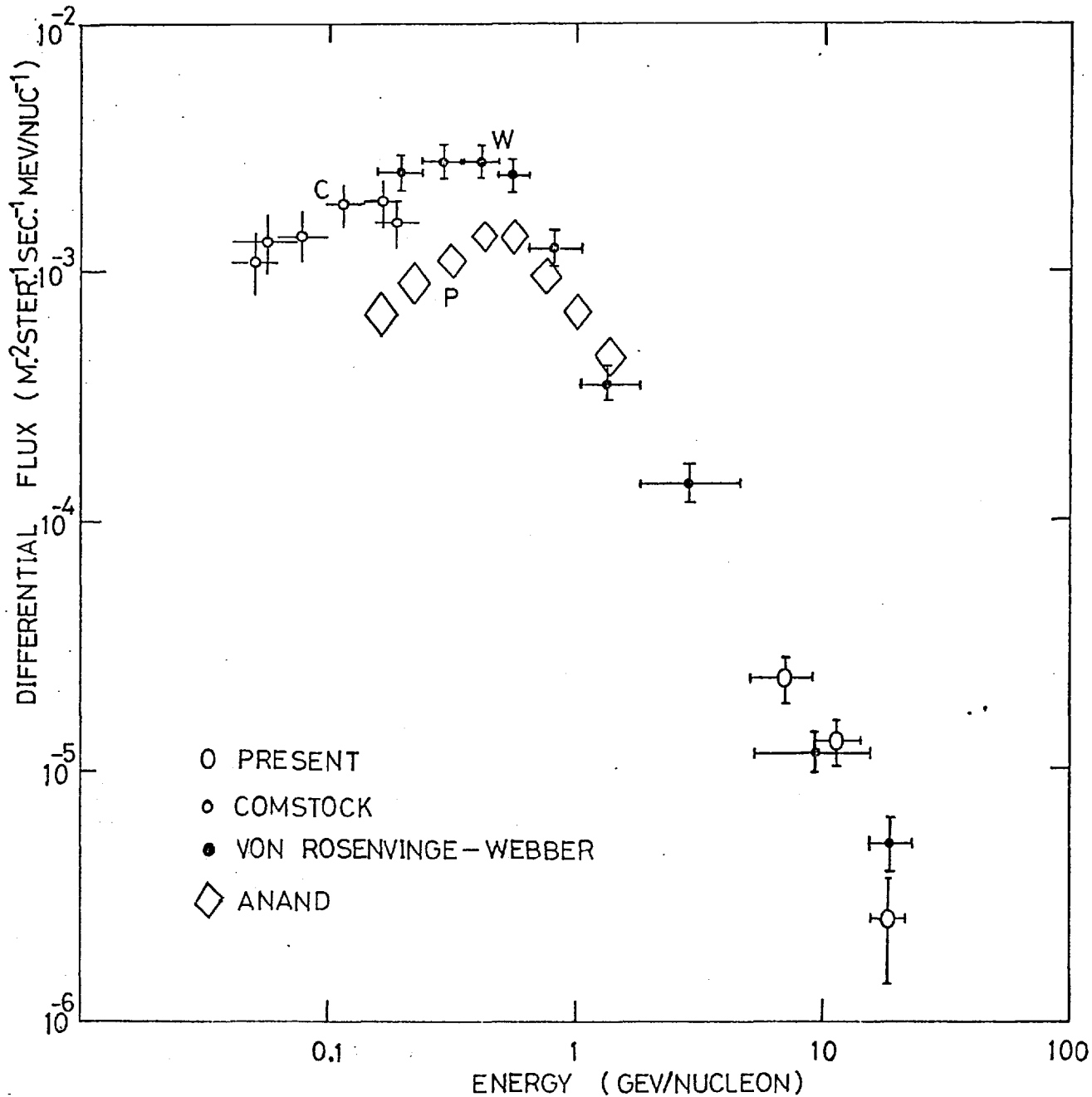


FIG. 35 DIFFERENTIAL ENERGY SPECTRUM OF NITROGEN - COMPARISON WITH PREVIOUS RESULTS.

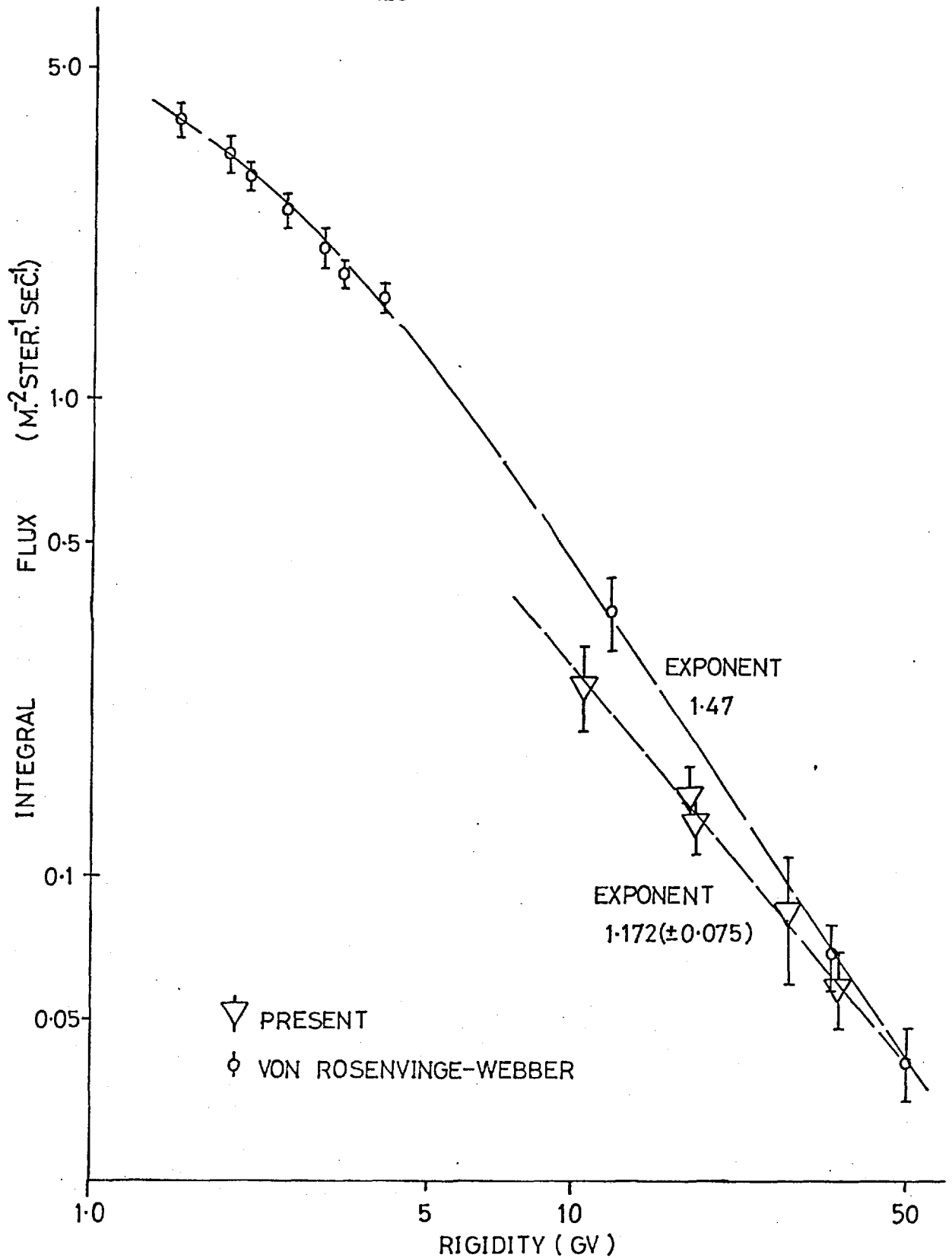


FIG. 36 INTEGRAL RIGIDITY SPECTRUM OF LH( $10 \leq Z \leq 14$ ) NUCLEI AT TOP OF ATMOSPHERE

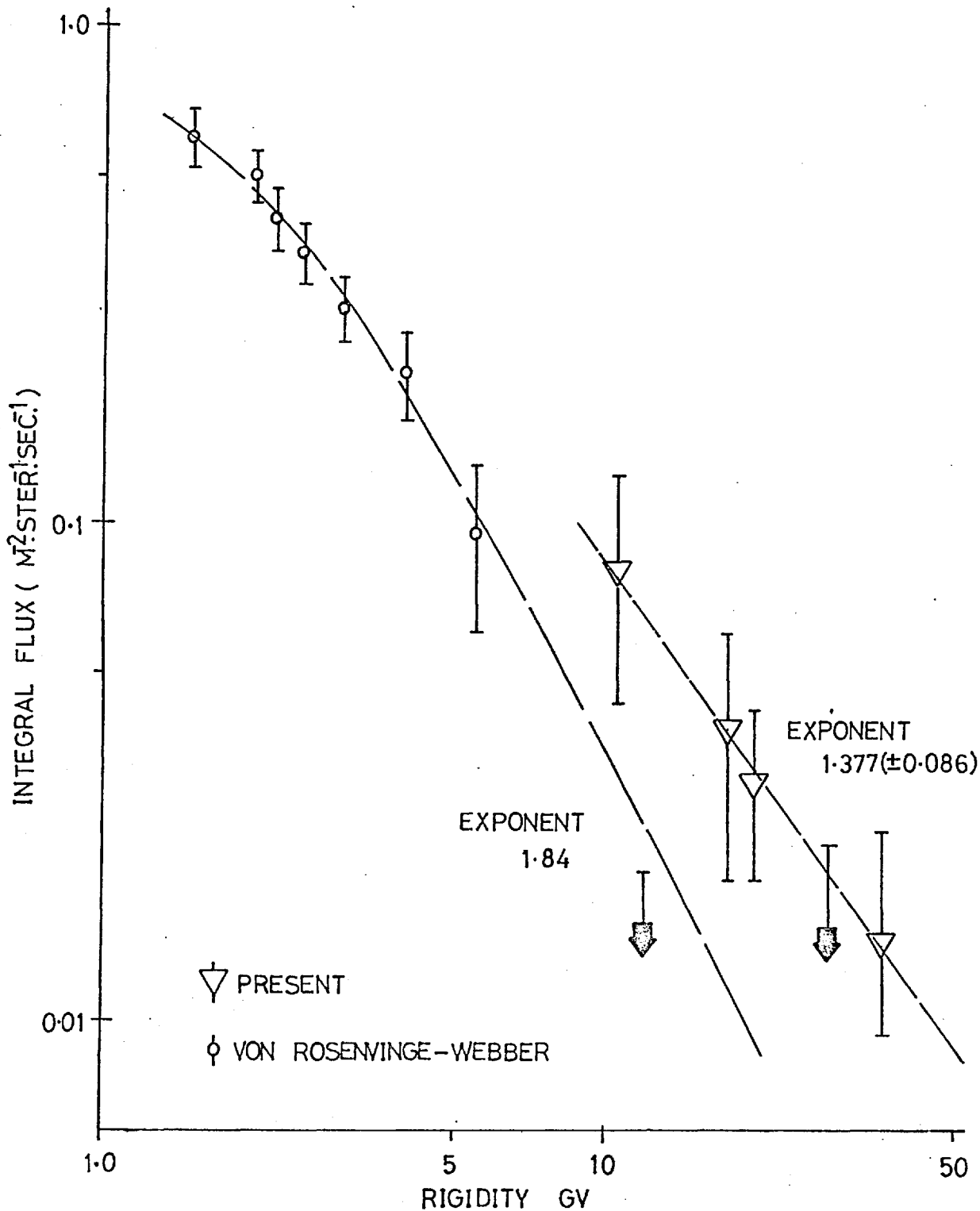


FIG. 37 INTEGRAL RIGIDITY SPECTRUM OF  $15 \leq Z \leq 19$  NUCLEI AT TOP OF ATMOSPHERE

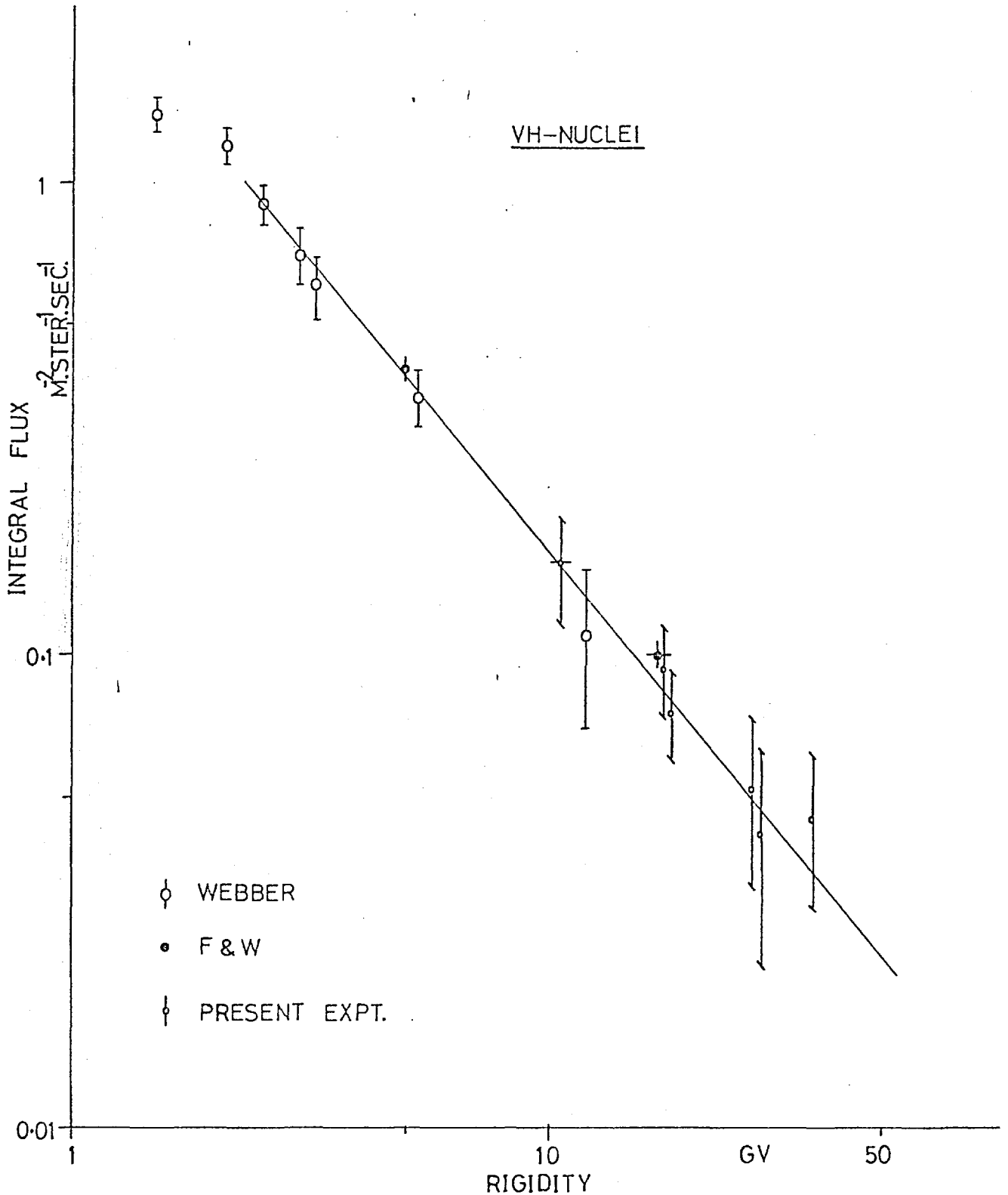


FIG 38 INTEGRAL RIGIDITY SPECTRUM OF VH (IRON GROUP) NUCLEI AT TOP OF THE ATMOSPHERE

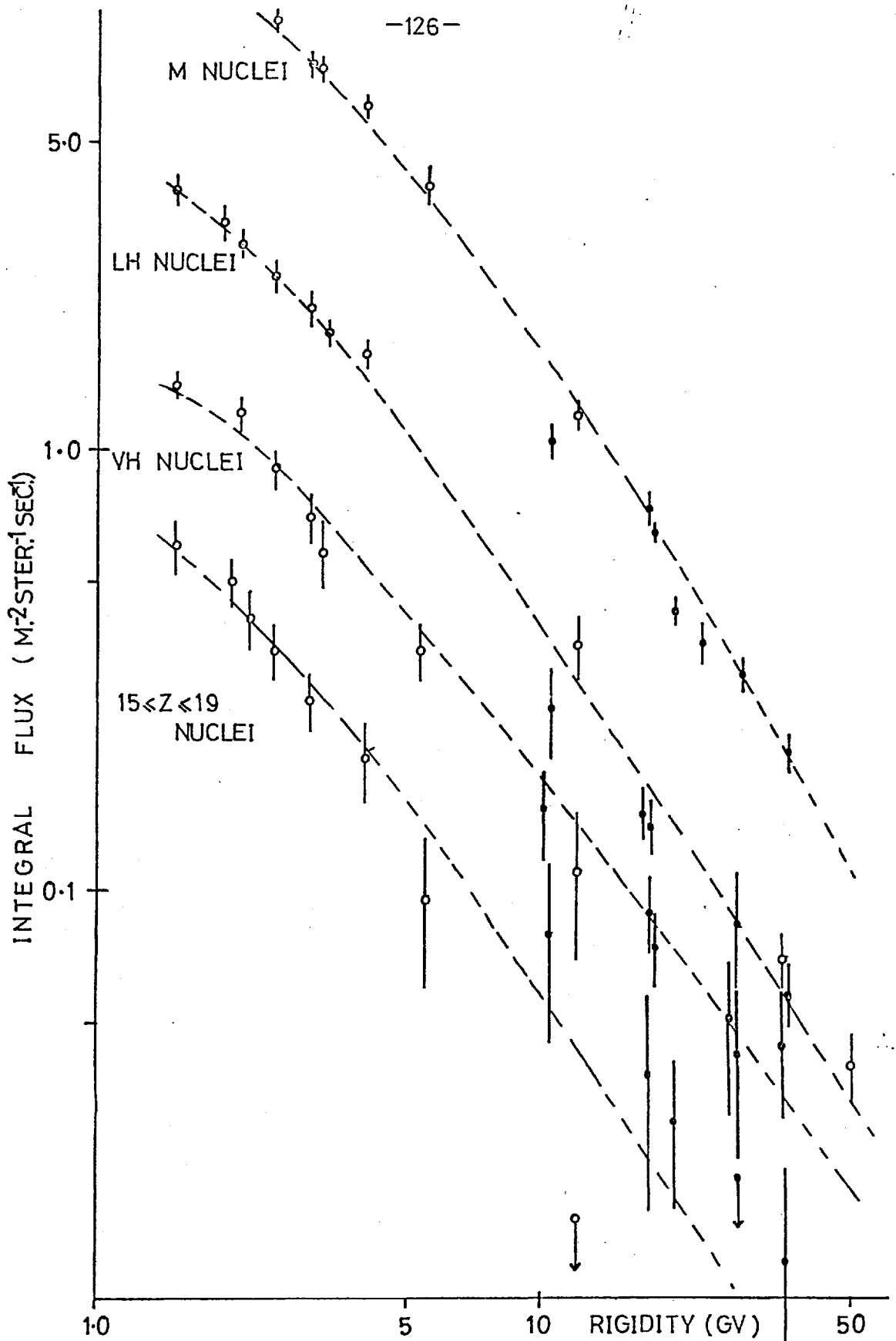


FIG. 39 COMPARISON OF INTEGRAL RIGIDITY SPECTRA OF HEAVY NUCLEI CHARGE GROUPS (AT TOP OF ATMOSPHERE)

$$j_{\text{EAST}}(Z_i) = \frac{N_{\text{EAST}}}{\Delta T_{\text{EAST}}} = j(Z_i; R > 28 \text{ GV})$$

The North and South events were combined to give

$$j_{\text{N-S}}(Z_i) = \frac{N_{\text{N-S}}}{\Delta T_{\text{N-S}}} = j(Z_i; R > 18 \text{ GV})$$

(ii) For each charge species, the output from the Cerenkov device is a function of the velocity of the particles as shown in figure 12. Using the pre-flight calibration curves, it was possible to determine the number of events whose velocity,  $\beta$ , and therefore rigidity,  $R$ , exceeded a certain value. In this way, integral rigidity flux estimates in the range  $18 \lesssim R \lesssim 36 \text{ GV}$  were possible.

$$j(>R) = \frac{N_{S_1, S_2 C}}{\text{TOTAL EXPOSURE TIME}}$$

The flux estimates derived were all corrected for dead time and spallation in the detector - as discussed in sections 3.2.5. and 4.4., and the fluxes for both flights were combined to improve the overall statistical accuracy of the results.

It is worth noting that the two techniques employed in the derivation of the integral rigidity flux points are independent of each other, and hence provide a valuable check on the consistency of the data.

An inspection of the integral rigidity spectra after extrapolation to the top of the atmosphere shows reasonable agreement with the results of Von Rosenvinge et.al. With the exception of the poor statistical data on the nuclei within the charge range,  $15 < Z < 19$ , the absolute fluxes derived in the present experiment are consistently lower than Von

Rosenvinge's. One possible reason for this is the effect of solar modulation at 10 GV.

The differential flux of charge group,  $i$ , observed at the earth,  $j_e(i)$ , is related to the flux in interstellar space,  $j_\infty(i)$ , by

$$j_e(i) = j_\infty(i) \exp(-\eta(t)/R)$$

where  $R$  = rigidity value in GV.

The time dependent parameter,  $\eta(t)$  is composed of two parts

$$\eta(t) = \eta_0 + \eta_1(t) \quad \begin{array}{l} \eta_0 = \text{residual modulation} \\ \text{parameter} \approx 0.65 \end{array}$$

The parameter  $\eta_1(t)$  depends upon the time that the measurements were made relative to the amount of solar activity. In order to demodulate the results of the present experiment  $\eta_1(t) \sim 1.42$  (for May 1970), and the differential flux values must be increased by  $\sim 20\%$  to give a demodulated absolute flux value. However, von Rosenvinge's flights were made in 1966 and the demodulated flux values at 10 GV are only  $\sim 7\%$  greater than the flux estimates presented.

The only serious discrepancy is the lack of an apparent 'crossover' in the relative abundances of carbon and oxygen claimed by von Rosenvinge et.al. No evidence has been found for such a 'crossover' of spectra in the rigidity range under consideration, however, there is some evidence that the best fit slope of the carbon nuclei is steeper than that of the oxygen nuclei. The statistical errors are too large to make a definitive statement.



If one assumes that the integral rigidity spectrum can be represented by a power law of the form:

$$j_z (> R) = k_z R^{-\gamma_z}$$

one can derive the best estimate of the spectral exponent,  $\gamma_z$  by applying the least-squares principle - see Topping (85).

$$\gamma_z = \frac{\{w\}\{wXY\} - \{wX\}\{wY\}}{\{w\}\{wXX\} - \{wX\}^2}$$

and

$$b = \frac{\{wY\}\{wXX\} - \{wX\}\{wXY\}}{\{w\}\{wXX\} - \{wX\}^2}$$

where  $X = \log R$

$$Y = \log j_z (> R)$$

$$w = 1/\sigma^2, \quad \sigma = \text{error in flux estimates}$$

{ } denotes summation over all values

In the derivation of the exponent,  $\gamma_z$  one assumes that the error in the rigidity is negligible.

The standard error in the exponent,  $\alpha_\gamma$  is related to the standard error of the flux estimates about the best fit spectrum,  $\alpha$  by

$$\alpha_\gamma^2 = \frac{\{w\}\alpha^2}{\{w\}\{wXX\} - \{wX\}^2} \quad (\text{Bond (86)})$$

where

$$\alpha = \frac{\{w(Y_{\text{exp}} - Y_{\text{act}})^2\}}{(N - 2)}$$

$Y_{\text{act}}$  = actual experimental flux value

$Y_{\text{exp}}$  = expected flux value given by the best fit line  $Y_{\text{exp}} = -\gamma_z X + b$

$N$  = number of flux measurements

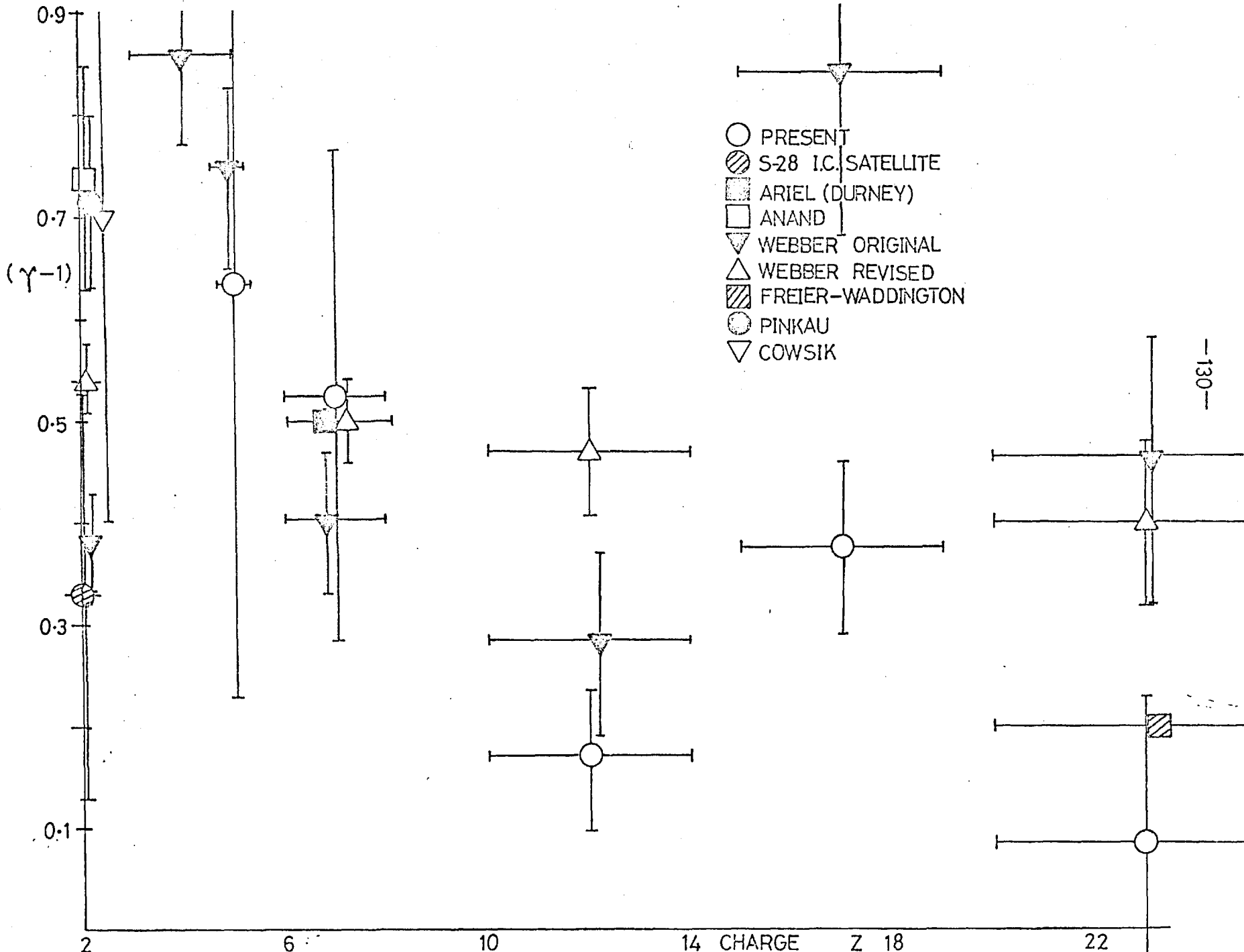


FIG 40 VARIATION OF INTEGRAL RIGIDITY SPECTRAL EXPONENTS WITH CHARGE FOR  $10 < R < 40$  GV

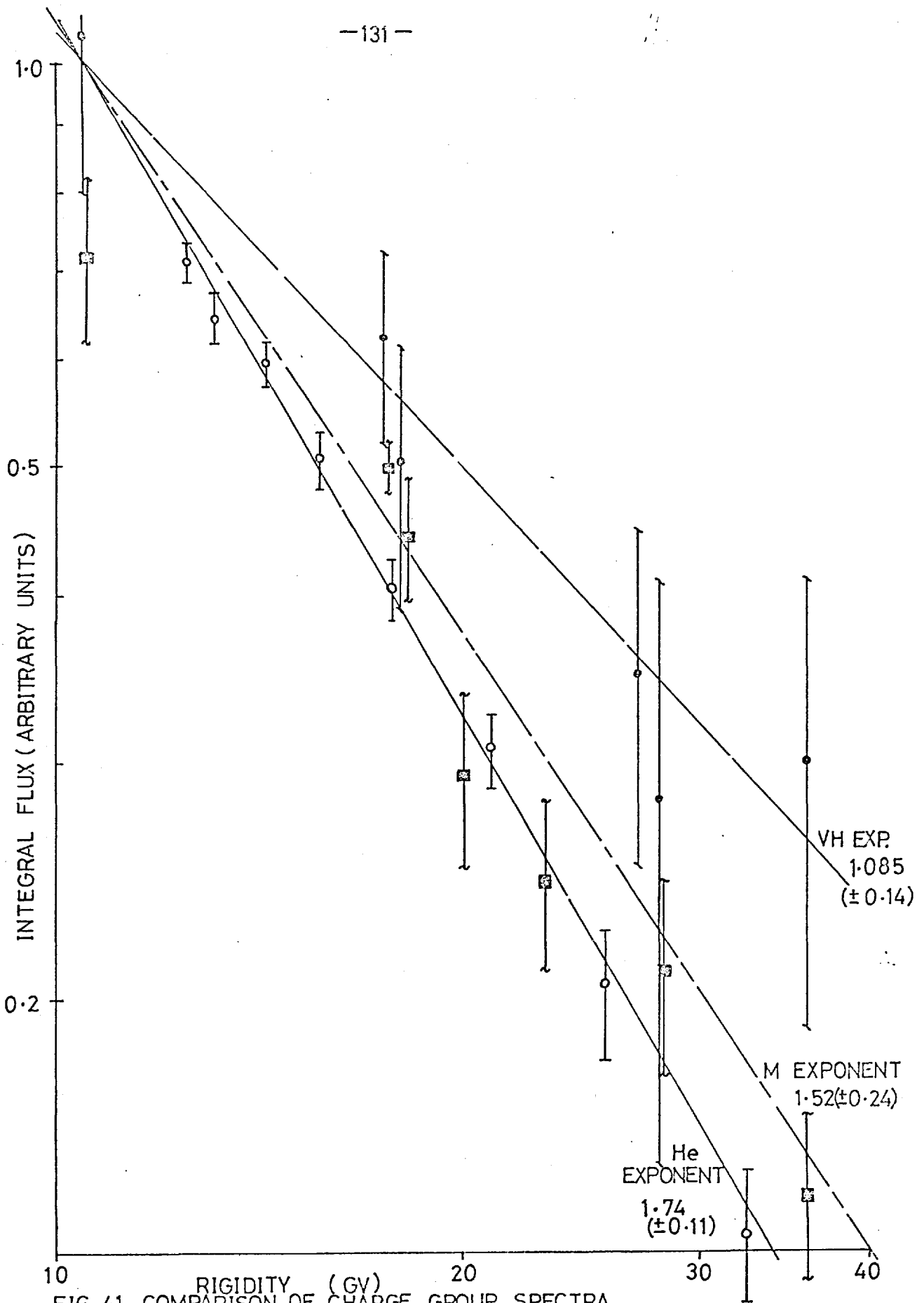


FIG 41 COMPARISON OF CHARGE GROUP SPECTRA

TABLE III: DISTRIBUTION OF EXPONENTS ABOUT THE MEAN

$\underline{\gamma}$	$\epsilon_{\underline{\gamma}}$	$\frac{w}{\underline{\gamma}}$	$\frac{w_{\underline{\gamma}}}{\underline{\gamma}}$	$\frac{d}{\underline{\gamma}}$	$\frac{w_{\underline{\gamma}} d_{\underline{\gamma}}}{\underline{\gamma}} \times 10^{-2}$
1.74	0.11	9.0	15.7	0.39	136.80
1.63	0.40	2.5	4.1	0.28	19.62
1.52	0.23	4.0	6.1	0.17	11.56
1.17	0.06	17.0	20.0	0.18	55.10
1.37	0.09	11.0	15.0	0.02	0.44
1.085	0.14	<u>7.0</u>	<u>7.5</u>	0.265	<u>49.00</u>
$\Sigma$		50.5	<u>68.4</u>		272.52

Weighted mean,  $\bar{\gamma} = \frac{\Sigma w_{\underline{\gamma}} \underline{\gamma}}{\Sigma w_{\underline{\gamma}}} = \frac{68.4}{50.5} = 1.35$

Standard error of weighted mean

$$\sigma = \frac{\Sigma w_{\underline{\gamma}} (\underline{\gamma} - \bar{\gamma})^2}{\Sigma w_{\underline{\gamma}} (n-1)}$$

$$= 0.100$$

Significance levels

+3 $\sigma$	+2 $\sigma$	+ $\sigma$	Mean	- $\sigma$	-2 $\sigma$	-3 $\sigma$
1.650	1.550	1.450	1.350	1.250	1.150	1.050

The values of the spectral exponents for the predominant charge groups, together with the estimated errors in the exponents are shown plotted as a function of the charge  $Z$  in figure 40. Also shown in this figure are the integral rigidity exponents derived by Anand et.al.(87), Freier and Waddington and the original and revised results of von Rosenvinge, Ormes and Webber. The satellite data of Durney et.al. (88) for medium nuclei is shown for comparison.

Whereas the results of von Rosenvinge et.al. are not inconsistent with a mean exponent of  $|\gamma| = 1.5$ , the present results (taken together with Anand's) suggest a functional relationship between the exponent,  $\gamma_Z$  and the charge,  $Z_i$ . It is clear that both the helium and the VH nuclei results are more than two standard deviations from the value, 1.5. This discrepancy cannot be explained in terms of solar modulation effects.

In figure 41 the fluxes of the VH-, M- and helium nuclei have been normalised to the same 'best-fit' flux value at a rigidity of 10.5 GV. Despite the relatively large error bars for the VH-nuclei, which reflect the smaller number of nuclei recorded, the conclusion must be that the integral rigidity spectra of the heavy nuclei in the primary cosmic rays are inconsistent with a fixed-spectral-exponent power-law (see Table III).

## 5.2. Rigidity Spectra, $10 < R < 40$ GV

### Review

In the past the experimental results of the spectral exponents at relativistic energies for heavy nuclei have been associated with large statistical errors, because of the low flux of heavy nuclei in the cosmic

radiation. Ginzburg (89) reviewed the experimental data, and concluded that the spectral exponent,  $\gamma_E$  of the total energy integral spectrum is given by

$$\gamma_E = 1.5 (\pm 0.2)$$

for any charge group. However, in reaching this conclusion, Ginzburg had to compare exponents relating to different energy ranges, and of low statistical accuracy. Singer (91) had proposed that the spectral exponent,  $\gamma_E$  should increase with increasing charge,  $Z$ , if, as was believed, the cosmic rays were accelerated by the process of collisions with magnetic fields suggested by Fermi (92).

If the integral spectrum can be denoted by

$$j(>E) = k E^{-\gamma_E}$$

then the differential spectrum is given by

$$j(E) = k E^{-(\gamma_E+1)}$$

Syrovatskii (93) has interpreted the exponent of the differential spectrum,  $(1+\gamma_E) = 2.5$  as being due to the equipartition of available energy between

(a) cosmic radiation

(b) magnetic fields

and (c) interstellar turbulence

Von Rosenvinge (90) has conducted the most accurate investigations into heavy nuclei spectra in the energy range  $500 < E < 10,000$  MeV/n, and he concluded that, although the spectral exponents of different nuclear

species showed wide variation, the results were still consistent with a variation about a mean value of  $\bar{\gamma}_E \sim 1.5$ . These measurements covered a lower energy range than that of the present experiment. Webber (94) suggests that there may be evidence that the spectral exponent increases with increasing charge. Hence, the question of the possible dependence of the spectral exponent on the charge has not yet been satisfactorily answered.

As far as the situation at higher energies is concerned, Abraham (95) and the ICEF team (96) have investigated cosmic ray jets in the energy range  $10^{10} < E < 10^{14}$  eV and conclude that the relative composition of heavies to helium and hydrogen is about the same as for lower energies. The presence of muon-rich extensive air showers of energies  $E > 10^{14}$  eV is thought to indicate heavy nuclei progenitors. McCusker (97) argues that the multicore extensive air showers may be due to heavy primaries, and if so, it is possible that there is an enrichment of heavies relative to protons in this energy range. As discussed in Section 1.2., the physical reason for this may be that cosmic ray nuclei of energy  $E > 10^{16}$  eV/n can escape from the galaxy, so that  $10^{16}$  eV protons are preferentially removed from the observed flux than the  $10^{16}$  eV heavies (which have a smaller energy per nucleon). This model is discussed quantitatively by Syrovatskii (11). At higher energies, Linsley and Scarsi (98) report that heavy primaries are completely absent - this may mean that these energetic cosmic rays are of metagalactic origin (and all initial heavy nuclei are destroyed during propagation by photodisintegration in collision with starlight photons).

Over the entire range of cosmic ray energies, it is impossible to fit a unique value for the spectral exponents. The integral exponent appears to vary between  $\gamma \sim 1$  at low energies, due to the shaping of the spectrum by ionization losses, to  $\gamma \gtrsim 1.5$  at very high energies where, presumably, leakage from the galaxy predominates. In the following section, the particular significance of the spectra in the rigidity range  $10 < R < 40$  GV will be discussed.

### 5.3. Significance of Spectra in Range $10 < R < 40$ GV

There are a number of mechanisms which can modify the source spectra of heavy nuclei during propagation through the interstellar space:

- (a) Leakage from the galaxy
- (b) Ionization energy losses
- (c) Solar modulation
- (d) Fragmentation energy losses
- (e) Interstellar acceleration mechanisms

#### 5.3.1. Leakage from the Galaxy

In the previous section it was argued that the effect of a possible leakage of different charge species out of the galaxy only became apparent at cosmic ray energies  $E \gtrsim 10^{16}$  eV/n. Hence, one would not expect leakage to be significant at the energies,  $E \lesssim 10^{10}$  eV discussed in the present experiment. Also, as pointed out by Ginzburg (89), the diffusion process is most likely due to the diffusion of the cosmic rays out of the magnetic, cloudlike irregularities within the galaxy. This process should depend



therefore on the rigidity of the cosmic ray, and any spectral shaping for one particular charge group should be identical to the shaping of any other charge group (with  $A/Z = 2$ ) as far as the integral rigidity spectrum is concerned - see Appendix C.

### 5.3.2. Ionization

Peters (99) shows that the specific ionization loss of a relativistic particle of charge,  $Z_i$  in interstellar hydrogen is  $4.7 Z_i^2$  MeV.grm.cm<sup>-2</sup>. As an estimate of the energy loss,  $\Delta E$  by ionization per nucleon per mean free path, one obtains

$$\Delta E = \frac{4.7 Z_i^2}{A_i} \cdot \frac{m_p}{\pi r_o^2 A_i^{2/3}} = 34.5 Z_i^{1/3} \text{ MeV}$$

where  $m_p$  = proton mass = 940 MeV

$r_o$  = nucleon radius,  $1.5 \times 10^{-13}$  cm

The expression is clearly a slowly varying function of the charge, and the total energy loss per nucleon per mean free path for iron is only 100 MeV. In the energy range under consideration ( $5.0 < E < 20$  GeV/n), it can be seen that the ionization losses in interstellar space, after the initial injection from the source, do not shape the spectrum.

### 5.3.3. Solar Modulation

The currently accepted theories of solar modulation, e.g. Parker (100) postulate a rigidity dependence of the modulation function, and the effect of any modulation should be to shape the integral rigidity spectra of different charge groups in exactly the same way. However, the present flights were carried out close to solar minimum, and the estimated residual

solar modulation at 10 GV is of the order of 2%, which is small enough to be negligible in the arguments which follow - see Appendix B.

#### 5.3.4. Fragmentation

For relativistic nuclei, the cross-section for nuclear collisions is proportional to the geometrical cross-section of the nuclei, and is energy independent - see Cleghorn et.al. (84). Also, Ginzburg (101) and Peters (99) agree that, in the relativistic region of energies, there is negligible energy loss during the fragmentation of a heavy nucleus because the secondary fragments are produced in the cosmic ray centre-of-mass frame of reference with small kinetic energies. The spectra of the fragmentation products should be the same as the spectra of the parent nuclei and it also follows that the passage of each charge group through the interstellar medium will simply reduce the intensity of the flux of particles within a certain rigidity range, but the observed rigidity spectra will be a facsimile of the source spectra unless charge-dependent interstellar accelerating mechanisms are present.

#### 5.3.5. Interstellar Acceleration Mechanisms

As Peters (99) points out, the very presence of heavy nuclei in the cosmic radiation with energies of the order of  $E > 10^{12}$  eV indicates that catastrophic nuclear events cannot be invoked to explain acceleration to such energies. The nuclei would be completely disrupted in such an event because

$$\frac{\text{Binding Energy}}{\text{Total Energy Imparted}} \ll 1$$

The early models proposed by Millikan et.al. (102) of the spontaneous annihilation of atoms in space or Klein (103) of matter-antimatter annihilations would seem unlikely. Fermi (92) proposed a theory of slow continuous acceleration of charged particles in interstellar space

in which the particles

gain energy from the kinetic energy of interstellar matter by colliding with magnetic fields assumed to be attached to highly ionised gaseous clouds in our galaxy. Fermi realised that there were numerous shortcomings to his original model, and these have been discussed by Morrison (104).

One problem was that the heavy nuclei required very high injection energies  $\sim 10^8$  eV before Fermi's statistical accelerations could take place, and this placed severe constraints on any acceptable injection mechanisms. Another, more important discrepancy between the model and the experimental results concerned the spectra of different charge groups.

The total energy increase per collision with a magnetic cloud can be represented by

$$\frac{dU}{dn} = \alpha U - \beta(U)$$

function of            radiation or collision loss term.  
velocity of  
clouds

The minimum energy for acceleration is when

$$\frac{dU}{dn} = 0$$

i.e.

$$U_{\text{critical}} = \beta(U_c) / \alpha = \text{injection energy}$$

The particle's energy increases exponentially with a time constant,  $1/\alpha$  during the acceleration process, but the particles of a particular charge group, i undergo simultaneous nuclear absorption. If the lifetime

of this group is  $\tau_i$  against absorption, it can be shown that

$$\text{Spectral exponent, } \gamma_i = 1 + \frac{1}{\alpha \tau_i}$$

Qualitatively this means that as the heavier nuclei have shorter lifetimes against ionisation and nuclear absorption (due to larger geometrical cross-section), fewer heavier nuclei survive long enough to be accelerated to the highest energies and hence, the energy/nucleon spectra or rigidity spectra should be much steeper for the heavies than for the light nuclei.

Note,

$$\tau_i \propto A_i^{-2/3} \quad \text{where } A_i \text{ is the atomic mass of the } i^{\text{th}} \text{ species.}$$

The experimental results, however, seemed to indicate that the exponents of each charge group were identical and Morrison suggested a possible way in which the model could be reconciled with this experimental fact. He assumed that the cosmic ray diffused around the galaxy for a long time compared to the average time for escape from the galaxy along straight line paths but for short times compared to the mean lifetime before collision with interstellar hydrogen. In this case, the exponent becomes

$$\gamma = 1 + \frac{1}{\alpha T} \quad \text{where } T \text{ is average lifetime in galaxy for all charge groups.}$$

Also, in order to explain the observed proton exponent, the model now required a greater rate of energy gain,  $\alpha$  and this reduced the required injection energy of the heavy ions. However, from an astrophysical point of view, this new rate of energy gain is difficult to believe.

To summarise, if appreciable, slow interstellar acceleration is effective, it is most likely to be a Fermi-type mechanism and the effect of this acceleration mechanism on the source spectra is either,

(a) negligible - if the propagation times through the interstellar medium after injection are short compared to the lifetime against nuclear absorption, or

(b) it will produce a marked dependence of the exponent of the rigidity spectrum on the charge,  $Z_i$ , and this dependence will be such that  $|\gamma_Z|$  increases as  $Z_i$  increases.

#### 5.4. Discussion of Results

Although the interpretation of the results of this experiment lean heavily upon the helium exponent of Anand et.al. (87), this experimental result is the most significant in the rigidity range  $10 < R < 40$  GV at the present time.

In what follows, it will be assumed that a functional relationship,  $\gamma(Z_i)$  does indeed exist, and the implication to the source accelerating mechanism and interstellar accelerating mechanism will be discussed briefly.

##### A. Interstellar Fermi Acceleration Mechanism

The results of the present experiment indicate that, in the rigidity range  $10 < R < 40$  GV, there is no evidence for a Fermi-type interstellar acceleration. In the statistical equilibrium model of cosmic ray propagation - see Ramaty and Lingelfelter (31) - it is argued that, in order to explain the discrepancy between cosmic ray age and the lack of isotropy, the lifetimes of the heavy nuclei must be dominated by the collision probability. Hence, we would expect to see a marked dependence of exponent,  $\gamma_i$  on the mass of the nuclear species under consideration. The present results can only be reconciled with the theory if one also assumes that

the rigidity spectra of the heavies from the source has an even greater dependence on the mass of the nuclei being injected into space. Freier and Webber (106) found no evidence for this when investigating the rigidity spectra of electrons, protons and alphas accelerated during flare conditions on the sun.

Ramadurai (48) proposed that the puzzling low-energy results reported by Comstock et.al. (45) and attributed by them to a two-component propagation model, could be explained if one assumed that ionisation losses were effective during Fermi acceleration for the simple one-component model. By this mechanism, Ramadurai could explain the constancy of the He/VH ratio down to low energies. However, another prediction of this theory is that the spectral exponents of the heavier nuclei should be steeper than for lighter nuclei - in contradiction to the present experiment. Hence, Ramadurai's model cannot be accepted on the basis of the present results.

It has been shown that ionisation processes during and after possible interstellar acceleration contradict the present results. There is the possibility, however, that the cosmic rays underwent ionisation at low energies and then were accelerated to their current energies.

#### B. Ionization at Low Energies - Kristiansson's Theory

Kristiansson (107) was the first to propose that cosmic rays had traversed matter at low energies and had then been accelerated to the energies observed. He based this conclusion on the charge distribution of heavies with  $15 < Z < 26$ . The observed relative abundances could be

reproduced if one assumed that an initially pure sample of iron nuclei had fragmented at energies of the order of  $E \sim 200 \text{ MeV/n}$ . Von Rosenvinge (108) criticised this theory on the basis of the observed  $^{Be}/M$  ratio. The currently available fragmentation probabilities show an energy dependence which Von Rosenvinge (108) believed would produce  $^{Be}/M \sim 0.18$  if Kristiansson's theory was correct, whereas the experimental values give  $^{Be}/M \rightarrow 0.42$ . However, this was on the assumption that  $^7\text{Be}$  was the dominant beryllium isotope. Present evidence - see Corydon-Peterson (109) - point to  $^9\text{Be}$  and/or  $^{10}\text{Be}$  as the dominant isotopes in the primary cosmic radiation, and the fragmentation probabilities of heavier nuclei into these isotopes is not well known at present. Hence, it is possible that the  $^{Be}/M$  experimental result is consistent with Kristiansson's model.

On the basis of this model, it is possible to see qualitatively how the observed charge-dependent rigidity exponents are produced. If the ionisation takes place before the acceleration, the heavy nuclei, especially those at lower energies, will be removed from the cosmic ray flux and the spectrum of the heavies will be flattened more than the spectrum of the lighter nuclei. Also, the abundance of the heavies will drop considerably. Hence, before the acceleration, the exponent of the heavy nuclei spectrum should be small, and  $\gamma_H \rightarrow 0$ . The effect of a subsequent Fermi-type acceleration would be to increase the exponent of the heavies more than the lighter ions, and so offset the initial difference in exponent values.

### C. Charge Dependent Injection Mechanism

This final possibility is that, when cosmic rays are ejected from supernovae, or other possible sources, the accelerating injection mechanism is charge dependent. In the past, it has been assumed that the accelerating process is independent of the charge, i.e. that all nuclear species have the same source spectra. Biswas and Fichtel (110) have discussed this idea which is based upon the correspondence between the compositions of nuclear species accelerated from the sun and the abundances compiled from spectroscopic data. They argue that a charge dependent acceleration would introduce large discrepancies between solar cosmic ray compositions and solar compositions (in situ.). Also, as mentioned before, Freier and Webber (106) found no evidence for a charge dependent effect.

However, it is probable that the flare mechanism on the sun is totally different from cosmic ray source accelerating mechanisms and hence, the extrapolation of the charge independent hypothesis to source regions may be totally unjustified. The supposition of charge-independency is the cornerstone of all arguments on the source composition. Hence, if the present results indicate that heavy nuclei are preferentially accelerated by the sources, all hopes of deducing the nucleosynthesis processes within the sources prior to acceleration will be squashed. This is certainly not a reason for distrusting the results, but it introduces another problem, namely, what acceleration mechanism can be invoked to explain the observed dependence of the integral rigidity exponent on the charge,  $\gamma (Z_i)$  ?

In this case, the Fermi mechanism or its variants cannot be invoked (see Kaplon and Skadron (14), Layzer (13)) and the Hayakawa (105) hydro-



magnetic shock mechanism is also ruled out. Melrose (16) and Tsyтович (17) discuss the possibilities of waveparticle interaction giving rise to the preferential acceleration of heavy ions. One such mechanism discussed is a resonant acceleration process, when the wave frequency is a harmonic of the ions gyrofrequency in the plasma. Another mechanism discussed is the acceleration of the particle by a random distribution of Alfvén waves. More theoretical work is required on the effects of such mechanisms on the final accelerated spectra.

#### 5.4.1. Conclusion

The results presented here are difficult to understand in terms of currently accepted source accelerating mechanisms and detailed propagation models. In order to explain these results by themselves, it is necessary to assume either

(i) that heavy nuclei are preferentially accelerated at the source, i.e. they have a hard spectrum. In this case it will be difficult to deduce how far the nucleosynthesis stage had progressed before the acceleration phase, and a new acceleration mechanism must be invoked, or

(ii) that the observed spectral shapes are due to cosmic ray propagation at low energies, during which time the particles underwent ionisation losses, in the source region followed by acceleration to the energies currently observed. This implies a two-stage acceleration mechanism. In stellar interiors, the energy distribution of particles is described by the Maxwell-Boltzmann law, because the mean free path is extremely small. The particles are accelerated by non-thermal mechanisms to energies probably of the order of a few hundred MeV/nucleon - as in solar flares, and undergo Coulomb interactions in the source regions before release into

the interstellar medium. The advantage of this model is that no new accelerating mechanisms need be invoked.

The ultimate test of either model must be further, more accurate measurements of the spectra of heavy nuclei in this range of rigidities, and comparison of the predictions of either model with present experimental data.

Chapter 6 - NUCLEAR COMPOSITION OF COSMIC RAYS - CHARGE SPECTRUM

Similarities and differences between the distribution of the elements in the cosmic radiation and in nature can be expected to give very important information about the history of the radiation. In particular, the comparison of extrapolated source abundances and the spectroscopic abundances for specific astrophysical objects may locate the dominant sources of the cosmic radiation.

6.1. Extrapolation to Top of Atmosphere

Heavy nuclei of charge,  $Z_i$  and mass number,  $A_i$  undergo fragmentation when they traverse matter. The cross-section for inelastic collision,  $\sigma$ , is best represented by the geometrical cross-section of the nucleus.

$$\sigma_i \sim \pi r_i^2 \sim \pi (1.3A_i^{1/3})^2 \times 10^{-26} \text{ cm}^2$$
$$\sigma_i \propto A_i^{2/3}$$

The heavier the nucleus, the more likely the possibility of collision. The measured cosmic-ray fluxes of a balloon-borne detector must be extrapolated to the top of the atmosphere in order to derive the true primary fluxes. The extrapolation to the top of the atmosphere is particularly simple because it is essentially a 1-dimensional diffusion problem in which the cosmic ray path length is energy independent.

The observed flux is the sum of the residual primary component  $j_1(x)$  and secondary fragmentation products  $j_2(x)$  after passage of the beam

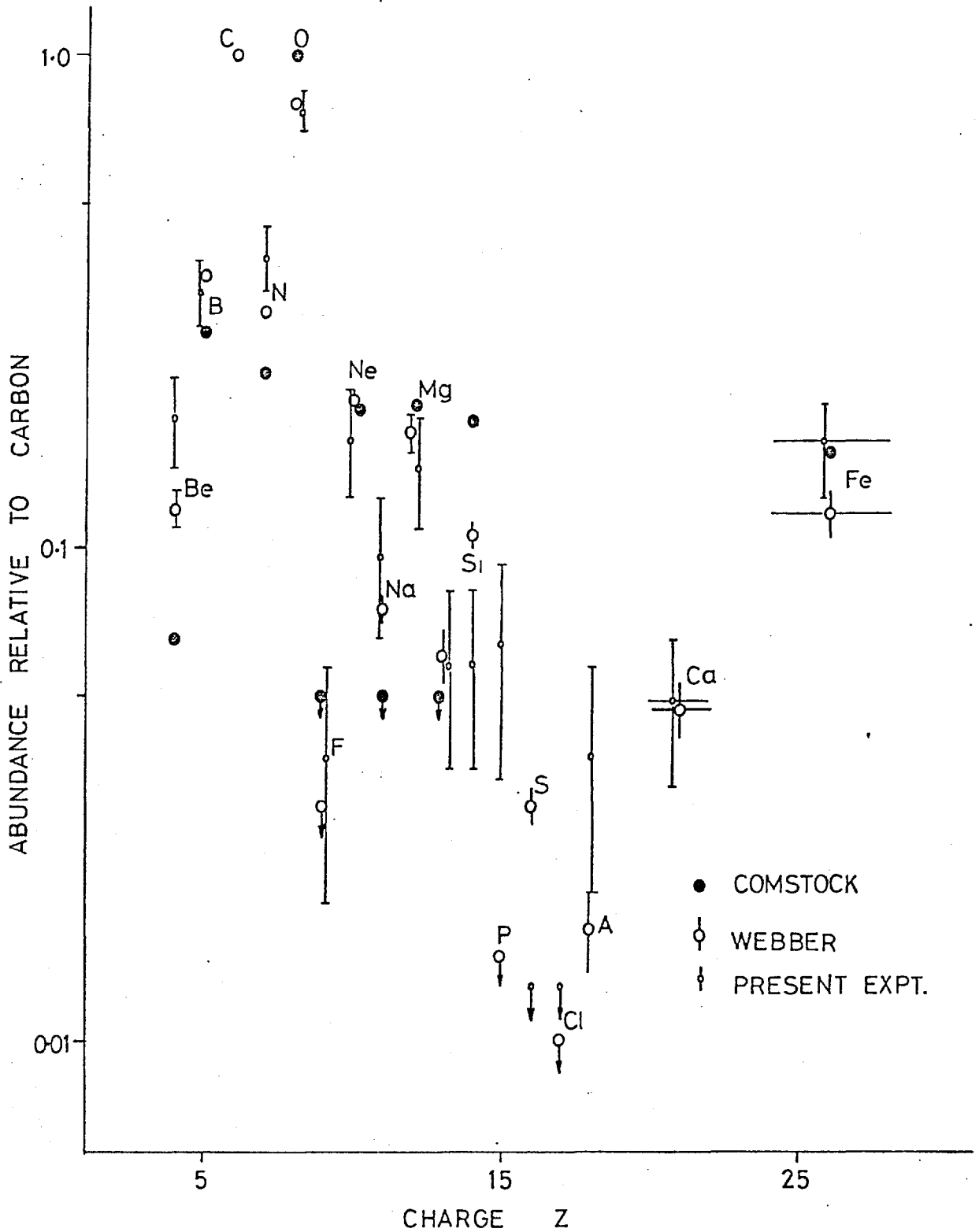


FIG.42 CHARGE COMPOSITION OF THE PRIMARY COSMIC RAYS

through  $x \text{ grm.cm}^{-2}$ . (Tertiary products and higher can be neglected at balloon altitudes because of the small amount of residual atmosphere.)

$$j(x) \Big|_i = j_1(x) + j_2(x)$$

$$j_1(x) = j_1(0) \exp(-x/\lambda_i) \quad \lambda_i = \text{mean free path}$$

between collision for  $i^{\text{th}}$   
species

$$j_2(x) = \sum_{j>i} j_j(0) \cdot P_{ij} \{1 - \exp(-x/\lambda_j)\}$$

$$P_{ij} = \text{fragmentation probability of } j^{\text{th}}$$

species into  $i^{\text{th}}$  species.

and  $j(0)$  refers to flux at top of atmosphere.

These equations can be solved systematically by considering firstly the heaviest nuclei present, the iron group and then successively lighter nuclei.

The results of the present flight were extrapolated to the top of the atmosphere by using the fragmentation probabilities deduced by Waddington (111) from the semi-empirical mass formulae of Rudstam (112) and the mean free paths,  $\lambda_i$  deduced by Cleghorn et.al. (84) and von Rosenvinge (90) whose values are derived from measurements on the spallation of heavy nuclei at different depths in the atmosphere. The float altitude of the combined results was 120,000 ft. which corresponds to  $5.0 (\pm 0.2) \text{ grm.cm}^{-2}$  residual atmosphere. As the telescope was inclined at  $50^\circ$  to the vertical, the effective mean path length of the cosmic ray beam was

$$\bar{x} = 7.5 (\pm 0.5) \text{ gm.cm}^{-2}$$

and this value was used in the extrapolation procedures.

The relative elemental abundances at balloon-altitude are shown in Fig. 42 together with von Roserving and Webber's (90) results at lower energies and also the satellite results of Comstock (45). The overall agreement between the present results and previous results is good, and is indirect proof that the charge groups were allocated correctly.

The elemental abundances after extrapolation to the top of the atmosphere are shown in table IV. It is now possible to compare the results of the present experiment with previous results on charge composition.

#### 6.1.1. ( $L/M$ ) Light to Medium Ratio

This ratio is important because it is an indicator of the effective path length traversed by medium nuclei. The value derived in the present experiment at the top of the atmosphere is

$$L/M = 0.285 (\pm 0.035)$$

This value is in excellent agreement with the results of O'Dell et. al. (24); Webber (72); Von Roserving et.al. (90); Durgaprasad (113); Anand et.al. (114); Balasubrahmanyam et.al. (115) as shown in Fig. 43.

Although the early results of this ratio indicated an energy dependence, the latest definitive results of von Roserving indicate that the ratio is constant over the whole energy range.

TABLE IV      EXTRAPOLATION TO TOP OF ATMOSPHERE

Element	Abundance relative to Carbon
Li	0.250
Be	0.150
B	0.225
C	1.000
N	0.368
O	0.825
F	(see text)
Ne	0.155
Ma	0.100
Mg	0.144
Al	0.060
Si	0.054
K	
Ca	} 0.050
Si	
Fe	0.274

TABLE V :  $(\frac{H}{M})$

$E$ (MeV/n)	$(\frac{H}{M})$	References
100	0.42(+0.05)	Comstock et.al. Ap.J., <u>146</u> , p.51
200-700	0.34(+0.05)	Aizu et.al., Suppl.Prog.Theor.Phys., <u>16</u> , p.54
700	0.39(+0.04)	Koshiha et.al., Phys.Rev., <u>131</u> , p.2692
1500	0.38(+0.04)	Judek et.al., Can.J.Phys., <u>44</u> , p.1121
1500	0.46(+0.04)	Durgaprasad et.al., Phys.Rev., <u>D1</u> , p.1021

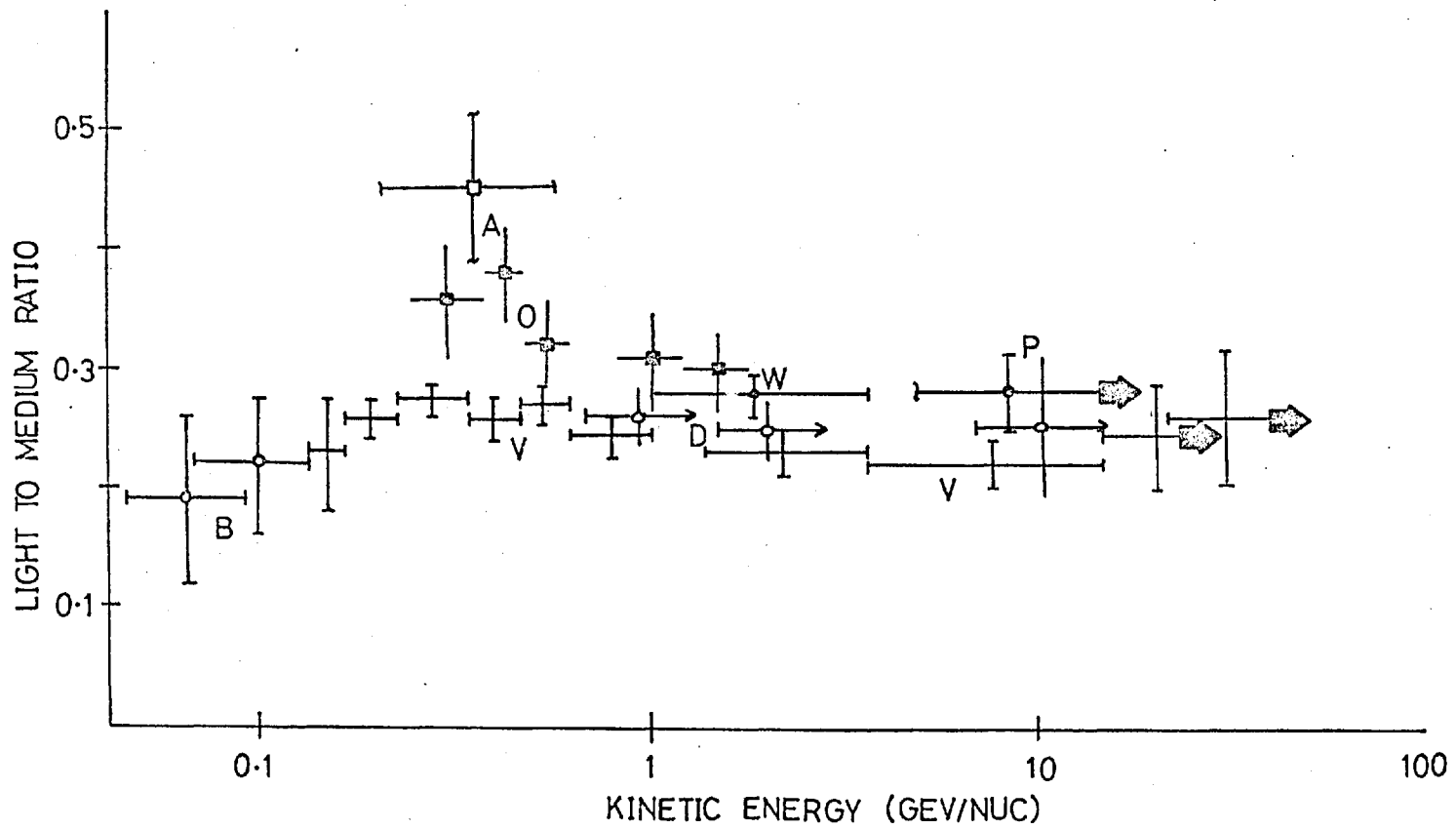
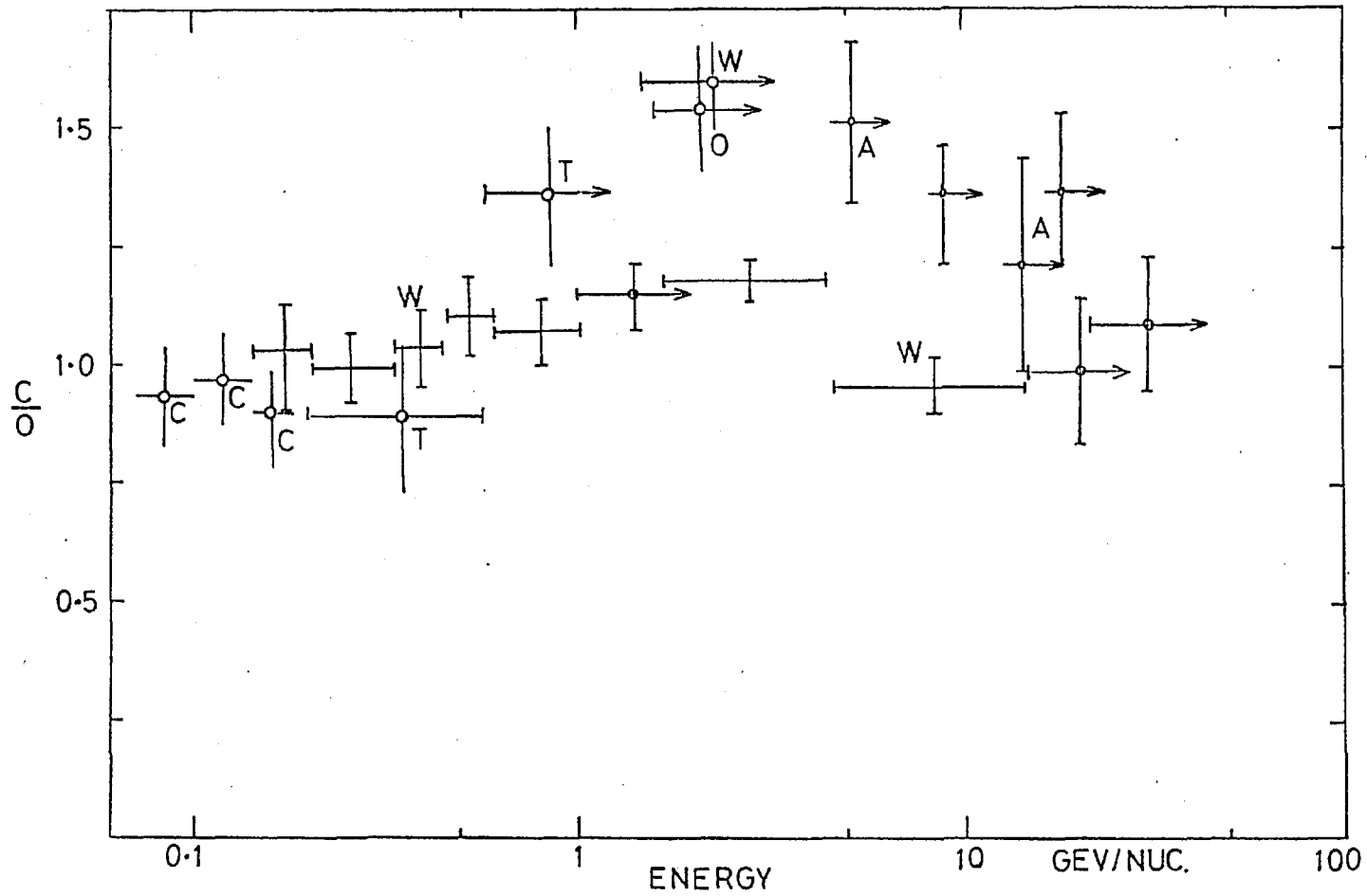


FIG 43 ENERGY DEPENDENCE OF THE LIGHT TO MEDIUM NUCLEI RATIO  
 A-ANAND B-BALASUBRAHMANYAN D-DURGAPRASAD O-O'DELL  
 P-PRESENT V-VON ROSENVINGE W-WEBBER





**FIG.44** ENERGY DEPENDENCE OF CARBON TO OXYGEN RATIO  
 T-ANAND C-COMSTOCK A-PRESENT W-VON ROSENVINGE  
 O-O'DELL

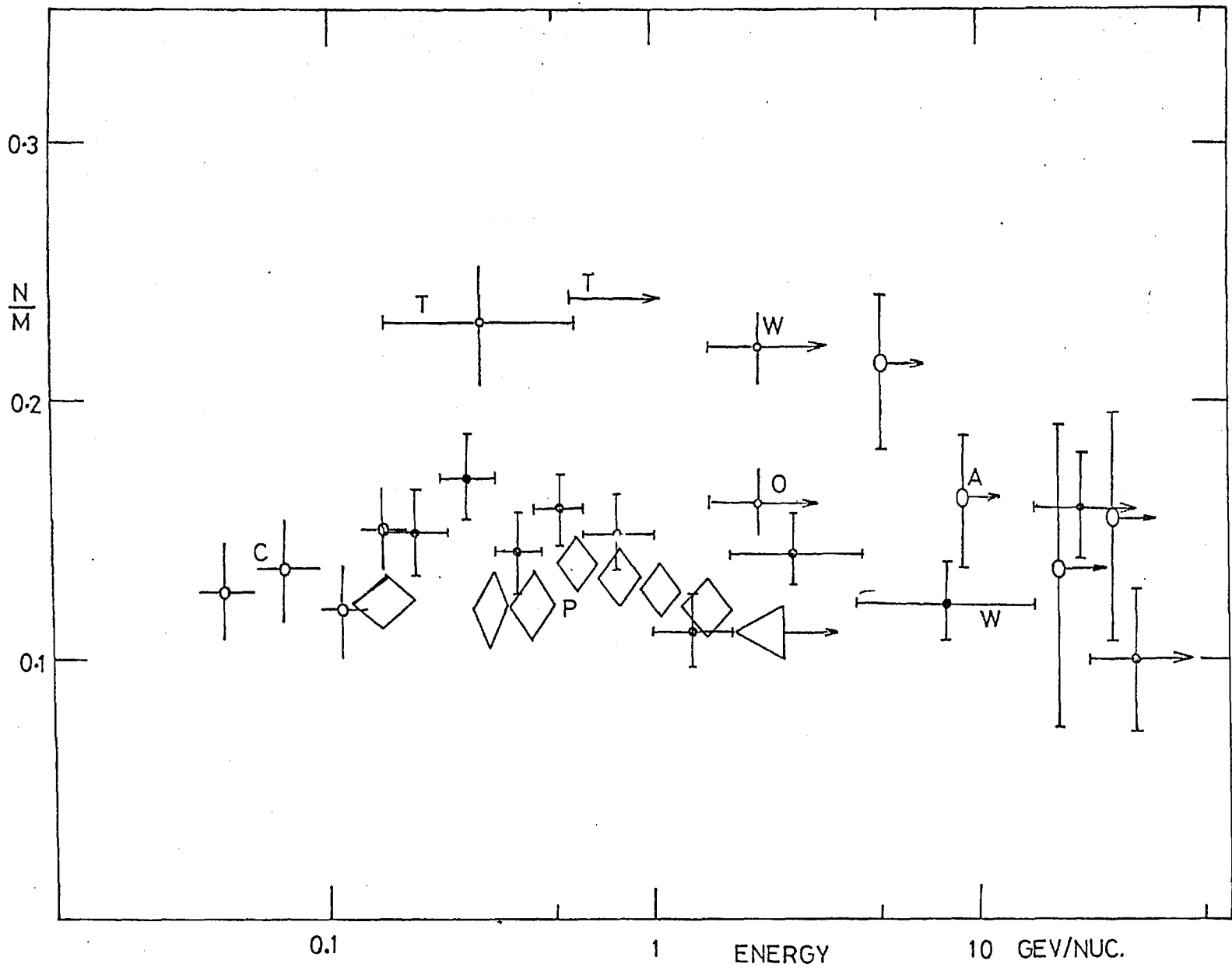


FIG.45 ENERGY DEPENDENCE OF NITROGEN TO MEDIUM NUCLEI RATIO  
 COMSTOCK(C) O'DELL(O) VON ROSENVINGE(W) PRESENT(A) BALASUBRAHMANYAN(P)  
 ANAND(T)

The effective path length deduced from the latest fragmentation parameters, for a ratio  $L/M = 0.25$  at relativistic energies is

$$\bar{x} = 3.5 (\pm 0.5) \text{ grm.cm}^{-2}$$

see Shapiro and Silberberg (116), and the present result does not conflict with this estimate.

#### 6.1.2. (C/O) Carbon-Oxygen Ratio

The mean value of this ratio at the top of the atmosphere is

$$C/O = 1.210 (\pm 0.085)$$

Again, this value is in good agreement with the results of von Rosenvinge, see Fig. 44, in the same energy range although they present evidence that the spectral exponents of carbon and oxygen are different in the energy range under consideration, leading to a decrease in the ratio at high energies, i.e.

$$\begin{aligned} |\gamma_c| &> |\gamma_o| \\ \text{and } C/O|_{E>5\text{GeV}} &\approx 1.0 \end{aligned}$$

The results of the present experiment on the rigidity spectra of carbon and oxygen, shown in Fig. 34, also indicate a difference in spectral exponent, but the  $C/O$  ratio is still greater than 1 in the rigidity range under consideration.

#### 6.1.3. $N/M$ Nitrogen to Medium Nuclei

The mean value of this ratio at the top of the atmosphere is

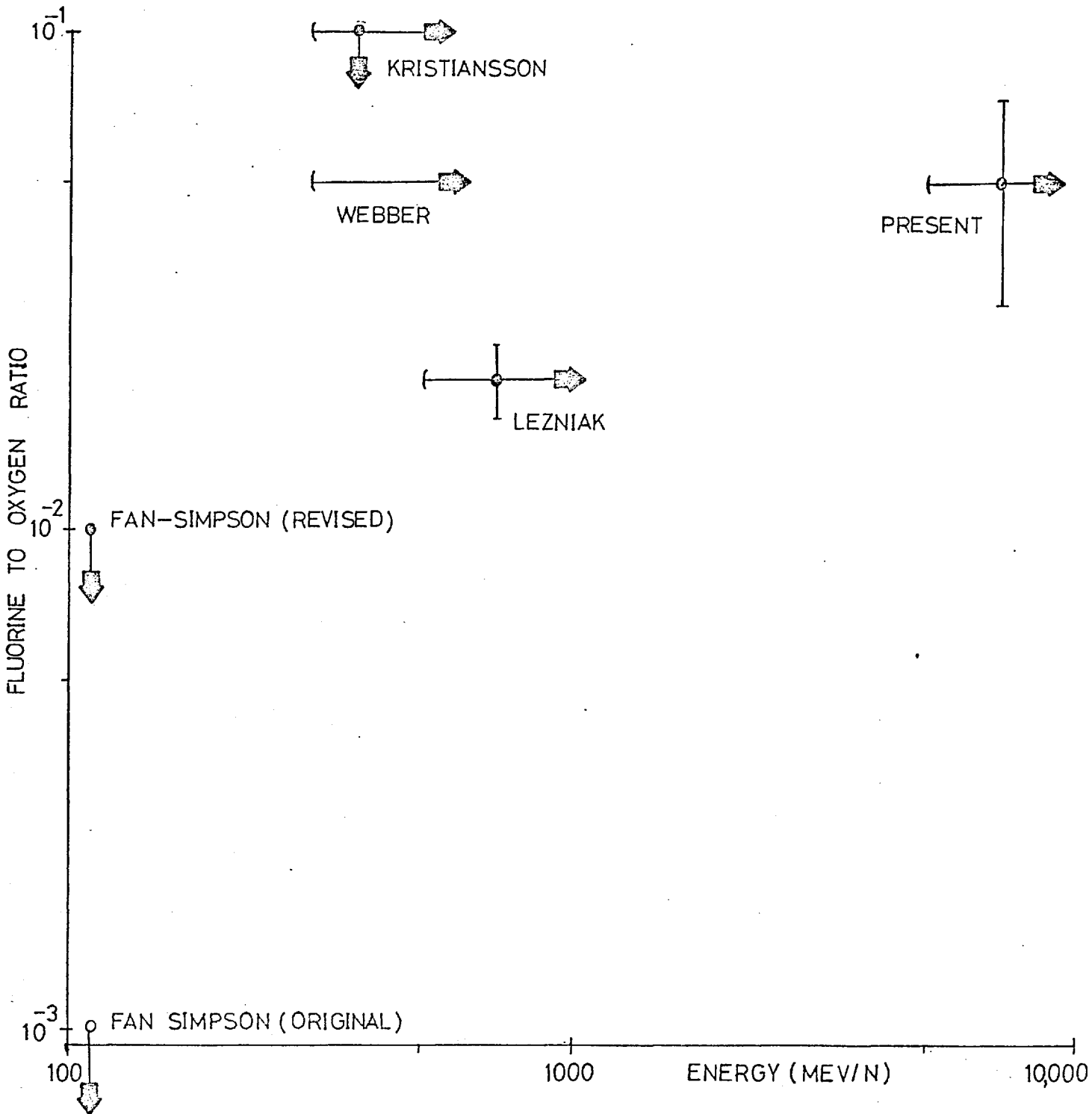


FIG.46 ENERGY DEPENDENCE OF FLUORINE TO OXYGEN RATIO

$$N/M = 0.168 \quad (\pm 0.017)$$

and, although consistent with the currently accepted ratios shown in Fig. 45, it is higher than the von Rosenvinge results. The points shown in this figure are derived from the variation of the rates with azimuth and also the Cerenkov output.

The significance of the  $N/M$  and  $C/O$  ratio to the source composition will be discussed in Section 6.4.

#### 6.1.4. F/O Fluorine to Oxygen

The value of this ratio at balloon altitudes (after passage through  $7.5 \text{ gm.cm}^{-2}$  of residual atmosphere) is

$$F/O \sim 0.05 \quad (\pm 0.022)$$

This agrees very well with previous measurements, see Fig. 46, but as the fragmentation probabilities for the spallation of heavier elements into fluorine are not well known, it is difficult to extrapolate to the top of the atmosphere.

#### 6.1.5. H/M Heavier ( $Z > 10$ ) to Medium Nuclei

The mean value of this ratio at the top of the atmosphere is

$$H/M = 0.39 \quad (\pm 0.015)$$

and this is in excellent agreement with previous results, tabulated in Table V. The ratio is essentially independent of energy. This result implies that, if both heavy and medium nuclei have traversed the same

region in space and were produced by the same source with the same spectrum, then the path length must be

$$\bar{x} < 1 \text{ grm.cm}^{-2}$$

which disagrees with the accepted values of  $\sim 3 \text{ grm.cm}^{-2}$ .

## 6.2. Source Composition

### 6.2.1. Extrapolation to Source Region

Although the slab model of propagation does not fit all the experimental data, as discussed in section 1.4, it is still suitable for the extrapolation of the observed charge spectrum at relativistic energies from the top of the atmosphere to the source region.

The assumed interstellar path length is

$$\bar{x} = 3.5 (\pm 0.5) \text{ grm.cm}^{-2}$$

The extrapolated source compositions are shown in Table VI. In the second column, the results refer to propagation through  $3.5 \text{ grm.cm}^{-2}$  at relativistic energies,  $E > 2 \text{ GeV/n}$  while in the third column, they refer to propagation at an energy  $E \sim 250 \text{ MeV/n}$ . (In Section 5.4.1. it is suggested that most of the matter may have been traversed at considerably lower energies than those observed, before acceleration into interstellar space, but it can be seen that the effect on the source compositions is minor, *if the interstellar acceleration is charge independent.*)

The mean path length applies for both models of propagation as shown by Kristiansson (107) from a consideration of the L-nuclei fragmentation probability energy dependence and the fragmentation probabilities assumed are those predicted by Rudstam's (112) semi-empirical formula.

TABLE VI : EXTRAPOLATION TO SOURCE

Element	E 2 GeV/n	E=250 MeV/n	$\lambda_H$ (m.f.p. in interstellar space)
	Source Composition Relative to Carbon		
Be	-	-	-
B	-	-	-
C	1.00	1.00	7.10
N	0.32	0.282	6.50
O	1.04	1.08	5.90
F	-	-	-
Ne	0.130	0.098	5.00
Na	0.121	0.122	4.54
Mg	0.062	0.146	4.42
Al	0.074	0.092	4.10
Si	0.031	0.090	4.00
*			
*			
*			
*			
Ca group	-	0.065	3.14
Fe group	0.770	0.805	2.5

\* These figures have not been extrapolated because there is meagre statistical evidence from the present experiment on the detailed flux values.

The best values of the ratios  $C/O$  and  $N/M$  at the source are

$$\left. \frac{C}{O} \right|_{\text{source}} \approx 0.95 (\pm 0.05)$$

$$\left. \frac{N}{M} \right|_{\text{source}} \approx 0.130 (\pm 0.10)$$

and  $\left. \frac{N}{O} \right|_{\text{source}} \approx 0.30 (\pm 0.02)$

The significance of these values is discussed in section 6.4.1.

### 6.2.2. Source Composition

The significance of the primordial composition of the cosmic radiation has been in doubt for some time. Aller (18) on the one hand maintains that the charge distribution reflects the history of a sample of high accelerated matter and has no bearing on the cosmic abundance distribution, whereas Shapiro (116) maintains that the elemental abundances of the primordial cosmic rays reflects the chemical composition in the regions of origin and may reveal the processes of nucleosynthesis which have been involved in the evolution of the source.

The nucleosynthesis processes can be deduced only if the acceleration mechanism is charge independent. The basis of the arguments supporting this conclusion is that the equality of the abundances of the elements in the outer layers of the sun (determined spectroscopically - see Pottasch (117) and Unsold (118)) to the elemental abundances in solar cosmic rays, implies no charge dependent preference. Biswas and Fichtel (119) suggested that this argument might be applied to the acceleration of galactic cosmic rays, but many models of charge dependent mechanisms have been suggested by Melrose (16); Tsytoovich (17) and Kaplon (14), and the



conclusion of the present experiment on source spectra question the validity of this assumption.

At the present time, the most statistically significant data on heavy nuclei is available for the M-nuclei, because these nuclei are the most abundant and charge resolution is  $\Delta Z \leq \pm 0.3$  units of charge for all scintillator detectors. The extrapolation of the abundances of carbon, nitrogen and oxygen to the source region is expected to give the most reliable information on nucleosynthesis.

### 6.3. Discussion.

#### CNO-Bicycle

Jonsson et.al. (120) have recently reported a new measurement of the ratio of two stable carbon isotopes,  $^{12}\text{C}$  and  $^{13}\text{C}$  in the cosmic radiation. The isotopic ratio  $\frac{^{13}\text{C}}{^{13}\text{C} + ^{12}\text{C}}$  is a sensitive probe of what happened to the cosmic ray matter before the acceleration started. If the source matter has been involved in nuclear reactions in the interior of stars or in a hot plasma, the  $\frac{^{13}\text{C}}{^{13}\text{C} + ^{12}\text{C}}$  ratio will reach a value characteristic for the reaction chain in which the carbon nuclei have taken part. The value derived for the ratio at the source is

$$R_c = \left( \frac{^{13}\text{C}}{^{13}\text{C} + ^{12}\text{C}} \right) < 0.11$$

The CNO-cycle has been studied by Caughlan (121) who has computed the expected relative nuclide abundances as a function of the reaction temperature and of the number of protons captured per initial CNO-nucleus.

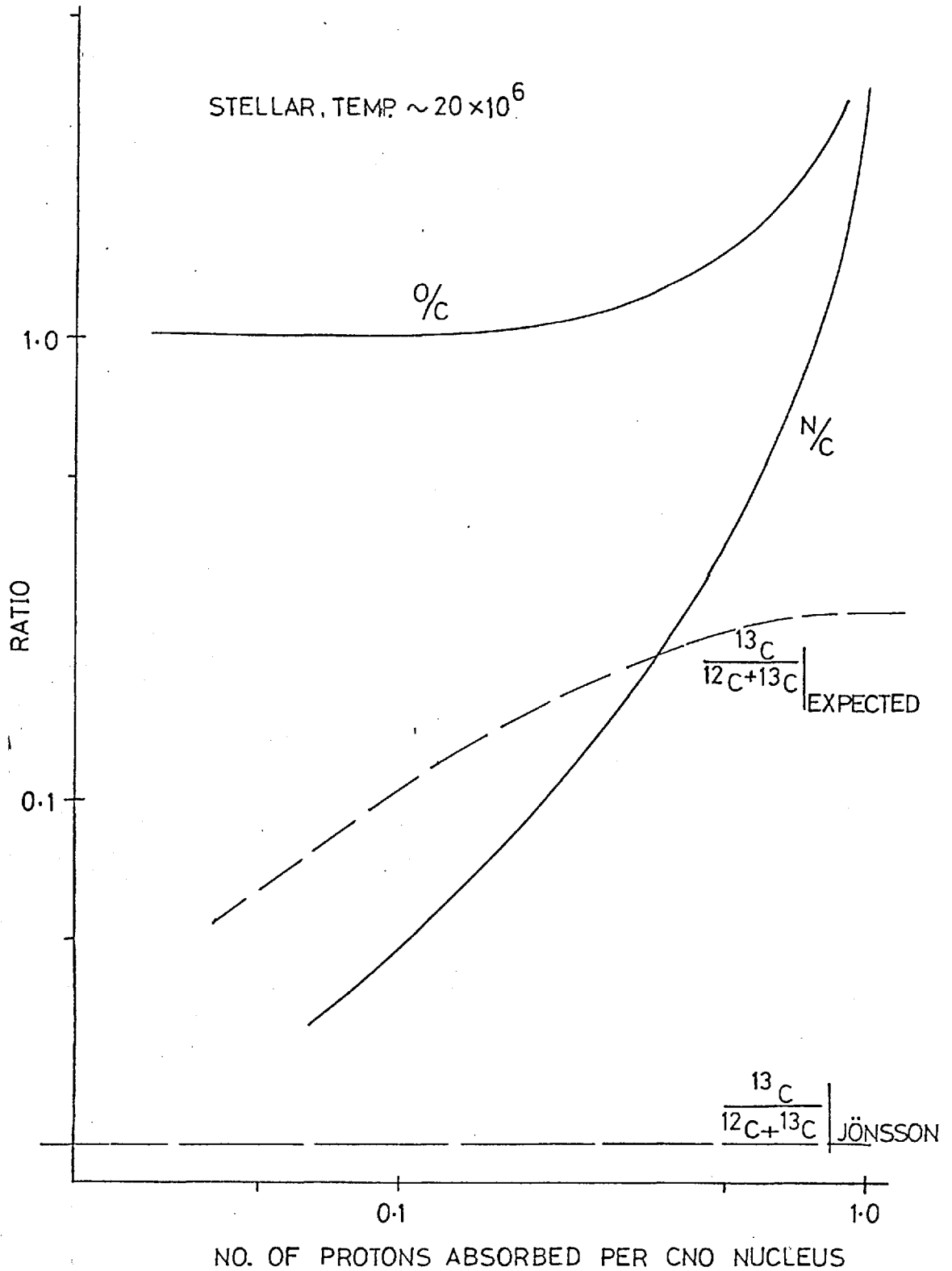


FIG. 47 DEPENDENCE OF CNO NUCLEI ON NO. OF PROTONS ABSORBED PER CNO NUCLEUS FOR CNO-BICYCLE.

The ratio of nitrogen to carbon,  $N/C$  of the CNO-cycle at equilibrium is temperature dependent and is typically  $10 \rightarrow 100$  for a temperature range  $(20-50) \times 10^6$  °K. As the currently accepted experimental ratio

$$N/C \approx 0.2 - 0.3$$

typified by the present experimental result of 0.282, it would seem that the CNO-cycle cannot have been active. Unfortunately, there has arisen some uncertainty, because Warburton et.al. (122) suggest that at the temperatures of interest, a possible resonance exists in the reaction  $^{14}\text{N}(p, \gamma)^{15}\text{O}$  which would decrease the  $N/C$  ratio.

In Fig. 47, the dependence of oxygen, nitrogen and carbon including the carbon isotopes, on the number of absorbed protons at a temperature of  $20 \times 10^6$  °K is shown. It can be seen that the value of  $R_c$  and the extrapolated source ratio of

$$C/O \approx 0.8 - 0.9 \quad (\text{derived in this experiment})$$

are consistent with the view that less than 0.1 protons are absorbed per CNO nucleus, and put another way, this means that the probability is very small that the M nuclei in the cosmic radiation have taken part in a CNO-bicycle.

#### Fast CNO-Cycle

At temperatures above  $10^8$  °K, cyclic reaction chains in which carbon, nitrogen and oxygen nuclei are involved are very fast so that an equilibrium can be reached in a time short compared to the CNO-bicycle discussed already. For example, in the presence of small amounts of neutrons, the

-decays of the ordinary cycle will be substituted by much faster neutron absorption reactions. Hayakawa (123) calculated the abundances of nuclides as a function of reaction temperature and neutron density. He found that carbon and oxygen had approximately the same relative abundances, and the nitrogen content was smaller than for the CNO bicycle. However, as Jonsson et.al. point out, the ratio of  $\frac{^{13}\text{C}}{^{13}\text{C} + ^{12}\text{C}}$  predicted by this model is  $\sim 0.6$ . This represents a serious discrepancy.

In Table VII, the cosmic ray abundance is compared with the universal abundances derived from stellar, meteoritic and terrestrial measurements. The universal abundances are usually weighted heavily towards solar composition data and hence a comparison with the cosmic ray abundances explores the possibility that the sources of cosmic rays are similar to the sun.

The comparison clearly shows that the lighter elements are underabundant and the very heavies overabundant in the cosmic radiation. These comparisons favour a cosmic ray origin in highly evolved stars, in which the processes of element synthesis have reached an advanced stage. An alternative point of view is that the observed cosmic ray abundances are due to the superposition of abundances of a spectrum of stars with different abundance anomalies, e.g. the so-called peculiar A stars. However, there is no evidence that such stars are capable of accelerating cosmic rays.

#### 6.4. Conclusion on Source Composition

It is currently accepted that supernovae are the most likely sources of cosmic rays because they are a class of object which have undergone

TABLE VII : ABUNDANCES FROM MEYER, P. (COSMIC RAYS IN GALAXY)

Element	Cosmic Ray Abundance Rel. to Silicon. 50 < E < 200 MeV/n.	Universal Abundance Rel. to Silicon. Cameron
Li	1	$4.5 \times 10^{-5}$
Be	0.5	$7 \times 10^{-5}$
B	1.7	$6 \times 10^{-6}$
C	5	13
N	1.4	2.4
O	5	24
F	$2 \times 10^{-2}$	$10^{-4}$
Ne	1	2.4
Na	0.3	0.06
Mg	1.5	1.00
Al	0.1	0.09
P-K	0.4	0.75
Ca-Cr	0.4	0.09
Mn-Ni	0.6	0.95

several stages of nucleosynthesis and, more importantly, they satisfy the stringent energy requirements.

As discussed in the previous section, it may be possible to deduce how far nucleosynthesis had progressed before the disruption of the star. However, in the Colgate et.al. (124) model of the acceleration of cosmic rays, it is assumed that a strong shock wave is formed by processes deep in the interior of the pre-supernova star, and that this wave moves outwards with increasing speed. Within this shock wave violent nuclear interactions may take place so that the 'apparent' source abundance reflect the acceleration mechanism rather than the nucleosynthesis within the stellar interior. Before any definitive statement can be made, more experimental measurements of isotopic abundances as well as elemental abundances must be forthcoming.

Another experimental result which favours the supernovae as the sources of cosmic rays is the discovery of the super-heavy nuclei ( $Z > 40$ ) in the cosmic radiation. Fowler et.al. (125) point out that their data favour an origin in rapid rather than slow neutron-capture processes. The rapid neutron capture has a time scale of seconds and might be expected in the rapidly expanding supernovae shells.

The present experiment cannot challenge any of the accepted theories on the possible sources of cosmic rays with the elemental abundance results, but the data on the rigidity spectra of different charge groups questions the basic premise of all such theories, i.e. that the acceleration mechanism is independent of charge. If the acceleration process is dependent on the charge, it will be necessary to develop a suitable theory of the accelerating process before the pre-explosion source composition can be determined.

## Chapter 7. - UPPER LIMIT TO ANTINUCLEI IN PRIMARY COSMIC RAYS

### 7.1.1. Experimental Method

The prime aim of the experiment was to place an upper limit to the ratio of antinuclei to nuclei in the charge, Z range and rigidity, R range given by

$$(i) \quad Z \geq 6$$

$$\text{and} \quad (ii) \quad 10.5 \leq R \leq 18 \text{ GV}$$

$$\text{i.e.} \quad 5.2 \leq E \leq 9.0 \text{ GeV/nucleon}$$

The physical reason for this particular selection of Z and R is described below. Meanwhile, the method depends on a knowledge of geomagnetic threshold rigidities and this topic will be discussed first.

### Cosmic Ray Trajectories in the Earth's Magnetic Field

The general three dimensional problem of computing trajectories in the Earth's magnetic field is a complex one, partly because the simple dipole model of the field is inadequate for many aspects of cosmic ray research.

The problem was simplified somewhat when it was realised that the motion of an incoming particle of one sign of charge could be simulated by a particle leaving the earth with the same physical parameters, except that the sign of its charge was opposite to that of the incoming particle.

Störmer (126) showed that, at any point on the Earth's surface, there were allowed and forbidden directions of incidence for particles of a particular rigidity. Another way of looking at this is that in order for a particle to escape from the earth's magnetic field, it must have a momentum, or rigidity greater than a certain critical value. This critical value  $R_G$ , the geomagnetic cut-off rigidity depends upon the initial azimuth,  $\theta_A$  and zenith,  $\phi$  of the escaping particle. Once found,  $R_G(\theta_A, \phi)$  for the escape of a particle with  $-Ze$  units of charge is identical to the geomagnetic threshold rigidity of a primary cosmic ray particle of  $+Ze$  units of charge detected by a cosmic ray telescope inclined at azimuth  $\theta_A$  and zenith  $\phi$  at the same point on the earth.

At high latitudes,  $\lambda_L$ , Störmer's theory has to be modified because there are certain values of rigidity,  $R > R_G$ , which, although they take the escaping particle to infinity, require that the particle trajectory pass through the earth at some stage - and this is physically impossible. These values  $R(\lambda_L, \theta_A, \phi)$  constitute the penumbra and are inaccessible to primary cosmic ray particles.

The simplest trajectories to consider are those confined to the geomagnetic equatorial plane. In Fig. 48 are shown the minimum rigidities required for positively charged particles arriving from the Western horizon, vertically and the Eastern Horizon. As the magnetic field lines,  $\underline{B}$  are perpendicular to this plane and the force,  $\underline{F}$ , on a particle, charge  $Ze$  and velocity  $\underline{v}$  is given by the vectorial relation



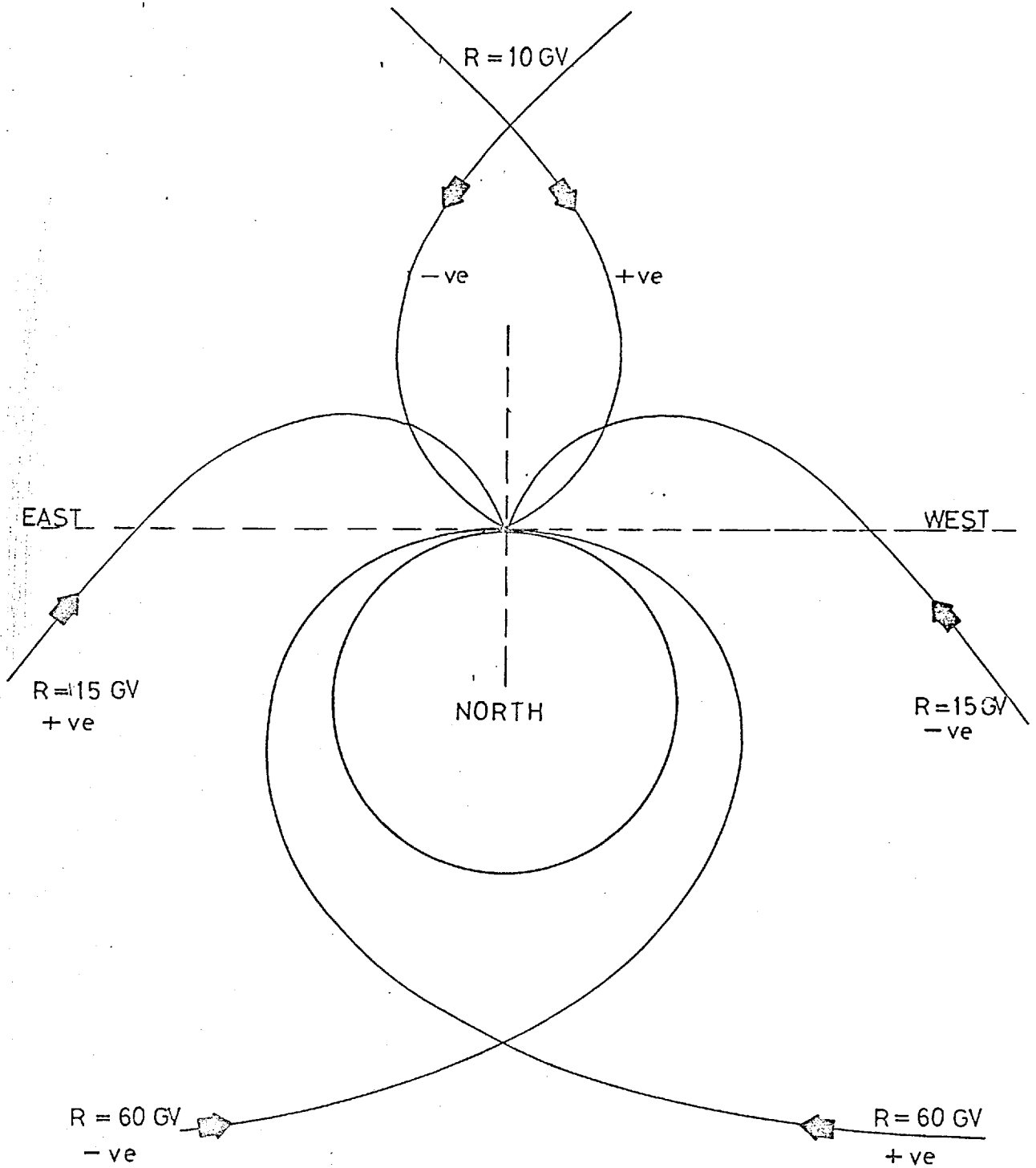


FIG. 48 PARTICLE TRAJECTORIES IN THE EQUATORIAL PLANE (WOLFENDALE)

$$\underline{F} = Ze \underline{v} \wedge \underline{B}$$

it can be seen that the trajectories of a negatively charged particle will be the mirror image of those for the positively charged particles about the vertical plane through the point of observation in Fig. 48.

Mathematically,

$$R_G(\theta_A, \phi) \Big|_{-Ze} \equiv R_G(\pi + \theta_A, \phi) \Big|_{+Ze}$$

The standard McCracken (127) programme was used to compute the geomagnetic cut-off rigidity values for all azimuths, and for zenith angles  $\phi$  within the opening angle of the detector ( $30^\circ \leq \phi \leq 70^\circ$ ).

The variation of the geomagnetic threshold rigidity with zenith and azimuth is shown in Fig. 32. If a Cerenkov device or rigidity selector is incorporated in the detector which determines whether or not the incident particle has a rigidity below a well-defined threshold  $R_c$ , it is possible to define the sign of the incident particle. The rigidity selector threshold is set such that

$$R_G(\theta_A, \phi) < R_c < R_G(\pi + \theta_A, \phi)$$

see Fig. 49.

Events which satisfy the criteria:

$$\left. \begin{array}{l} -60^\circ < \theta_A < +60^\circ \\ \text{and } R < R_c \end{array} \right\} \text{ must be nuclei with } R_G \Big|_{+Z} < R < R_c (N_Z)$$

whereas those which satisfy

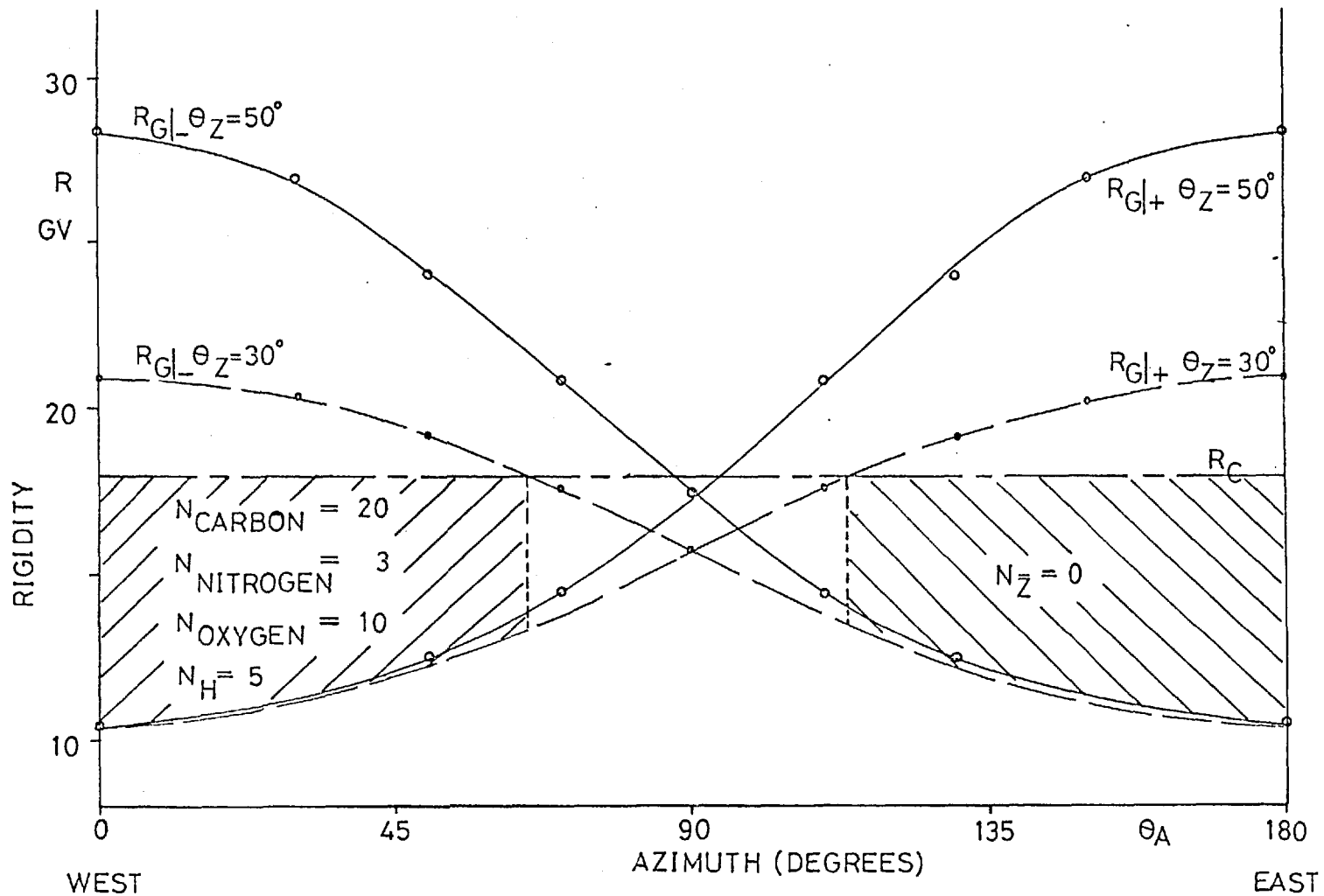


FIG. 49 VARIATION OF GEOMAGNETIC THRESHOLD RIGIDITY WITH AZIMUTH

$$\left. \begin{array}{l}
 (\pi - 60^\circ) < \theta_A < (\pi + 60^\circ) \\
 \text{and} \\
 R < R_c
 \end{array} \right\} \begin{array}{l}
 \text{must be antinuclei with} \\
 R_G \Big|_{-Z} < R < R_c \quad (N_Z^-)
 \end{array}$$

The criteria for selecting  $N_Z$  and  $N_Z^-$  are shown schematically in Fig. 49.

### 7.1.2. Derivation of Upper Limit

As no events with charge,  $Z \geq 6$  were recorded whilst the telescope was pointing within  $60^\circ$  of East with a zero Cerenkov output, it is possible to place an upper limit to the fraction of antinuclei in the cosmic radiation. The number of ordinary nuclei within the same rigidity range,  $10 \leq R \leq 18$  GV is given by the total number of events recorded which had zero Cerenkov output while pointing West ( $\pm 60^\circ$ ). The total number of nuclei observed which satisfied this criterion was 38, as shown in Fig. 49. As the detector pointed within  $60^\circ$  of East for 3% longer than the corresponding time for the Westerly direction, the number of ordinary nuclei which would have been seen in the same time as no anti-nuclei were seen is 40.

It follows that the ratio of antinuclei ( $Z \geq 6$ ) to nuclei in the rigidity range  $10 \leq R \leq 18$  GV is

$$N_A^- / N_A < 7.5\% \quad (95\% \text{ confidence limit})$$

In the following section, the possible sources of spurious anti-nuclei events are discussed.

### 7.1.3. Spurious 'Antinuclei' Events and Detector Sensitivity

#### Sources of Error

##### 1) Penumbra

In equatorial regions, the penumbra effect is thought to be absent. Not one of the trajectory computations indicated a penumbra and so this is not considered a possible source of error.

##### 11) Opening Angle of Telescope

Due to the large geometrical factor and opening angle of the telescope a wide range of geomagnetic cut-off rigidities is sampled for a given mean value of azimuth,  $\theta_A$  and zenith,  $\phi$ .

This finite opening angle imposes a restriction on the range of azimuths used in the determination of the upper limit to antinuclei. Referring to Fig. 49, the range of azimuth which can be used:

$$-45^\circ \leq \theta_A \leq +45^\circ \quad \text{for opening angle } \pm 10^\circ.$$

##### 111) Physical Processes Responsible for Spurious Antimatter Events

Every detector has an intrinsic limit below which particle fluxes of interest cannot be distinguished from spurious events and/or noise. This limit defines the sensitivity of the detector and in order to make meaningful measurements, the flux measured should be an order of magnitude higher than this lower limit.

The following physical processes were thought to be possible progenitors of spurious antimatter events in the detector.

a) Chance Coincidence

A possible 'antinucleus' would be generated if there were a chance coincidence between noise pulses in the pm tubes looking at the top and bottom scintillators. As the coincidence gate is only open for 200 nanoseconds, the expected rate of chance coincidences is given by

$$R_{cc} = 3 N_1 N_2 N_3 \tau^2 \quad \text{- see Janossy (128)}$$

where  $\tau = 200 \times 10^{-9}$  sec,

$N_1 =$  singles rate for tube 1, etc.  
 $= 5000/\text{min} = N_2 = N_3$

Substituting,

$$R_{cc} = 7 \times 10^{-11} \text{ sec}^{-1}$$

and this is negligible.

Another possibility is that a particle will traverse the top scintillator and a chance coincidence could be generated with noise in the bottom tube. The expected rate for this process would be

$$R_{NC} = 2 N_1 \cdot \gamma_N \cdot \tau \quad \gamma_N = \text{particles traversing the top scintillator per sec}$$

$$\approx 10^{-5} \gamma_N$$

Hence, the lower limit imposed by this chance coincidence is

$$\eta_{\min} \approx \frac{R_{NC}}{\gamma_N} \frac{1}{\alpha} = 10^{-3} \% \quad \begin{array}{l} A = \text{area of top scintillator} \\ \alpha = \text{geometrical factor of telescope.} \end{array}$$

The limit is less than this value, because a spurious event would only occur if the noise pulse had the same magnitude as the pulse due to the particle in the top tube.

b) Albedo

The term albedo is given to particles which are generated by nuclear interactions of the primary cosmic rays. The proton and alpha particle albedo background have been discussed extensively in Chapter 4. Referring to figure 27, only those albedo particles within well-defined energy intervals can be confused with antinuclei:

(a) Splash and re-entrant protons with  $39 \lesssim E_p \lesssim 41$  MeV give a zero Cerenkov pulse and are 'apparent' relativistic antilithium nuclei.

(b) Splash and re-entrant alpha particles with  $350 \lesssim E_\alpha \lesssim 450$  MeV are apparent relativistic antiberyllium nuclei.

(c) Splash and re-entrant alpha particles with  $220 \lesssim E_\alpha \lesssim 280$  MeV could look like relativistic antiboron nuclei.

(d) Splash and re-entrant alpha particles with  $155 \lesssim E_\alpha \lesssim 160$  MeV could look like relativistic anticarbon nuclei.

In sections 4.3.1. and 4.4.1., the proton and alpha particle albedo spectra have been derived from the inflight data. The differential fluxes of the albedo particles  $dj_{ALB}$  in each of the energy intervals (shown above) have been computed from the derived spectra. Also the differential fluxes of relativistic lithium, beryllium and boron,  $dj_{REL}$  have been derived for the rigidity range  $10 \leq R \leq 18$  GV from the spectra in Chapter 5. The ratio

$$R_\eta = \frac{dj_{ALB}}{dj_{REL}} \times 100 \%$$

represents the lowest limit to the ratio of antinuclei to nuclei which could be assigned by the present detector. The limits obtained are

$$\begin{aligned} R_{\bar{n}} (\text{Li}) &\sim 100\% & R_{\bar{n}} (\text{Be}) &\sim 20\% \\ R_{\bar{n}} (\text{B}) &\sim 20\% & R_{\bar{n}} (\text{C}) &\sim 0.1\% \end{aligned}$$

Hence, this physical process prevents the unambiguous assignation of antilithium, antiberyllium and antiboron in the primary cosmic ray flux with the present detector. In the derivation of the upper limit to the ratio of antinuclei to nuclei, the light-nuclei events have been ignored.

c) Isotopic Compositions

The relationship between the critical energy required to give an output from the Cerenkov and the charge, Z of the particle may be represented by

$$E_c = A \cdot m \cdot \gamma_c^2 \quad \text{GeV}/c^2$$

Expressing this energy in terms of a critical rigidity  $R_c$  and rearranging

$$\gamma_c = \left( \frac{Z}{A} \right) \cdot \frac{R_c}{m} \quad \text{where } m = \text{mass of nucleus}$$

A = atomic number of nucleus.

As the Cerenkov device is preset before the flight to give an output if a nucleus with a  $(Z/A)$  ratio of 0.5 has a rigidity,  $R_c = 18$  GV, then the value of the critical velocity,  $\beta_c$  is such that

$$\gamma_c = (1 - \beta_c^2)^{-\frac{1}{2}} = \frac{1}{2} \times \frac{18}{0.94}$$

$$= 9.60$$



For values,  $Z \geq 6$ , the charge to mass ratio approaches 0.5 for all stable isotopes, that is nuclei with the same number of protons, but different numbers of neutrons. However, the elements Li, Be and B all have stable isotopes which have a charge to mass ratio smaller than 0.5.

The effect of this can be seen in the following calculation:

Consider the two stable isotopes of Lithium:

Li<sup>6</sup>

$$\frac{Z}{A} = \frac{1}{2} \quad \therefore \gamma(19 \text{ GV}) = 10.1$$

Li<sup>7</sup>

$$\frac{Z}{A} = \frac{3}{7} \quad \therefore \gamma(19 \text{ GV}) = 8.65$$

As  $\gamma_c = 9.60$ , it can be seen that whereas  $\text{Li}^6$  gives an output in the Cerenkov channel, the  $\text{Li}^7$  isotope will not give an output because

$$\gamma < \gamma_c$$

Hence, it is possible for particular isotopes to be indistinguishable from antinuclei in the range of charge, Z

$$2 < Z \leq 6$$

In table VIII, the different stable isotopes are listed. In column 3, the maximum rigidity that the isotope may have in order to give zero output in the Cerenkov is computed. In column 4, the azimuthal angles which could give rise to spurious antinuclei events due to that particular isotope are listed.

The table indicates that, if the isotopes  $\text{Li}^7$ ,  $\text{Li}^9$ ,  $\text{Be}^9$ ,  $\text{Be}^{10}$ ,  $\text{B}^{10}$ ,  $\text{B}^{11}$ , and  $\text{C}^{14}$  are present in the cosmic radiation there is a possibility

ISOTOPE	$Z/A$	$R_{MAX}$ (GV)	AZIMUTH ANGLE $\theta_A$
$Li^6$	$1/2$	18.0	$\theta < 115^\circ$
$Li^7$	$3/7$	21.0	$\theta < 180^\circ$
$Li^9$	$1/3$	27.0	$\theta < 180^\circ$
$Be^7$	$4/7$	15.8	$\theta < 115^\circ$
$Be^9$	$4/9$	21.2	$\theta < 180^\circ$
$Be^{10}$	$2/5$	23.5	$\theta < 180^\circ$
$B^{10}$	$1/2$	18.0	$\theta < 115^\circ$
$B^{11}$	$5/11$	19.9	$\theta < 145^\circ$
$C^{10}$	$3/5$	15.0	$\theta < 115^\circ$
$C^{11}$	$6/11$	16.5	$\theta < 115^\circ$
$C^{12}$	$1/2$	18.0	$\theta < 115^\circ$
$C^{13}$	$6/13$	19.5	$\theta < 135^\circ$
$C^{14}$	$3/7$	21.0	$\theta < 180^\circ$

TABLE VIII

of their being confused with antinuclei.

d) Pion Production in Jets

One conceivable way in which a high-Z nucleus could be simulated, is by the passage of a large number of particles of unit charge through the scintillator at a particular instant of time. This condition is satisfied when a high energy primary interacts with a nucleus in the styrofoam covering around the detector and produces a number,  $n_s$ , of pions. See section 4.2.

However, in order to be confused with a lithium nucleus,  $n_s \geq 9$ , and using the functional relationship

$$\bar{n}_s = 2.1 E_p^{1/4} \quad \text{where } E \text{ is in GeV}$$

it can be seen that the energy of the incident primary,  $E_p$  must exceed 500 GeV. However, the Cerenkov device responds to any particle with a velocity  $\beta \approx 10.0$ , and if the pions are produced in the C.M.S. frame

$$\gamma_{C.M.S.}^\pi \geq 1$$

Transforming into the laboratory frame

$$\begin{aligned} \gamma_{LAB}^\pi &= \gamma_{C.M.S.}^\pi \left( \frac{\gamma_p}{2} \right)^{1/2} \quad \text{where } \gamma_p \text{ is velocity of} \\ &\quad \text{primary} \\ &= \gamma_{C.M.S.}^\pi \left( \frac{E_p}{2m_p} \right)^{1/2} \\ &\approx 16 \gamma_{C.M.S.}^\pi \end{aligned}$$

$$\therefore \gamma_{LAB}^\pi \geq 16$$

The pions will each produce  $\approx 10$  photons in the gas Cerenkov and hence the probability of confusing such an event with an antiparticle is the probability of  $> 90$  photons producing no output. This probability is negligible.

e) Stars

Nuclear interactions due to primary particles with energy

$$E_p \approx \text{few GeV/nucleon}$$

give rise to 'stars' in emulsions. The secondary products of such an interaction are protons, mesons and nuclear fragments. The protons have energies of the order of 150 MeV or less whereas the nuclear fragments have energies of the order of a few MeV.

It is possible for such interactions to produce spurious events which look like antinuclei, but the protons are the only secondaries capable of reaching the scintillators, and so any such events cannot deposit more energy than the slow proton events discussed already. Although it is possible that, under exceptional circumstances, the event could look like a boron nucleus, this mechanism is considered unimportant.

f) Fragmentation of High-Z Primary

The two types of fragmentation in the earth's atmosphere are

- (i) break-up of an atmospheric nuclide by a very high energy proton
- (ii) break-up of a relativistic primary high-Z nucleus due to an interaction with an atmospheric nuclide.

The first type can be ignored, because the kinetic energy of the nuclear fragments is too low to be important and so the second process only will be considered.

It is possible to generate a spurious antimatter event at balloon altitudes if a primary nucleus,  $Z_p$  fragments in the atmosphere into a nucleus, charge  $Z_F$  and in doing so imparts a smaller energy per nucleon to this secondary particle. If the secondary particle has a rigidity  $R < R_{\text{Cerenkov}}$ , it will be indistinguishable from an antinucleus of rigidity,  $R$ .

In a high energy collision, some of the energy of the incident particle disappears in the production of relativistic pions. The fraction of the incident energy lost is denoted by the inelasticity coefficient,  $K$ . This factor varies from one interaction to another. Hayakawa (129) maintains that its value

$$K \lesssim 0.1$$

for a fragmentation interaction, because the fragmentation process involves the emission of low energy particles in the rest system of the incoming nucleus. This implies that the energy/nucleon of the fragmentation products is almost identical to the energy/nucleon of the primary.

If this assumption is correct, then the sensitivity of the detector is unaffected by this physical process. However, it was thought worthwhile to derive a sensitivity function,  $S(Z_p, K)$  and see exactly how it would be affected by variations in the inelasticity coefficient.

Let the fragmentation probability,  $P_{Z_p, Z_F}$  denote the probability that a heavy nucleus,  $Z_p$  will fragment into a lighter nucleus,  $Z_F$  and

let  $P_{Z_p}(\lambda)$  be the probability of a collision of the heavy nucleus with an atmospheric nuclide. Then, the flux of spurious background, charge  $Z_F$  is given by

$$j(Z_F) = \sum_{Z_p > Z_F} j_{Z_p}(R_G \leq R \leq R_{CRIT}) \cdot P_{Z_p}(\lambda) \cdot P_{Z_p, Z_F}$$

To a good approximation  $P_{Z_p}(\lambda) \approx X_{ATMOS} / \lambda_{Z_p}$

$R_{CRIT}$  depends upon the inelasticity coefficient,  $R_{CRIT} = (1 - K)^{-1} R_C$

The sensitivity function, which is the ultimate sensitivity of the detector to antinuclei of charge,  $|Z_F|$  due to fragmentation becomes:

$$S(Z_F, K) = X_{ATMOS} \left\{ \sum_{Z_p} \frac{j_{Z_p}(R_G \leq R \leq R_{CRIT}) \cdot P_{Z_p, Z_F} / \lambda_{Z_p}}{j_{Z_F}(R > R_{G'})} \right\} \times 100\%$$

where  $R_G$  is the geomagnetic threshold rigidity of nuclei in the East quadrant and  $R_{G'}$  is the threshold rigidity of nuclei in the West quadrant.

This function has been evaluated for a mean amount of residual atmosphere traversed of  $7.5 \text{ grm.cm}^{-2}$  and for representative charge group flux values,  $j_z$  given by Webber (71). The only simplifying assumption used is that each charge group can be represented by the integral spectrum

$$j_z(>R) = k_z R^{-1.5}$$

The results are shown in Fig. 50. They show that it is desirable to conduct the experiment as high in the atmosphere as possible, if the value of  $K$  is in the region  $0.1 < K \leq 0.2$ .

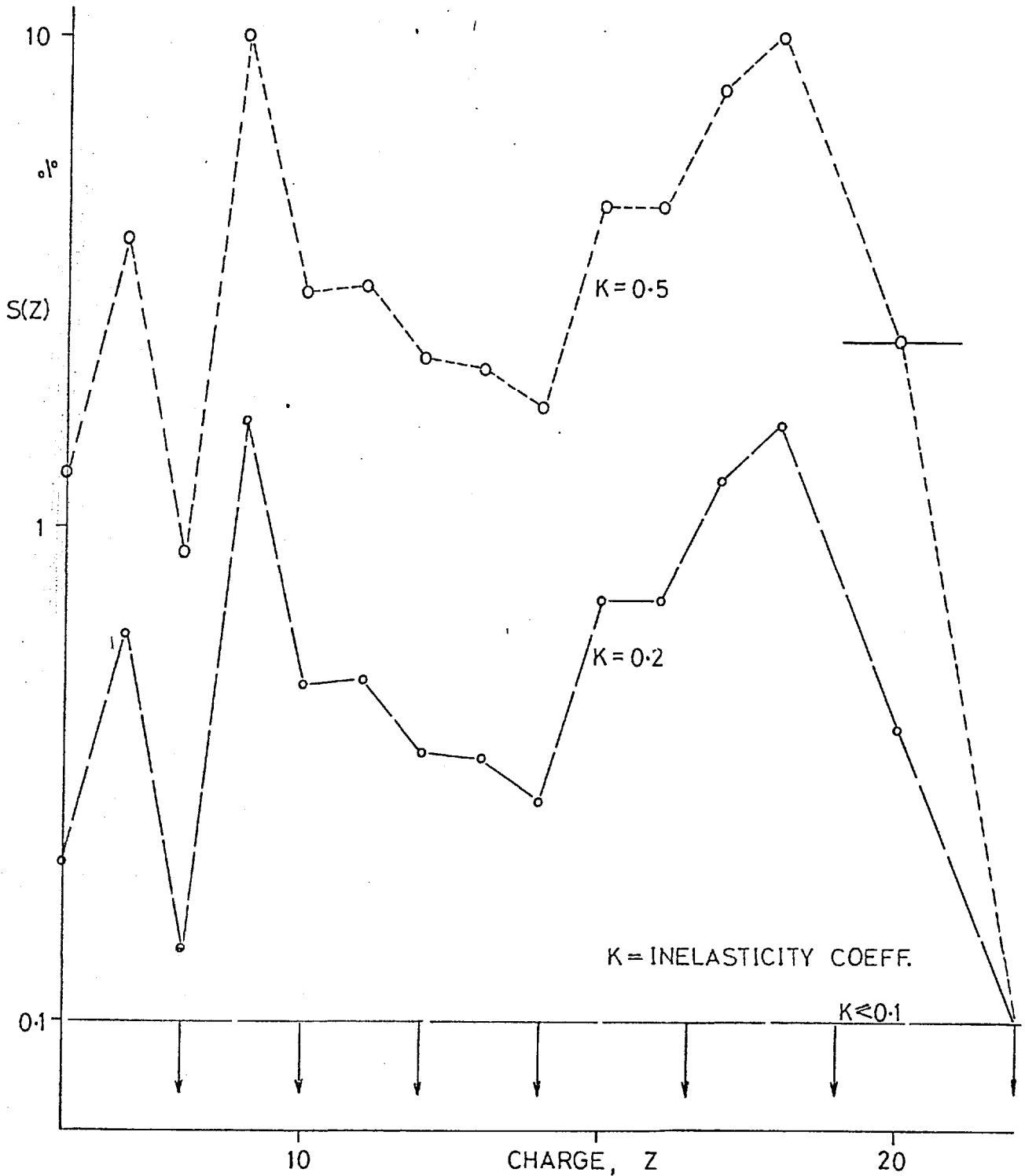


FIG. 50 SENSITIVITY OF DETECTOR TO ANTINUCLEI

If the value of  $K$  exceeds 0.2, then the limit to the instrument sensitivity is 1%. However, the current body of opinion assumes the inelasticity coefficient to lie between

$$0 \lesssim K \lesssim 0.1$$

in which case the ultimate sensitivity is less than  $10^{-3}\%$ .

### Conclusion

Various physical mechanisms which may provide spurious antinuclei events have been discussed and the conclusion is that, if the present detector is to be used to reduce the upper limit to the ratio of antinuclei to nuclei in the cosmic radiation, it is necessary to increase the exposure time at altitude and unambiguously define the large albedo fluxes of protons and alphas. If this can be successfully achieved, the ultimate sensitivity limit to the ratio of antinuclei to nuclei is governed by chance coincidences. This limit is

$$\bar{n}_A/n_A \sim 10^{-3} \% \text{ (for } Z \geq 6)$$

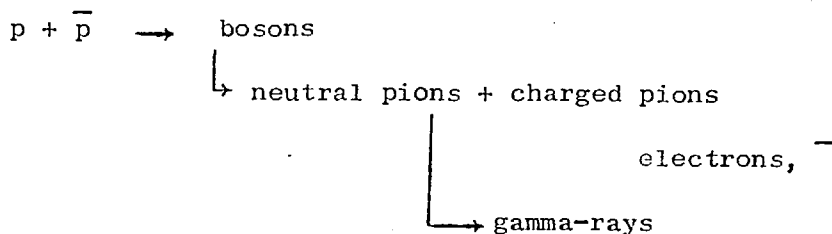
### 7.2. Antimatter in the Galaxy - Significance of Gamma Ray Astronomy

It has been seen that the presence or absence of regions of antimatter cannot be deduced from observational astronomy alone. It is necessary to detect the presence of antinuclei or the products of the annihilation mechanism in the cosmic radiation in order to prove that such regions exist. (This begs the question as to whether the cosmic radiation is a representative sample of matter-antimatter regions of the



Universe.)

There is much experimental information on the decay modes for the annihilation reactions of antiprotons,  $\bar{p}$  with protons,  $p$  from high energy accelerator data, e.g. CERN and Serpukhov, and this data is predicted by well-established theories, e.g. Matsuda (130). The decay scheme is typified by



and it has been established that the product of c.m.s. velocity and annihilation cross-section is essentially constant

$$(\sigma \beta_{\text{c.m.s.}})' \sim 25 \text{ mbarn.}$$

for

$$25 \lesssim E_p \lesssim 7000 \text{ MeV}$$

see Stecker (131) on  $\gamma$ -ray production

Other products of the decay are neutrinos, but as their interaction with matter is extremely small

$$\sigma_{\text{int}} \Big|_{\nu} \sim 10^{-44} \text{ cm}^2$$

it is impossible, with present day experimental technique, to hope to detect these elementary particles to any degree of accuracy.

Some experimental results on the ratio of positrons to electrons in the primary cosmic radiation have been reported by Daniel and Stephen (132) and Fanselow (133), and Kojoian (134) has developed a theory linking the

positron-electron ratio to the rate of matter-antimatter annihilation. In this way, Kojoian deduced an antimatter-matter ratio,  $n_{\bar{A}}/n_A$  of at least 3-4% if the annihilation mechanism is the dominant contributor to the electron flux.

The experimental determinations of the flux of positrons is difficult due to terrestrial background and also, there are many theories for production of cosmic electrons, e.g. Ginzburg (135) and Hayakawa (136). This led Morrison (137) to suggest that, of all the decay products, the  $\gamma$ -rays provide the best chance of "detecting" antimatter.

The technique of  $\gamma$ -ray balloon-borne detectors have been improving all the time, and Kraushaar and Clark (138) and Sood (139) have placed very low finite values to the isotropic  $\gamma$ -ray background of

$$\frac{dj_{\gamma}}{d\Omega} \approx (1.1 \pm 0.2) \times 10^{-4} \text{ cm}^{-2} \text{ sec}^{-1} \text{ ster}^{-1}$$

and report a higher flux of  $\gamma$ -rays from the galactic centre, for which

$$\frac{dj_{\gamma}}{d\Omega} \approx 2 \times 10^{-4} \text{ cm}^{-2} \text{ sec}^{-1} \text{ ster}^{-1}$$

Steigman (51) has pointed out that, if one assumes a homogeneous mix of particles and antiparticles, the annihilation rate, S is given by

$$S = n_+ n_- \sigma v$$

$n_{\pm}$  are densities of matter and antimatter

$\sigma$  = annihilation crosssection

$v$  = velocity

$$(\sigma v)_{\text{exp}} = 25 \text{ mb.}$$

and the flux of  $\gamma$ -rays is a value  $dV$  at a distance R from the annihilation

region is 
$$dJ_{\gamma} \approx \frac{g_{\gamma} S dV}{4 \pi R^2}$$

where  $g_\gamma$  is the number of  $\gamma$ 's produced per annihilation ( $3 \rightarrow 4$ ).

Annihilations in intergalactic space would produce the flux

$$(A) \quad \frac{dj_\gamma}{d\Omega} \approx \left( \frac{g_\gamma R_o}{4\pi} \right) S_{I.G.} \frac{\text{photons}}{\text{cm}^2 \text{ster. sec.}}$$

$$\text{where } R_o = c H_o^{-1} \approx 10^{28} \text{ cm}$$

Annihilation in our own galaxy would tend to produce a line source in the galactic plane - as observed, where

$$(B) \quad \frac{dj_\gamma}{d\Omega} \approx \left( \frac{g_\gamma R_G}{2\pi} \right) S_G \frac{\text{photons}}{\text{cm}^2 \text{ster. sec}}$$

$$\text{where } R_G = \text{galactic radius} \approx 3 \times 10^{22} \text{ cm}$$

Annihilation, if at galactic centre, would produce a flux given by

$$(C) \quad \frac{dj_\gamma}{d\Omega} \approx \left( \frac{g_\gamma}{4\pi} \right) \frac{SV}{R^2} \frac{\text{photons}}{\text{cm}^2 \text{ster. sec}}$$

where  $V$  = volume of galactic nucleus,  $R$  = distance of nucleus from observer.

The low flux values of the observed  $\gamma$ -radiation places an upper limit to the annihilation rates as shown below

$$S_{IG} \leq 4 \times 10^{-32} \text{ ann.cm}^{-3} \text{.sec}^{-1}.$$

$$S_G \leq 10^{-26} \text{ ann.cm}^{-3} \text{.sec}^{-1}.$$

$$(SV)_{\text{centre}} \leq 4 \times 10^{41} \text{ ann.sec}^{-1}.$$

As  $(\sigma V)_{\text{exp}} \approx 10^{-10} \text{ cms}^3/\text{sec}$ , one obtains limits to the density of

$n_+$  and  $n_-$  in the three regions:

$$(1) \quad n_+ n_- \Big|_{\text{I.G.}} \lesssim 4 \times 10^{-22} \text{ cm}^{-6}$$

and

$$(2) \quad n_+ n_- \Big|_{\text{G}} \lesssim 10^{-16} \text{ cm}^{-6}$$

The intergalactic result (1) is not inconsistent with the limits on the neutral density of intergalactic gas set by lack of Ly $_{\alpha}$  absorption lines in the spectra of quasars of large red shift as reported by Burbidge (140).

However, the galactic result (2) implies a density of protons and antiprotons of

$$n_{\pm} \lesssim 10^{-8} \text{ cm}^{-3}$$

whereas the density of the interstellar medium is known, from other observations to be  $n_+ \lesssim 1.0 \text{ cm}^{-3}$ . The conclusion is therefore that the interstellar gas is overwhelmingly of one kind - the result certainly means that a homogeneous mix of matter and antimatter cannot exist within the galaxy.

The final conclusion concerns the galactic centre. It can be shown that the observed flux could be explained by the annihilation of

$$\frac{dM}{dt} \sim 10^{-8} M_{\odot} / \text{yr.} \quad \text{where } M_{\odot} = \text{solar mass}$$

Although this possibility cannot be ruled out it seems unlikely that the antimatter could have survived the early stages of galactic evolution.

It has been speculated that the annihilation mechanism is responsible for the energy release from quasars and radio galaxies - see Omnes (59); Alfvén (141); Teller (142).

On the assumption that the annihilation electrons in the source regions produce synchrotron radiation, one expects twice as much energy in the form of  $\gamma$ -radiation. Oke et.al. (143) and others predict that the  $\gamma$ -ray flux from 3C273 should be  $F_{\gamma} = 3 \times 10^{-5} \text{ } \gamma\text{'s cm}^{-2} \text{sec}^{-1}$  and hence the annihilation mechanism is losing ground in the face of these accurate experiments. However, an observation such as this one, of specific objects like 3C273 cannot state categorically that the antimatter does not exist in these regions because more information must be obtained on the relative opacity of the intervening space and of the source regions to  $\gamma$ -radiation.

The other valid argument which confuses the issue of the annihilation products is that the flux of the secondary products is a function of the relative mixing of matter and antimatter. In Alfvén and Klein's (50) original theory, they pointed out the Leiden-frost phenomenon could separate regions of pure matter and regions of predominantly antimatter, so that annihilation could only take place slowly at the boundary of these regions. The amount of annihilation radiation therefore depends upon the physical extent of the regions such that the larger the extent, the smaller the annihilation per unit volume.

The presence of antimatter in the galaxy and/or metagalaxy would be proved if a significant flux of antinuclei were seen in the cosmic radiation. As antiprotons and positrons can be synthesised in very high energy nuclear interactions, it is to be expected that both should be

present to some extent in the primary cosmic radiation due to the propagation of high energy cosmic rays through interstellar space and the probability of nuclear collisions en route. However, the presence of anticarbon, antineon or anti-iron for example would indicate that these antiparticles were synthesised at a source, or in regions of space which were predominantly antimatter. Grigorov et.al. (145) and Ivanova et.al. (146) exposed emulsions in a satellite flight and looked for annihilation stars amongst the nuclei which stopped in their emulsions. From these results, they concluded that for  $E_n \lesssim 1.4$  GeV/n the upper limit to the antimatter-matter ratio is

$$\bar{A}/A \lesssim 0.59\% \quad (1.8\% \text{ at } 95\% \text{ confidence limit})$$

At somewhat lower energies, Aizu et.al. (147) have, by employing the same technique, derived an upper limit for  $E_n \lesssim 700$  MeV/n of

$$\bar{A}/A \lesssim 0.1\% \quad (0.3\% \text{ at } 95\% \text{ confidence limit})$$

for the total cosmic radiation, i.e. predominantly protons (whereas the Russian results were for charge,  $Z > 3$ ).

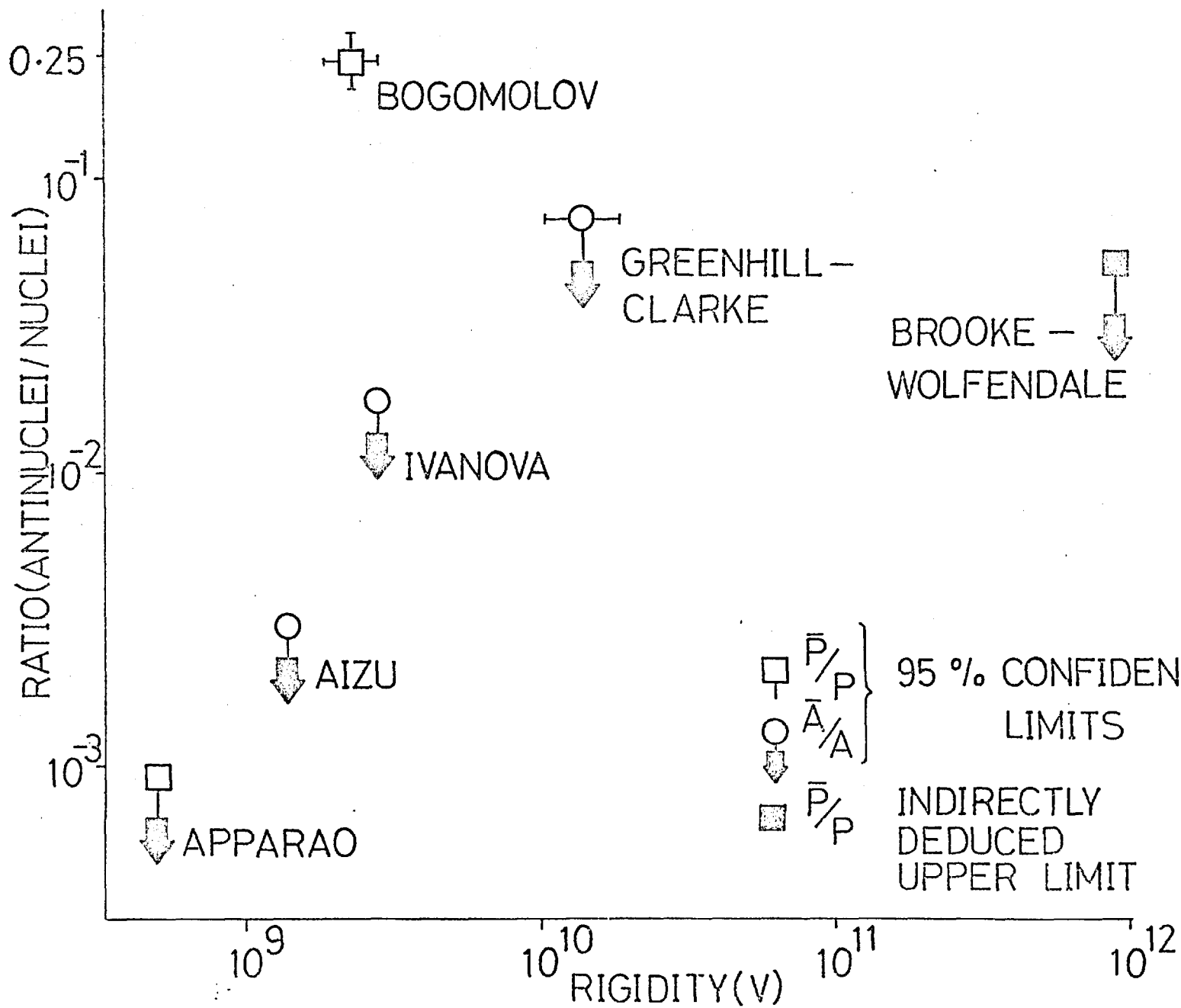
All other experiments have placed upper limits to the ratio of antiprotons to protons. Apparao et.al. (148) has placed the limit of

$$\bar{p}/p \lesssim 3 \times 10^{-4} \quad (10^{-3} \text{ at } 95\% \text{ confidence limit})$$

for  $E_p \lesssim 150$  MeV which is the lowest limit so far obtained. This limit is surprising, not because of the implications to antimatter, but because of the lack of secondary antiprotons. Rosen and Milford (149) estimate that for  $E_p \lesssim 0.5$  GeV, the ratio should be

$$\bar{p}/p \lesssim 3 \times 10^{-3}$$

FIG. 51 EXPERIMENTAL RESULTS ON ANTINEUTRONS IN THE PRIMARY COSMIC RAYS



and predict larger values for lower energies. Hence, Apparao's results contradict theory.

Some experimental and theoretical upper limits are plotted in Fig. 51. One Russian group, Bogomolov (OG63 - Budapest Conference) has reported a 25% ratio of antiprotons to protons at the recent Budapest Conference, but until this is confirmed by another group, it must be regarded as invalid. If this flux is upheld, the antiproton/proton ratio of Apparao's is totally inconsistent with the Russian value.

### 7.3. Antimatter in the Galaxy - Conclusions

The present experiment has established a new upper limit to anti-nuclei of charge,  $Z \geq 6$  in the primary cosmic radiation within the rigidity range  $10 \leq R \leq 18$  GV of

$$\frac{n^-}{n_A} \leq 7.5\% \text{ (95\% confidence limit)}$$

In order to draw conclusions on the antimatter content of the galaxy from this result, it is necessary to make assumptions about the sources and propagation of the primary cosmic radiation.

There is little doubt that the sources of the cosmic rays are distributed throughout the galactic disk, and, as has been discussed, the most likely candidates are supernovae and novae. In the previous section, the evidence on the propagation models was summarised, and three variants of the galactic disk model were discussed. It is now possible to place limits to the amount of antimatter in the galaxy for



each of the three models.

(a) Cosmic Radiation Representative of Whole Disk

This point of view could be valid if either of two propagation models is correct.

If the observed isotropy of the cosmic radiation is not a real effect, and is produced locally in the interplanetary space, then for an observed lifetime of  $\tau_{CR} \simeq 10^6 - 10^7$  yrs it is possible that the net flux of the cosmic radiation is the superimposed effect of sources spread throughout the disk.

Marshal Libby (150) has argued that another possible model is that the cosmic rays are produced in the disk and that they leak out of the disk into the halo region after  $\tau \simeq 10^6$  yrs. The composition of the halo, on this model, would be representative of the whole disk (because cosmic rays can propagate more freely in the low density,  $n \simeq 10^{-2} \text{ cm}^{-3}$ , halo than in the disk,  $n \sim 1 \text{ cm}^{-3}$ ). He further argues that, as the electron energy spectrum takes  $10^8$  yrs to reach a steady state, the electrons (and positrons) must be accelerated in the disk, leak into the halo for long storage and leak back into the disk in steady state equilibrium with the physical forces which degrade their energies - thereby implying that the nuclei and antinuclei could have the same lifecycle. If this were true and accepting the constancy of the cosmic ray flux for  $10^9$  yrs, the cosmic rays in the disk must be leaking into the halo at the same rate that cosmic rays in the halo are leaking into the disk.

For both of these models, the derived upper limit is thus the upper limit to antimatter in the galaxy.

(b) Cosmic Radiation of Local Origin

This model depends upon the validity of the isotropy measurements. The fragmentation of the nuclei with charge  $Z > .6$  during propagation into the L-nuclei indicates that  $3-4 \text{ gm.cm}^{-2}$  of interstellar material has been traversed, and for the accepted density of interstellar space of  $n_H \sim 1 \text{ cm}^{-3}$ , this implies a lifetime in the disk of  $\tau_{CR} \sim 10^6$  yrs. The bulk velocity of the cosmic radiation is reflected by the isotropy measurements, and the conclusion drawn is that the velocity is less than or equal to 20 km/sec i.e. 20 pc per  $10^6$  yrs. - See Meyer (151), due to diffusion processes.

Hence the cosmic radiation observed at the earth, allowing for errors, cannot have sampled more than  $\sim 2\%$  of the galaxy - see Marshall Libby (150) and this percentage represents the interstellar material in the vicinity of the solar system.

If this model is correct and the lifetime of the heavy nuclei in the cosmic radiation is governed by the probability of interaction rather than leakage as proposed by Ramaty and Lingenfelter (152), the derived upper limit to the ratio of antinuclei to nuclei tells us little about the average antimatter content of the galaxy. All the limit tells us is that in the vicinity of the solar system, the amount of antimatter is less than 7% that of matter. In order to generalise the limit, one might argue that the observed presence of Faraday rotation throughout the galaxy - Woltjer (153) - denies the presence of a patchy distribution of matter and antimatter, and as one observes less than 7% of antimatter in a region of the order of  $1/50$ th the size of the galaxy, it is unlikely

that antimatter exceeds this limit in other parts of the galaxy.

From an aesthetic point of view, if antimatter exists at all in our galaxy, it must exist as either a small scale homogeneous mix with matter, or as one single pure-antimatter region at the centre of the galaxy. The homogeneous-mix can be disproved by lowering the present upper limits to the flux of annihilation  $\gamma$ -radiation, but the alternative theory cannot be disproved by  $\gamma$ -ray astronomy, unless the galactic centre is transparent to  $\gamma$ -radiation, and this seems unlikely.

If the presently accepted views on the propagation of cosmic rays are upheld, it is difficult to see how the galactic-centre theory can be disproved, or proved. The only possibility is that the halo storage model is verified, and then the presence of antinuclei in the cosmic radiation will imply that the centre of the galaxy does indeed consist of antimatter.

#### Extragalactic Cosmic Rays

It was mentioned in section 1.2 that there was evidence at energies  $E \approx 10^{16}$  eV/n that the cosmic radiation was of extragalactic origin. The fraction of the cosmic radiation at lower energies which may be extragalactic is  $\sim 10^{-2}$ . Very little is known about the galactic boundary conditions for particle propagation and it is possible that a substantially smaller fraction of lower energy cosmic rays is of extragalactic origin. This fact emphasises the need for a lower upper-limit to antinuclei at relativistic energies rather than the

subrelativistic region measurements with emulsions.

The  $\gamma$ -ray measurements imply that the intergalactic space contains negligible antimatter, but it is possible that there are neighbouring galaxies in the local cluster which are made of antimatter. If, however, the extragalactic flux was found to contain antinuclei, this would present considerable problems to the cosmologists, because in any charge-symmetric cosmology, there is, at present, no plausible mechanism for the separation of region of matter and antimatter on a galactic scale (Defouw (154)).

The conclusions drawn is that more measurements of the antinuclei to nuclei ratio, and the isotropic  $\gamma$ -ray background flux are required in order to improve upper limits. If antinuclei were found in the cosmic radiation, cosmologists would be forced to introduce charge symmetry into their theories and, as shown in section 1.6., this is beset with difficulties. But astrophysicists and astronomers would then be able to explain the phenomenal energy outputs of radio galaxies and quasars in terms of a controlled annihilation mechanism. In short, the research on antinuclei and the appropriate cosmic ray propagation model will certainly clarify many current problems, and undoubtedly pose many more.

APPENDIX A

Hall-Probe Magnetometer

The outline of the magnetometer has already been given. Below are a few significant design criteria:

(i) Field-Concentrators

The Hall Probe chosen was the commercially available type with the highest sensitivity. The sensitivity of the two Hall Probes used

were (a) 0.646 millivolt/mA. Kgauss

(b) 0.831 millivolt/mA. Kgauss

When these probes are used, without field concentrators and with the maximum permissible control current of 200 milliAmps, it can be seen that the change in output voltage at the terminals of the Hall Probes, for an orientational change of  $\theta_A = 180^\circ$  - which means a change in the magnetic field strength of 0.400 gauss is given by

$$(a) \quad 0.646 \times 200 = \frac{0.4}{1000} \text{ millivolts}$$

$$\Delta V_o = 51.68 \text{ microvolts}$$

$$(b) \quad 0.831 \times 200 \times \frac{0.4}{1000} \text{ millivolts}$$

$$\Delta V_o = 66.88 \text{ microvolts}$$

Hence, in order to achieve an orientational accuracy of 1 degree of arc, very high gain circuits are necessary. However, the use of very high gain circuits will not only increase the sensitivity, but also increase the intrinsic drifts in the H.E.P. The output of the Hall Probe may be represented by

$$v_o = V_{HALL}(B) + \epsilon$$

where  $\epsilon$  represents a misalignment voltage susceptible to drifts (and any other unwanted voltage) and  $V_{HALL}$  is a function of the magnetic field strength  $B$  at the sensor.

If ferrite rod field concentrators are used, the effective field at the sensor becomes  $(\alpha B)$  where  $\alpha$  is the effective permeability of the rods. It follows that

$$v_o = V_{HALL}(\alpha B) + \epsilon$$

$$v_o = \alpha \cdot V_{HALL}(B) + \epsilon$$

and the signal to noise ratio has been improved by a factor,  $\alpha$ .

Using the relationship

$$1/\mu F = 1/\alpha - N/4\pi$$

where  $N$  = demagnetising factor

and  $\mu F$  = true permeability of the ferrite material.

and Table IX, taken from Bozorth\*, which relates the physical size of the rods to the demagnetising factor, the effective permeability of the rods used was

$$\alpha \approx 150$$

\* TABLE IX :

$1/d$	$N/4\pi$
2	0.14
5	0.055
10	0.020
15	0.010
20	0.007
30	0.0035

Hence, the output from the Hall Probe for a swing of  $\Delta\theta \approx 180^\circ$  was  $\Delta V_O \approx 10$  millivolts.

(ii) Sensitivity - Transfer Coefficient

The behaviour of the complete electronic cct is conveniently summarised by the transfer coefficient, S which is synonymous with the sensitivity of the device. It is defined as the change in the output variable for a change in the input variable, namely the azimuthal orientation,  $\theta_A$ .

Mathematically, as the output variable of interest is the subcarrier frequency,  $f_t$ :

$$S = \frac{\Delta f_t}{\Delta \theta_A}$$

Considering the responses of the individual circuits

$$\frac{\Delta f_t}{\Delta \theta_A} = \frac{\Delta f_t}{\Delta V_{v \rightarrow f}} \cdot \frac{\Delta V_{v \rightarrow f}}{\Delta V_{INT}} \cdot \frac{\Delta V_{INT}}{\Delta V_{TWIN-T}} \cdot \frac{\Delta V_{TWIN-T}}{\Delta V_O} \cdot \frac{\Delta V_O}{\Delta \theta_A}$$

i.e.

$$S \equiv \{S_{v \rightarrow f}\} \cdot \{S_{INTEGRATOR}\} \cdot \{S_{P.S.D.}\} \cdot \{S_{TWIN-T}\} \cdot \{S_{H.E.P.}\}$$

where

$$S_{v \rightarrow f} = \left\{ \frac{R_G}{R_{E_1} R_{E_2}} \cdot \frac{(R_{BIAS} + R_{fb})}{R_{fb}} \cdot \frac{1}{C \eta V_{cc}} \right\}$$

$$S_{INT} = \left\{ \frac{1 - \tau_{OX}/2R.C}{0.707} \right\}$$

$\tau_{OX}$  = period of master oscillator

$$S_{P.S.D.} = \cos(\phi_{SIG} - \phi_{OX})$$

$$S_{\text{TWIN-T}} = \frac{R_f}{R_B} \{1 - 0.003 \{f_{\text{OX}} - f_C\}^2\}$$

assuming Gaussian response  
of Gain. v freq.

$$S_{\text{H.E.P.}} = S_{\text{H.P.}} i_{\text{H.P.}} \sin \theta_A \cdot B_{\text{MAX}} \alpha_{\text{FERRITE}}$$

$S_{\text{H.P.}}$  = sensitivity of sensors in  
mV/mA Kgauss



APPENDIX B.

Solar Modulation.

In order to interpret the energy or rigidity spectra of the cosmic radiation one has to take into account any processes that may modify or modulate the shape of the spectra as the radiation propagates through interstellar space from source to observer. One such process which has been extensively studied is called solar modulation which affects cosmic radiation in interplanetary space.

The magnitude of the effect is correlated with the sun's rotational period and, in the long term, with the 11 yr. cycle of magnetic disturbances on the sun. When the balloon flights were conducted, the solar modulation effect was near minimal, but the effect of this residual modulation must still be considered on the results in the rigidity range of interest.

The presently accepted model of solar modulation is the solar wind theory of Parker (1958) which envisages a continuous stream of plasma flowing outward from the sun (the solar wind). Magnetic field lines are frozen into the plasma and form an archimedean spiral shape throughout the interplanetary space which is the composite effect of the plasma outward flow and the rotation of the sun. At a certain distance from the sun the plasma becomes unstable and the magnetic field becomes disordered. In this region the galactic particles will undergo isotropic diffusion whereas, in the inner solar system where the field lines are ordered, the cosmic ray particles will diffuse more readily inward along the lines of force rather than across them, i.e. a state of anisotropic diffusion.

Parker obtains the following result for the case of isotropic diffusion by considering the continuity equation and assuming the steady state condition for the cosmic ray spectrum:

$$j_i(R) = \rho_i(R) \exp \left\{ \frac{-3vr \left( 1 + \frac{m^2 c^2}{Z_i^2 R^2} \right)^{\frac{1}{2}}}{c L(R)} \right\}$$

where  $V$  = solar wind speed

$r$  = thickness of diffusing region

$L(R)$  = magnetic scattering mean free path

and

$$L(R) = \lambda \left( 1 + \frac{\pi R^2}{4 \times 300^2 B^2 d^2} \right)$$

where  $B$  = average field strength in diffusion

$d$  = average scale size of magnetic irregularity

$\lambda$  = mean separation of irregularities

The values of the parameters at solar minimum are given by Parker as  $v = 3 \times 10^7$  cm/sec,  $r = 3 \times 10^{14}$  cm,  $B = 2 \times 10^{-5}$  gauss,  $d = 2 \times 10^{11}$  cm and the equation for the observed rigidity spectra,  $j_i(R)$  in terms of the galactic rigidity spectra  $\rho_i(R)$  becomes

$$j_i(R) = \rho_i(R) \exp \left\{ - \frac{1 + \frac{0.88 A_i^2}{Z_i^2 R^2}}{1 + 1.76 R^2} \right\}$$

If  $R > 1$  GV,  $j_i(R) \approx \left( 1 - \frac{2}{R^2} \right) \rho_i(R)$

If  $R < 1$  GV  $j_i(R) \approx \exp \left( - \frac{0.94 A_i}{Z_i A} \right) \rho_i(R)$ .

In the rigidity range of interest,  $R > 10$  GV, the relations above show that the intensity of the 10 GV particles is reduced by only 2% ( $\approx 2/R^2$ ) and so the effect of solar modulation on the rigidity spectral exponents is negligibly small compared to the statistical errors.

APPENDIX C

Preferential Loss by Diffusion

Whether diffusion from a source region, or the galactic disk is being considered, it is to be expected that the appropriate diffusion coefficient,  $D$  is purely a function of the rigidity,  $R_i$  of each charge group and not the charge,  $Z_i$ .

The confinement of cosmic rays is thought due to the presence of magnetic fields. The particles diffuse out of the regions if their radii of curvature,  $r_i$  are comparable to or greater than the typical linear dimensions of the regions considered

$$r_i = \frac{c p}{Z_i e H}$$

$c$  = velocity of light  
 $H$  = magnetic field strength  
 $p$  = transverse momentum.

But the rigidity is defined as

$$R_i = \frac{p c}{Z_i e}$$

Hence,  $D_i = f(r_i) = f(R_i)$

Particles of different charge should leak out of the regions in exactly the same way provided that their rigidities are the same. Put another way, this implies that the integral rigidity spectra of each charge group,  $Z_i$  should be identical after the diffusion if their spectra were the same before the diffusion.

REFERENCES

1. Burbridge, E.M., Burbridge, G.R. and Hoyle, F., (1963), Ap.J., 138, p.873.
2. Burbridge, G.R. and Hoyle, F., (1964), Proc.Phys.Soc., 84, p.141.
3. Burbridge, E.M. and Burbridge, G.R., (1965), Proc.Int.Conf.Cosmic Rays, London, 1, p.92.
4. Sciama, D.W., (1964), Quart.J.Roy.Astron.Soc., 5, p.196.
5. Ginzburg, V.L. and Syrovatskii, S.I., (1964), "Origin of Cosmic Rays", Pergamon Press N.Y.
6. Webber, W., (1967), Bull.Am.Phys.Soc., 12, p.591.
7. Durgaprasad, N., (1967), J.Geophys.Res., 72, p.965.
8. Cowsik, R., Yash Pal, Tandon, S.N. and Verma, R.P., (1967), Tata Inst. Preprint.
9. Walker, R. - as reported in Meyer, P., (1969), Ann.Rev.Astronomy & Astrophys., 7.
10. Anders, E., (1964), Space Science Revs., 3, p.583.
11. Syrovatskii, S.I., Fomin, Yu.A. and Khristiansen, G.B., (1963), J.E.T.P., 45, p.1595.
12. Colgate, S.A. and McKee, C., (1969), Ap.J., 157, p.623.
13. Layzer, D., (1965), Ap.J., 141, p.837 and Nature, 214, p.772.
14. Kaplan, M.F. and Skadron, G., Univ. of Rochester, Rpt.no. URPA-124.
15. Michel, F.C., (1969), Ap.J., 157, p.1183.

16. Melrose, D.B., (1968), *Can.J.Phys.*, 46, p.638.
17. Tsyтовich, V.N., (1964), *Soviet Astronomy*, 7, p.471.
18. Aller, L.H. (1961), "Abundance of the Elements", *Interscience Monographs*, Vol. VII.
19. Cameron, A.G.W., (1959), *Ap.J.*, 130, p.429.
20. Gold, T., (1968), *Nature*, 218, p.731 and *Nature*, 221, p.25.
21. Ostriker, J.P. and Gunn, J.E., (1969), *Ap.J.*, 157, p.1395.
22. Burbidge, E.M., Burbidge, G.R., Fowler, W.A. and Hoyle, F., (1957), *Rev. Mod. Phys.*, 29, p.547.
23. Biswas, S., Ramadurai, S. and Sreenivasan, N., (1966), *Phys. Rev.*, 149, p.1037.
24. O'Dell, F.W., Shapiro, M.M. and Stiller, B., (1962), *J. Phys. Soc. Japan*, 17, Suppl.A-III, p.23.
25. Elliot, H., Peacock, D. and Thambyahpillai, T., (1970), 11th Int.Conf. Cosmic Rays, *Acta Physica Hungaricae*, 29, Suppl.1.
26. Ginzburg, V.L. and Syrovatskii, S.I., (1964), "Origin of Cosmic Rays", Pergamon Press N.Y.
27. Wentzel, D.G., (1968), *Ap.J.*, 152, p.987 and (1969), *Ap.J.*, 157, p.545.
28. Lerche, I., (1967), *Ap.J.*, 147, p.689 and (1966), *Phys.Fluids*, 9, p.1073.
29. Parker, E.N., (1969), *Space Sci. Rev.*, 9, p.651.

30. Parker, E.N., (1970), Proc.Int.Conf.Cosmic Rays, Budapest, Acta Physica Hungaricae.
31. Ramaty, R. Reames, D.V. and Lingenfelter, R.E., (1970), Phys. Rev. Letters, 24, No.16, p.913.
32. Hayakawa, S., Ito, K. and Terashima, Y., (1968), Prog. Theoretical Phys. Suppl. (Kyoto), 6, p.1.
33. Peters, B., (1963), Pontificiae Academiae Scientiarum Scripta Varia, 25, 1.
34. Shapiro, M.M. and Silberberg, R., (1970), 11th Conf. Cosmic Rays, Budapest, Paper OG-89.
35. Von Rosenvinge, T.T. and Webber, W.R., (1969), Astrophysics and Space Science, 3, p.4.
36. Lund, N., Peters, B., Cowsik, R. and Yash Pal, (1970), Phys. Rev. Letters, 31B, p.553.
37. Reames, D.V., (1970), Bull.Am.Phys.Soc., 15, p.619.
38. Shapiro, M.M. and Silberberg, R., (1970), Ann.Rev. Nuclear Science, Vol.20.
39. Fan, C.Y., Gloeckler, G. and Simpson, J.A., (1966), Phys. Rev. Letters, 17, p.329.
40. Cowsik, R., Yash Pal, Tandon, S.N. and Verma, R.P., (1967), Phys. Rev., 158, p.1238.
41. Balasubrahmanyam, V.K., Boldt, E., Palmeira, R.A.R., (1967), J. Geophys. Res., 72, p.27.
42. Fichtel, C.E. and Reames, D.V., (1968), Phys. Rev., 175, No.5, p.1564.

43. Comstock, G.M., Fan, C.Y., Simpson, J.A., (1969), *Astrophys.J.*, 155, p.609.
44. Waddington, C.J. and Freier, P.S., (1967), *Can.J.Phys.*, 46, p.
45. Comstock, G.M., (1969), *Ap.J.*, 155, p.619.
46. Burbidge, G.R., Fowler, W.A. and Hoyle, F., *Nature*, 216, p.22.
47. Teegarden, B.J., McDonald, F.B. and Balasubrahmanyam, V.K., (1970),  
11th Conf. Cosmic Rays, Budapest.
48. Ramadurai, S., (1967), *Proc. Ind. Acad. Sci.*, 65A, p.219.
49. Klein, O., (1958), "La Structure et l'Evolution de l'Univers",  
Institut Internat. de Physique Solaire, Bruxelles, p.33-51.
50. Klein, O. and Alfvén, H., (1962), *Arkiv fur Fysik*, 23, p.187.
51. Steigman, G., (1969), *Nature Centenary Issue*, Vol. 224, Nov. 1st.
52. Hawking, S. and Ellis, G.F.R., (1968), *Ap.J.*, 151, p.25.
53. Gamow, G., (1946), *Phys. Rev.*, 70, p.572.
54. Penzias, A.A. and Wilson, R.W., (1965), *Ap.J.*, 142, p.420.
55. Field, G.B. and Hitchcock, J.L., (1966), *Phys. Rev. Letters*, 16, p.817.
56. Zeldovich, Ya.B., (1965), *Adv. Astron. Ap.*, 3, p.241.
57. Chiu, H.Y., (1966), *Phys. Rev. Letters*, 17, p.712.
58. Harrison, E.R., (1968), *Phys. Rev.*, 167, p.1170.
59. Omnes, R., (1969), *Phys. Rev. Letters*, 23, p.38.
60. Ek spong, A.G., and Ronne, B.E., (1959), *Nuovo Cimento*, 13, p.27.
61. Cork, B. et.al., (1962), *Nuovo Cimento*, 25, p.497.



62. Koba, Z. and Takeda, G., (1958), Prog. Theor. Physics, 19, p.269.
63. Hoyle, F. and Narlikar, J.V., (1963), Proc. Roy.Soc. A, 273, p.1.
64. Burbidge, G.R. and Hoyle, F., (1950), Nuovo Cimento, 4, p.558
65. Hoyle, F., (1969), Nature (Centenary Issue), 224, p.477.
66. Jelley, J.V., (1966), Nature, 211, p.472.
67. Heristchi, (1967), Nucl. Instr. and Methods, 47, p.39 (French)
68. Crabb, (1966), Nucl. Instr. and Methods, 45, p.301
69. Briancon, A., (1967), Nucl. Instr. and Methods, 48, p.64.(French).
70. Dubbs, C., (1966), IEEE Trans. NS-13, No.1, p.729.
71. Von Rosenvinge, T.T. and Webber, W.R. (1968), Nucl. Instr. Methods.
72. Webber, W.R. and Ormes, J.F., (1967), J. Geophys. R., 72, p.5957.
73. Frank, I.M. and Tamm, I.G., (1937), Dokl. Acad. Nauk. SSSR, 14, No.3, p.109.
74. Jelley, J.V., (1958), 'Cerenkov Radiation and its Applications' (Pergamon Press).
75. Camerini, U. et.al., (1952), Progress in Cosmic Ray Physics, Vol.1, p.56.
76. Fowler, P.H., (1950), Phil. Magazine, 41, p.169 (III).
77. Rotelli, P., (1969), Phys. Rev., 182, No.5, p.1622.
78. Spergel, M.S.(1966), Nuovo Cimento Vol. XLII A, p.251.
79. Hillas, A.M.(1970), Leeds University Lecture Notes.
80. Treiman, S.B. (1953), Phys. Rev., 91, p.957.
81. Webber, W.R., (1967), Univ. of Minnesota Technical Rpt., CR-94.
82. Daniel, R.R. and Stephen, S.A., (1966), Phys. Rev. Letters, 17, p.935.
83. Dev Verma, S., (1967), J.G.R., 72, No.3, p.915.

84. Cleghorn, T.F. et.al., (1968), Can.J.Physics, 46, S572.
85. Topping, J., (1955) "Error of Observation and their Treatment"  
(Institute of Physics).
86. Bond, W.N., (1935), Probability and Random Errors, p.96 (Ed. Arnold Co.).
87. Anand, K.C. et.al., (1967), Phys. Rev. Letters, 20, p.764.
88. Durney, A.C. et.al., (1963), Imperial College Preprint.
89. Ginzburg, V.L., (1964), "Origin of Cosmic Rays" (Pergamon Press).
90. Von Rosenvinge, T.T. and Webber, W.R., (1969), Astro. Space Sci., 5, p.34
92. Fermi, E., (1949), Phys. Rev., 75, p.1169.
93. Syrovatskii, S.I., (1964), see ref. 26.
94. Webber, W.R., (1965), Univ. Minnesota Techn. Rpt., CR-82 (Proc. London Conference).
95. Abraham, F. et.al. (1967), Phys. Rev., 159, p.1110.
96. I.C.E.F. Team, (1963), Nuovo Cim. Suppl., 1, p.1039.
97. McCusker, C.B.A., (1963), Int. Conf. Cosmic Rays - Jaipur, 4, p.35.
98. Linsley, J. and Scarsi, L., (1962), Phys. Rev. Letters, 9, p.123.
99. Peters, B., (1952), Prog. Cosmic Ray Phys., p.193
100. Parker, E.N., (1958), Phys. Rev., 110, p.1445.
101. Ginzburg, V.L., (1963), Space Sci. Rev., 2, p.778.
102. Millikan, (1942), Phys. Rev., 61, p.397.
103. Klein, O., (1944), Ark. Mat. Astr. Fys., 31A.
104. Morrison, P., (1954), Phys. Rev., 94, p.440
105. Hayakawa, S., (1958), Suppl. Prog. Theor. Phys., No.6.
106. Freier, P.S. and Webber, W.R., (1963), J. Geophys. Res., 68, p.1605.
107. Kristiansson, K., (1964), Arkiv fur Fysik, 25, p.513.
108. Von Rosenvinge, T.T. and Webber, W.R., (1969), Astro.Space Sci., 3, p.80.

109. Corydon-Peterson, O. et.al., (1970), Phys. Letters, 31B, p.553.
110. Biswas and Fichtel, (1965), Space Sci. Rev., 4, p.709.
111. Waddington, C.J., (1968); Univ. Minnesota Preprint.
112. Rudstam, G., (1966), Zeitschrift fur Naturforschung, 21A, p.1027.
113. Durgaprasad, N., (1965), Proc. Ind. Ac. Sci., 62, Sec. A, p.330.
114. Anand, K. et.al., (1966), J. Geophys. Res., 71, p.4687.
115. Balasubrahmanyam, V.K., (1966), J. Geophys. Res., 71, p.1771.
116. Shapiro, M.M. and Silberberg, R., (1970), Ann. Rev. Space Sci., 20,
117. Pottasch, S.R., (1965), Proc. IAU-Symposium, Utrecht, 200.
118. Unsold, A.O.J., (1969), Science, 163, p.1015.
119. Biswas, S. and Fichtel, C.E., (1965), Space Sci. Rev., 4, p.709.
120. Jonsson, G., Kristiansson, K. and Malmqvist, L., (1970), Astro. and Space Sci., 7, p.231.
121. Caughlan, G.R., (1965), Ap.J., 141, p.688.
122. Warburton, E.K., Olness, J.W. and Alburger, R.E., (1965), Phys. Rev., 140, B1202.
123. Hayakawa, S. et.al., (1960), Proc. Moscow Cosmic Ray Conf., 3, p.171.
124. Colgate, S.A. and White, R.H., (1966), Ap.J., 143, p.626.
125. Fowler, P.H. et.al., (1970), Proc. Roy. Soc. Lond. A 318, p.1.
126. Stormer, C., (1955), "The Polar Aurora", (Oxford Clarendon Press).
127. McCracken, K.G., Rao, U.R. and Shea, M.A., (1962), M.I.T. Techn. Rpt. No. 77, NYD 2670.
128. Janossy, L., (1948), "Cosmic Rays", (Oxford Clarendon Press).
129. Hayakawa, S., (1969), "Cosmic Ray Physics", Vol.XXII (Interscience Mono

References to "Review of Antimatter in Cosmic Radiation".

130. Matsuda, S., (1966), Phys. Rev., 150, p.1197.
131. Stecker, F.W., (1966), Smithsonian Astrophys. Obs. Spec. Rpt., No.261.
132. Daniel, R.R. and Stephens, S.A., (1966), Phys. Rev. Letters, 17, p.935
133. Fanselow, J.L., (1968), Ap.J., 152, p.783.
134. Kojoian, G., (1967), Ames Research Centre (preprint).
135. Ginzburg, V.L., (1958), Prog. El. Particles and Cosmic Ray Physics, 4.
136. Hayakawa, S., (1952), Prog. Theor. Phys., 8, p.571.
137. Morrison, P., (1958), Nuovo Cimento, 7, p.858.
138. Kraushaar, W.L. and Clark, G.W., (1968), Ap.J.Letters, 153, L203.
139. Sood, R.K., (1969), Nature, 222, p.650.
140. Burbidge, G. and Burbidge M., (1967), "Quasi-Stellar Objects", p. 145, (Freeman & Co.).
141. Alfvén, H. and Elvius, A., (1969), Science, 164, p.911.
142. Teller, E., (1966), "Perspectives in Modern Physics", p.449 (Interscience Press).
143. Oke, J.B., (1965), Ap.J., 141, p.6.
144. Frye, G.M. and Wang, C.P., (1967), Physic. Rev. Letters, 18, p.132 and (1968), Can. J. Phys., 46, S448.
145. Grigorov, N.L. et.al., (1961), Artificial Earth Satellites, 10; Izd-vo An. SSSR (1961) p.96.
146. Ivanova, N.S. Gagarin, Yu.F., and Kulikov, V.N., (1968), Kosmicheskie Issledovaniya, 6, No.1, p.83.
147. Aizu, H. et.al., (1961), Phys. Rev. 121. p.1206.

148. Apparao, M.V.K., (1968), Can. J. Phys., 46, S654.

149. Rosen, S and Milford, S.N., (1965), Nature 205, p.582.

References to "Conclusion of Antimatter".

150. Marshall Libby, L., (1970), Nature, 225, p.166.

151. Meyer, P., (1969), Ann. Rev. of Astron. and Astrophys., 1.

152. Ramaty, R and Lingenfelter, R.E., (1970), Phys. Rev. Letters, 24,  
No.16, p.913.

153. Woltjer, L., (1967), I.A.U.-Symposium, 31, p.480.

154. Defouw, R.J., (1970), Nature, 228, p.1068.